Initial Access in Millimeter Wave Systems

By

Sadaf Nawaz

NUST201490196PSEECS0514F

Supervisor

Dr. Syed Ali Hassan

Department of Electrical Engineering

School of Electrical Engineering & Computer Science (SEECS)

National University of Sciences and Technology (NUST)

Islamabad, Pakistan

2021

Initial Access in Millimeter Wave Systems

By

Sadaf Nawaz

NUST201490196PSEECS0514F

Supervisor

Dr. Syed Ali Hassan

A thesis submitted in conformity with the requirements for

the degree of *Doctor of Philosophy* in

Electrical Engineering

Department of Electrical Engineering

School of Electrical Engineering & Computer Science (SEECS)

National University of Sciences and Technology (NUST)

Islamabad, Pakistan

2021

This thesis is dedicated to *my beloved son, Muhammad Azaan Shami*

Acknowledgments

I pay my heartiest gratitude to my advisor Dr. Syed Ali Hassan who has always been a source of inspiration for me, both technically and morally. The completion of this thesis would not have been possible without his continuous guidance and support on each step. I am grateful for his patience, compassion, calm and positive attitude that encouraged me to work enthusiastically and achieve my goals. I can never repay what he has taught me, but I have prayers which would always thank him for his endless support.

I am grateful to our research collaborators, Professor Haejoon Jung, Dr. Syed Ali Raza Zaidi and Professor Mounir Ghogho for their time, guidance and help in improving the research papers. Special thanks to Dr. Hassaan Khaliq, Dr. Sajid Saleem, Dr. Qaiser Choudhry, Dr. Sajjad Hussain and Dr. Imran Rashid for their time and valuable feedback during this thesis. I would also like to thank my IPT lab colleagues, Hamnah Munir, Rehan Zahid, Saad Zia, Aneeqa Ijaz, Aamra Arshad, Shahmeer Omar, Rida Mustafa, Shahzeb Khan, M. Waseem and my friend Anam Haq who have always helped me in the hour of need.

I don't have words to thank my dear husband, Dr. Muhammad Ali Shami for his love, patience, support and guidance throughout this thesis. Whenever I was breaking down, he aided me in getting back to my path. He stood by me through thick and thin and helped me become a better person and achieve this challenging target.

I would like to pay special thanks to my parents, siblings and grandfather for their continuous love, support and prayers throughout my studies that have made it possible for me to complete this thesis.

Table of Contents

List of Figures

List of Tables

List of Abbreviations

IA	Initial Access
mmWave	Millimeter Wave
MIMO	Multiple-Input Multiple-Output
mMIMO	Massive MIMO
BF	Beamforming
D2D	Device-to-Device
HetNet	Heterogeneous Network
ULA	Uniform Linear Array
UPA	Uniform Planar Array
AoA	Angle-of-Arrival
AoD	Angle-of-Departure
PMD	Probability of Miss Detection
DD	Discovery Delay
AH	Auxiliary-Half
AF	Auxiliary-Full
ABP	Auxiliary Beam Pair
SNR	Signal-to-Noise Ratio
SINR	Signal-to-Interference-plus-Noise Ratio

LTE	Long Term Evolution
GSM	Global System for Mobile Communications
TX	Transmitter
RX	Receiver
BS	Base Station
CSI	Channel State Information
EE	Energy Efficiency
QoS	Quality of Service
ODND	Oblivious Directional Neighbor Discovery
BW	Beamwidth
HPBW	Half-Power Beamwidth
UE	User Equipment
LoS	Line-of-Sight
NLoS	Non Line-of-Sight
ASE	Area Spectral Efficiency
PPP	Poisson Point Process
UHF	Ultra-High Frequency
UAVs	Unmanned Aerial Vehicles
FKM	Fredricksen, Kessler and Maiorana
CI	Context Information
GPS	Global Positioning System
RF	Radio Frequency

List of Symbols

N_t	Total number of antenna elements at transmitter
N_r	Total number of antenna elements at receiver
λ	Wavelength
d	Antenna element separation
θ_t	Angle-of-Departure
θ_t	Angle-of-Arrival
$\phi_{t\alpha}$	Steering direction of α beam
$\phi_{t\beta}$	Steering direction of β beam
$Y_{t\alpha}$	Radiation pattern of α beam
$Y_{t\beta}$	Radiation pattern of β beam
N_{tAH}	Total number of search sectors
δ	Separation between α and β beams
γ	Ratio metric
h	Positive integer
S	Stages
θ°_{start}	Start of search sector
θ°_{end}	End of search sector
k	Search sector index

ψ	Direction of main probing region
μ	User location
$G_{t\alpha}$	Beamforming gain of α beam
$G_{t\beta}$	Beamforming gain of β beam
G_{TX}	Transmit antenna gain
G_{RX}	Receive antenna gain
G	Total antenna gain
L	Path loss
ρ	Fixed path loss factor
r	Distance between the TX and R
α_L	LoS path loss exponent
α_N	NLoS path loss exponent
χ_L	Zero mean lognormal random variables for LoS
χ_N	Zero mean lognormal random variables for NLoS
P_r	Received power
P_t	Transmit power
ζ	Squared envelope of multipath fading channel
τ	SNR
σ^2	Noise variance
α_{th}	SNR threshold
T_{syn}	Synchronization signal
T_{sig}	Scanning time
T_{per}	Waiting time

α_l	Loose SNR threshold
f_c	Carrier frequency
M	Devices in the network
E	Extended ID sequence
L	Extended address length
t	Number of time slots
p_m	Smallest odd prime number
q_m	Smallest power of 2
${e_t}^m$	A bit in E
W	Worst-case disocvery delay
N	Necklaces
b	Beads
c	Colors
U_α	Antenna scan sequence of α beam
U_β	Antenna scan sequence of β beam
T	Maximum time slots

List of Publications

1. Sadaf Nawaz and Syed Ali Hassan, "Optimal beam separation in auxiliary beam pair-based initial access in mmWave D2D networks ", IEEE Vehicular Technology Conference (VTC), May 25-29, 2020.

2. Sadaf Nawaz, Syed Ali Hassan and Haejoon Jung, "Auxiliary beam pair enabled initial access for mmWave D2D networks", Physical Communication Journal, vol. 39, pp. 1-12, April 2020.

3. Sadaf Nawaz and Syed Ali Hassan, "Auxiliary beam pair enabled initial access in wwWave systems: Analysis and design insights", IEEE International Conference on Communications (ICC), May 20-24, 2019.

4. Sadaf Nawaz, Syed Ali Hassan, Syed Ali Raza Zaidi and Mounir Ghogho, "Throughput and energy efficiency of two-tier cellular networks: Massive MIMO overlay for small cells", IEEE International Wireless Communications and Mobile Networking Conference (IWCMC), September 5-9, 2016.

Abstract

The 5G technology will achieve high data rates, reduced latency, increased bandwidth, enhanced coverage, seamless connectivity, low cost and energy efficient systems through the union of multiple new technologies. For example, the existing macro band is insufficient to accommodate the ever increasing wireless traffic. Therefore, the high frequency millimeter wave (mmWave) spectrum should be utilized. On the other hand, the traffic load on existing base stations (BSs) should be reduced by offloading users to a device-to-device (D2D) network. Similarly, the initial access (IA) scheme of the existing 4G long term evolution (LTE) system is not suitable for 5G environment due to issues related to connectivity, blockages, deafness, discovery range etc. Hence, for the successful implementation of an efficient 5G network, a novel IA scheme is the need of the hour. This dissertation is motivated from these technologies where the amalgamation of novel IA schemes, mmWave system and D2D network improves the network performance.

Our research work consists of three phases. In the first phase we propose and implement two novel beamforming (BF) techniques, i.e., auxiliary-half (AH) and auxiliary-full (AF) at the transmitter (TX) side. In AH, two beams are generated simultaneously at the BS side, whereas, in AF, the beams are generated in a time division manner. The BS scans for the desired user by pointing the beam pair in a particular direction. The scanning process occurs in a sequential way and the user discovery process is successful only when the received signal-to-noise-ratio (SNR) is above a certain threshold value. We also develop a mathematical model for BF in the exhaustive and iterative search methods for a comprehensive analysis. Our results show dependence on beam-pair separation in both AH and AF schemes. AH achieves a lower discovery delay (DD) than iterative method and also lower probability of miss detection (PMD) than exhaustive scheme. Moreover, AF has a lower DD than exhaustive method and AF outperforms all other schemes in terms of PMD.

In the second phase, we implement BF at both TX and receiver (RX) side and propose a novel antenna scan sequence scheme. Both TX and RX scan the desired region in a non-sequential manner by utilizing the proposed antenna scan sequences. We also implement BF in the oblivious directional neighbor discovery (ODND) and Polya's Necklaces schemes for a detailed comparison. Simulation results show that both AH and AF rely on beam pair separation for optimal results. We also show a high dependence on SNR for the DD process, which contradicts the worst-case upper bound proposed by the ODND scheme. Furthermore, we show that AH and AF can achieve a lower DD for a certain range of TX-RX separation, SNR threshold and beam-pair separation. AF also outperforms all other schemes in terms of PMD.

The third phase discovers the optimal value of beam pair separation at both TX and RX side. BF is implemented at both TX and RX through non-sequential antenna scan sequences and a beam pair is investigated that achieves the least DD and PMD. It is also shown that the narrowest possible beam pair separation at both TX and RX does not ensure a least DD in either AH and AF schemes.

Chapter 1

Introduction

In this chapter, we briefly discuss about 5G and its relevant technologies. We also highlight our motivation behind this work and our valuable contributions to literature. The details are as follows.

1.1 5G Overview

Over a few decades, the mobile communications have evolved from voice only systems to multimedia applications. This rapid growth has attracted many users and according to statistics the mobile traffic increased by 70% in 2014 out of which more the half of the traffic consists of video mobile users [3]. It is expected that by 2020, around one terabyte data will be downloaded by an average mobile user annually [4]. On the other hand, augmented reality is gaining popularity as well and applications like Machine-to-Machine (M2M), D2D, Internet of vehicles (IoV), Internet of Things (IoT), etc. require high data rates and connectivity for successful communication. It is a crucial task for existing 4th generation (4G) long-term-evolution (LTE) systems to support these high-level applications. Although LTE is utilizing the concepts of multiple-input multiple-output (MIMO), heterogeneous networks (HetNets), small cells, multiple antennas etc. to sustain this heavy traffic load yet it seems unlikely to hold on to such a heavy load in the long run [4]. Hence, to satisfy this increasing mobile traffic and to ensure maximum capacity and seamless connectivity, the generation of 5G emerged.

5G envisions a massive increase in data rates (1-10 Gbps), high bandwidth, reduced latency, enormous connected devices, full coverage (almost 100%), increased battery life and reduced

energy consumption [5], [6]. The details of these technical requirements are as following:

1.1.1 Data Rate and Coverage

It is expected that 5G will maintain seamless connectivity anytime and anywhere with the data rate of at least 1 Gbps. The peak data rates along with quality of service (QoS) for different users, i.e., high-mobile and low-mobile users must always be ensured. The existing 4G network can support mobility of around 250km/h whereas, 5G will support mobility of 500 Km/h as well [2].

1.1.2 Latency

The latency requires that the data is delivered from source to destination within a set time period. 5G is expected to achieve a round trip time of around 1-5ms (10ms for 4G) [2, 7].

1.1.3 Connected Devices

5G will help achieve connectivity of devices at a massive level, which may reach around 100 times more devices in the network as compared to the existing wireless networks. The devices may vary with respect to technology (IoTs, wireless sensors, machine communication etc.) and require different data rates, reliability and delay [2].

1.1.4 Cost and Energy Efficiency

5G must ensure a cost-effective network to address mobile operators concerns regarding revenue flattening. Specifically, the energy-efficiency (EE) must improve by up to 1000 times compared with existing cellular technologies [2, 8]. This reduced power consumption will automatically lead to improved battery life [9].

1.1.5 Multiple RATs

5G will co-exist with the current wireless technologies, i.e., global system for mobile communications (GSM), 3G, LTE, Wi-Fi etc. to get integrated in a seamless manner for a unified system [2].

1.1.6 Higher Bandwidth

5G will also enable connectivity between multiple devices for a long duration and with high bandwidths in a specific area [9].

5G can achieve its above stated targets through a collection of different technologies such as D2D, millimeter wave (mmWave), beamforming (BF), initial access (IA), massive MIMO (mMIMO), HetNets etc. as shown in Fig. 1.1. The details of these technologies are as following

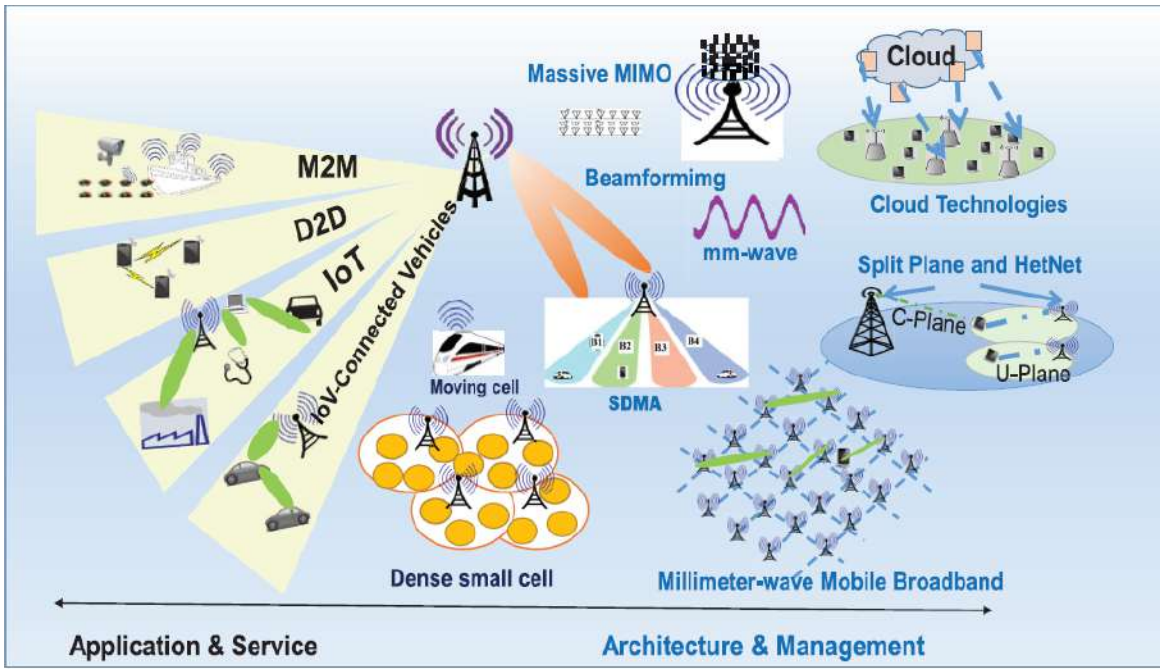

Figure 1.1: Schematic diagram of next generation 5G wireless networks [1].

1.2 Massive MIMO

A mMIMO system consists of a huge number of antennas deployed at both transmitter (TX) and receiver (RX). In particular, the expected number of antennas is 10 times larger than the total streams served to all cellular terminals. This in turn, leads to high BF gains and enhanced system capacity. The increased BF gains help reduce the inter-stream and intercell interference. Also, the capacity increase in a mMIMO system occurs by mere increase of the number of antennas and without increasing the transmit power and bandwidth. mMIMO achieves better signal-to-noise ratio (SNR) through zero pilot contamination and perfect channel state information (CSI). Although, mMIMO deployment can help satisfy

the increased capacity demand in the upcoming 5G systems, yet, the improved capacity leads to a dense cellular network, higher cost and complexity [10], [11].

mMIMO system can also enhance the EE of a system in two ways. First, the transmission power of users is reduced significantly when the number of antennas is increased and secondly, when the number of users increase, large throughput gain is achieved. This high gain is achieved through linear processing techniques of maximal ratio transmission and combining on the downlink and uplink side, respectively. The EE achieved through mMIMO is very high as compared to conventional systems [12].

1.3 Millimeter Wave

One of the key features of 5G technology is to support massively increasing mobile traffic along with high data rates and seamless connectivity. This target can be achieved by utilizing large chunks of spectrum in the very high frequency range such as mmWave spectrum [13]. The mmWave consists of a spectrum ranging from 30GHz-300GHz. Although, huge bandwidth can enable high capacity, high transmit power and flexibility for gigabit wireless communications, yet mmWave experience high propagation losses and expensive components [14]. High propagation loss makes mmWave unsuitable for long-distance communications. Recently, mmWave is utilized for point-to-point or high-resolution multimedia communications for outdoors and indoors, respectively. However, for future networks the support for non-line-of-sight (NLoS) cellular communication and long-range geographical coverage must exist. A key solution to make NLoS communication possible is through directional BF at TX and/or RX side [15, 16].

1.4 Heterogeneous Networks

HetNets is the collection of different cellular types, such as macro, pico, micro and femtocells. This combinational network is a key to enhance network coverage, capacity and EE. HeNets are being deployed in the existing 4G cellular networks. However, in the upcoming 5G architecture, not only multi-tier HetNets but relaying and multihop communications will be the essential part of the 5G network. The resource allocation algorithms that emphasize on efficient utilization of transmit power, bandwidth, antennas etc. while reducing inter-user and intercell interference and ensuring acceptable QoS will be the key features of the 5G

network. Also, the combination of mmWave and mMIMO systems will help resolve the critical challenges of 5G HetNets by seamless integration into the existing network as shown in Fig. 1.2 [2].

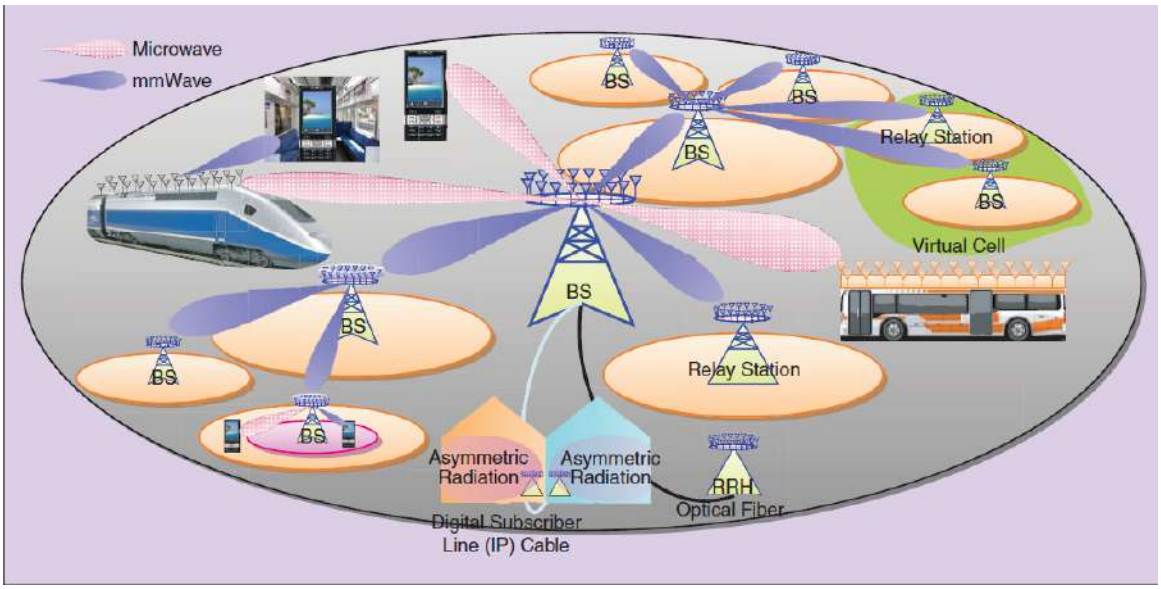

Figure 1.2: The potential 5G HetNet network architecture [2].

1.5 Device-to-Device Communication

When two devices communicate with each other in a licensed cellular bandwidth without or with limited base station (BS) involvement, it is known as a D2D communication. In the existing cellular generations, the concept of D2D does not exist mainly because D2D communication reduces the cost of local service provision. However, to satisfy the ever-increasing demand of context-aware applications and services, D2D is envisioned in the 5G network. D2D functionality can play a key role in mobile computing and resource sharing among users who are spatially close to each other. D2D communication can also help offload the network load by allowing direct transmission between nearby users. Moreover, it can prove a life savior at the time of natural calamities, for example, during hurricane or earthquakes, urgent communication network can be setup through D2D [17]. The network capacity can also be enhanced in a 5G network through mmWave usage in a D2D system for short-range communication. mmWave experience low multi-user interference and many mmWave D2D links can occur simultaneously, hence, improving the network capacity [18].

Although D2D communication has attracted a lot of attention for a 5G network, yet there

are certain challenges associated with D2D network as well. The details of which are as following [18]:

1.5.1 Synchronization

Synchronization among devices is important for discovering each other in correct time and frequency. However, it becomes a challenge when the devices belong to different BSs or when the users lie outside the coverage network.

1.5.2 Peer Discovery

Neighbor node discovery in less time and with reduced power consumption is important for successful communication. The cooperation among multiple BSs in a multi-tier network makes device discovery a challenging task.

1.5.3 Resource Allocation

Resource allocation is a critical step in establishing and maintaining links between D2D pairs. An optimal resource allocation scheme is required to achieve this target.

1.5.4 Interference Management

Devices may suffer from inband and outband interference. Interference can be mitigated if the devices operate at low power, but it reduces the QoS at the receiver. Therefore, new interference mitigating techniques are required.

1.5.5 Mobility

Mobile users pose a challenge for D2D communication and optimal performance is required by addressing the handover and interference challenges.

1.5.6 Pricing

Another critical issue is controlling the direct link between devices and charging the users. An efficient pricing model is required to address this problem.

1.5.7 Security

Security is a vital issue in D2D because data is not stored centrally. The devices are prone to common attacks such as internet protocol (IP) spoofing, eavesdropping, impersonification, malware attacks etc.

Hence, all the above stated challenges must be addressed in the 5G cellular network.

1.6 Initial Access

IA is a mechanism that allows both mobile users and BS to develop a physical link to initiate communication. In the existing network, IA is only deployed through omnidirectional channels, whereas, in 5G, IA will be utilized through directional BF [19]. The main factors that make IA of 4G-LTE unsuitable for 5G are as following [20]:

1.6.1 Discovery Range Mismatch

LTE acquire synchronization through omnidirectional transmission during cell search process. BF in LTE is utilized after the physical link is established. However, for 5G, it may be essential to utilize BF during cell search process, since omnidirectional communication may pose a mismatch during cell detection and data transmission/reception.

1.6.2 Multi-Connectivity

5G is a dense network with multiple devices detecting and communicating simultaneously, hence IA technique should be redesigned.

1.6.3 Blockage and Deafness

The existing 4G-LTE network increases the transmission power and waits for a random backoff time to cater the issues of deafness and blockages, whereas, 5G mmWave will not deal with these issues in a similar manner. Hence, new adaptive techniques are required.

1.6.4 Dynamics-Aware Access

The existing reference signal receiver power (RSRP) association scheme would not be supported by 5G network due to dense topology, Therefore, new access techniques are required to handle intermittency and directionality in a 5G system.

1.7 Thesis Motivation

The 5G technology promises high data rates, seamless connectivity, reduced latency, higher bandwidth, enhanced coverage, an energy efficient and cost efficient system [2]. To achieve these targets, multiple new technologies should co-exist. For example, the increasing wireless traffic cannot be accommodated on the existing microwave band only. Therefore, the high frequency mmWave spectrum must be utilized. Also, the bursting traffic load on existing BSs should be reduced by offloading traffic to a D2D network. Similarly, the IA mechanism of a 4G-LTE system is unsuitable for the 5G network because of issues related to multi-connectivity, discovery range mismatch, blockages, deafness, etc. [20]. Therefore, to overcome the challenges of a 5G network, a novel IA scheme for 5G networks is the need of hour. Our work was motivated from these technologies where we would like to propose some novel IA schemes in a mmWave-based D2D network for enhanced performance. Initially, the research work was focused on enhancing the capacity of a heterogenous network by deploying massive MIMO and small cells. However, the focus shifted from a HetNet to a single small cell to better understand the TX and RX connection by utilizing the mmWave band.

1.8 Thesis Contribution

We formulate our research problem in different stages and the contributions in each stage are as following.

1.8.1 Stage 1

We propose two novel BF techniques for a mmWave network. The BF techniques are implemented at the BS and a complete mathematical model is presented. In our algorithm, the BS forms two beams, either simultaneously or in a time division manner. The BS then

scans the entire region in a sequential manner and searches for the user through directional BF. If the received SNR is above a certain threshold value, only then the detection process is successful. Our proposed schemes aim at minimizing the user detection time and maximizing the detection probability.

1.8.2 Stage 2

We implement BF in a mmWave-based D2D network. We proposed BF at both the TX and RX sides. Two simultaneous or time-division based beam pairs are formed at RX and TX. However, the user detection process is not sequential. We proposed novel antenna scan sequences for beam sweeping at both TX and RX. The devices scan the region according to the antenna scan sequence. The search process continues until the devices have discovered each other or the maximize time bound is achieved. The proposed algorithms aim at reducing the discovery time and improving the detection probability.

1.8.3 Stage 3

BF is implemented by generating two beams simultaneously or in a time-division fashion. We investigate the optimal separation between a beam pair. The beam pair separation is a key factor in determining the efficient device detection mechanism. The optimal selection of beam pair separation results in reduced discovery delay and increased device detection probability.

1.9 Thesis Organization

The dissertation is organized as follows. Chapter 2 highlights the existing work in literature with respect to different 5G technologies. Chapter 3 gives a brief overview about the beamforming mechanism and different beamforming methods. Our proposed algorithms for a mmWave cellular network are discussed in chapter 4. Chapter 5 sheds light on the proposed algorithms and non-sequential BF techniques in a mmWave-based D2D network. The role of proposed beams with respect to optimal beam-pair separation is discussed in chapter 6. Finally, chapter 7 summarizes all our contributions and highlights the proposed future directions.

Chapter 2

Literature Review

In this chapter we discuss some important 5G technologies in the light of existing literature. The main discussion revolves around BF, IA, D2D, mmWave, Massive MIMO and Heterogeneous networks. The details of each technology are as following.

2.1 Millimeter Wave

mmWave is a high-frequency, low-range system that is studied extensively with respect to 5G communications. mmWave in terms of spectrum management is studied in [21]. A control-data separation architecture is proposed. The network consists of a control BS (CBS) and data BS (DBS) operating at sub-6 GHz single band and mmWave dual-band, respectively. An optimization problem is solved to improve the EE and spectral efficiency.

mmWave is also studied in combination with non-orthogonal multiple access (NOMA) technique [22]. An uplink NOMA system based on MIMO architecture is proposed. Multiple users are categorized as strong and weak users according to their CSI. Successive interference cancellation technique is used by the BS to overcome weak user interference [23]. It is shown that a mmWave-based NOMA system achieves better sum rate as compared to ultra-high frequency (UHF) and orthogonal multiple access networks.

2.2 Heterogeneous Networks

HetNets is a key technology to enhance data rate and coverage of a 5G network. Coverage and data rate are also increased in a HetNet through interference mitigation techniques [24].

A reverse frequency allocation (RFA) mechanism is utilized to reduce the cross-tier interference in a HetNet. The close-form expressions for coverage and data rate are derived through stochastic geometry and it is shown that RFA help achieve better outage capacity gains and performance gains.

HetNets are also investigated in terms of resource optimization. The existing resource allocation mechanism are insufficient in capturing the complete picture of a physical environment due to their reliance on single-slope loss model. Therefore, a multi-slope path loss model is investigated in a HetNet in [25], [26]. A HetNet with pico and macro cell is analyzed and a user association algorithm for dual slope path loss model is proposed. The dual slope outperforms single slope path loss model by offloading traffic from macro to pico cell [26]. A joint power allocation, user association and subcarrier allocation framework is proposed. The algorithm is formulated as a maximization problem of weighted sum rate while maintaining the QoS criteria. The proposed algorithm outperforms the single-slope path loss models and also improves system load by offloading users from macro BS to small cells [25].

A HetNet with macro and femto cells is investigated in [27]. A RFA scheme is proposed to provide intercell orthogonality which results in improved data rates. The impact of adjacent cell interference is also studied and a hybrid RFA scheme is developed. The modified RFA outperforms the conventional RFA in terms of sum rate capacity and user fairness. HetNet is also studied in the context of flexible duplexing in [28]. The system performance can be improved through switching between half-duplex (HD) and full-duplex (FD). A duplex scheme based on distance is proposed to study the impact of dual slope path loss model. Based on maximum received power, a user connects with the BS. Afterwards, the mode of operation i.e., FD or HD is chosen based on threshold distance. It is shown that distance in path loss model and threshold distance in FD directly impacts the system sum rate.

A HetNet with femto and macro cell is discussed in [29] based on a hierarchical game theory approach. In the first step, a non-cooperative game is played by femto access points (FAPs) to maximize rate by choosing between open or close access policy. In the second step, macro cell users decide connectivity between either FAPs or macrocell BS such that rate and network performance is maximized. The network-assisted user-centric is the best method to improve the HetNet performance. The use of femto cells in a HetNet to enhance system capacity is studied in [30]. A RFA scheme is proposed by dividing the service region into multiple parts and assigning frequencies to avoid interference in the network.

It is concluded that for a reasonable value of signal-to-interference-plus-noise-ratio (SINR), multiple regions help reduce the outage probability. HetNets with femto cells and RFA scheme is also proposed in [31]. A closed-form expression is derived for coverage probability under different RFA schemes. It is shown that the use of multiple regions enhance the coverage probability.

HetNets are also studied in combination with mmWave. The details are as following.

2.2.1 mmWave in a HetNet

A three-tier HetNet consisting of macro cell with sub-6GHz and small cells with sub-6 GHz and mmWave bands is studied in [32], [33]. A stochastic geometry model is utilized to analyze the spectral efficieny, coverage, EE and rate of a HetNet. It was shown that mmWave small cells increases the network coverage and spectral efficiency. Resource management in mmWave is also investigated in [34]. A framework is proposed to improve the QoS of a mmWave-based HetNet. The results are formulated in the light of computationally intelligent (CI) techniques. The simultaneous operation of both micro and mmWave links is a challenging phenomenon in terms of resource allocation. Hence, efficient CI techniques such as optimization routines and game theory are proposed to improve resource management in mmWave HetNet.

A multi-tier HetNet with unmanned aerial vehicles (UAVs) is proposed in [35]. The mmWave and sub-6GHz aerial BSs are utilized to maintain the data rate and network coverage requirements. Multiple network configurations are implemented to study the impact of bias factor and number of users. It is concluded that the combination of mmWave and sub-6GHz improves performance in terms of network capacity and SNR coverage, respectively. A game theoretic model of two layers for hybrid HetNet is proposed in [36] to maximize EE. In the outer layer, the FAPs can maximize the data rate through the selection of mmWave or sub-6GHz frequency band. The inner layer enables user association efficiently by maximizing transmission power and minimizing data rate. It is concluded that the inclusion of mmWave help improve EE and sum-rate as compared to single sub-6GHz network.

To overcome mmWave path loss and penetration losses, a HetNet is proposed in [37] that brings the BS close to the end user. The downlink-uplink effect is studied in detail and it is concluded that the proposed system design improves the data rate and coverage.

2.3 Massive MIMO

Currently, mMIMO is an attractive sub-6GHz technology in a 5G network that can provide good communication serves to high mobility users. mMIMO is studied in multiple contexts. A lower throughput bound for a mMIMO system is derived in [38]. A hexagonal geometry with uniform user distribution is evaluated. The lower bound is limited by pilot contamination, intra and inter cell interference. It is shown that the throughput performance is highly affected by the reuse factor and a minimum reuse factor is quantified.

An ergodic rate analysis is presented for a mMIMO system in [39]. Multiple antennas are deployed at the BS. The pilot contamination process occurs in the uplink, while the CSI is acquired by the BS through minimum mean squared error (MMSE) estimation. It is shown that shadowing is not affected by increasing the antennas under different precoding methods. The impact of Rayleigh fading and lognormal shadowing in mMIMO is investigated in [40]. SNR is analyzed utilizing the maximum-ratio-combining (MRC) RX. Furthermore, utilizing the SNR analysis, the SINR in a multi-user environment is determined for MRC, zero forcing (ZF) and MMSE receivers. The effect of outage is also studied and it is shown that large-scale fading is not averaged out by an increase in number of antennas at the BS.

A closed form expression for outage proabability in a mMIMO system is analyzed in [41]. MRC is utilized by the BS under path loss and Rayleigh fading environment. It is shown that SINR is approximated through lognormal random variable and increasing the antennas did not average out the shadowing effect. The recent concept of virtual MIMO (vMIMO) is investigated in [42]. Single antenna nodes cooperate to form clusters and enable transmission in vMIMO technology. A MIMO-based distributed antenna systems (DAS) and vMIMO-based DAS is discussed to improves spectral efficiency and successful end-to-end communication.

mMIMO is also investigated along with mmWave and HetNet. The details are as following.

2.3.1 Massive MIMO with mmWave

mmWave mMIMO in terms of encoding and detection is studied in [43]. A lower bound on system throughput is derived. However, the lower bound is limited by pilot contamination intracell and intercell interference. It is shown that the reuse factor is crucial in determining the least achievable throughput. A mMIMO system in combination with mmWave and

sub-6GHz small cells is studied in terms of security in [44]. A stochastic geometry model is proposed to investigate the secrecy EE (SEE), secrecy outage probability and secrecy spectrum efficiency (SSE). The impact of directional BF, cell density, large antenna arrays and transmit power is also investigated. The results show a tradeoff between improved secrecy and coverage.

A mMIMO-enabled multi-tier HetNet with sub-6GHz bands and mmWave in terms of secrecy outage is also analyzed in [45]. The network is overlaid with numerous eavesdroppers. A poisson point process (PPP) is used to analyze location of both desired user and eavesdropper. The results show that the mmWave-based HetNet significantly reduces the secrecy outage probability and connection outage. An UHF and mmWave-based mMIMO system is studied in [46]. A pilot reuse algorithm is proposed to obtain a lower bound on throughput. It is concluded that the performance of UHF system is highly dependent on reuse factor, whereas, mmWave is almost independent.

2.3.2 Massive MIMO and Heterogeneous Networks

The co-existance of a mMIMO system in a Hetnet fulfills the data rate requirement of a 5G network. mMIMO helps increase the network capacity and a Hetnet ensures seamless conenctivity. Our previous work in [47] implements this architecture to enhance network capacity. A two-tier network is implemented with mMIMO deployed at the macro-tier and single antennas for the femto cell. A novel channel allocation scheme is proposed to maximize the network throughput and EE. The results show that there exits an optimal split between number of channels allocated to the macro and femto cells. Also, an optimal trnasmit power exists that enhances the network EE. Under different scenarios, mMIMO plays a crucial role in enhancing the sum rate capacity as compared to single antenna femtocells.

mMIMO and small cells can also improve EE of a network through soft-cell coordination approach, where the mobile user is served by non-coherent BF from multipe transmitters [48]. The users are allocated optimally to a transmitter by solving a complex optimization problem. The results show a great improvement in the total power consumption of the network through the combination of mMIMO and small cells. mMIMO and small cells are also used to suppress interference through directional transmission of multiple antennas at the macrocell and creating gaps for small cell transmission in other directions [49]. Also, the inter-tier interference can be coordinated by either intelligently switching OFF the small cells or

offloading macrocell traffic to small cells, hence, increasing the throughput significantly.

2.4 D2D Communication

To enhance data rate in the context of live video and data sharing in a 5G network, D2D system plays a vital role [50]. The network capacity is improved by offloading traffic from BS to D2D entities. However, D2D communication poses several challenges such as network discovery, interference management, network security and proximity services. Some emerging techniques such as mmWave, V2V communications, simultaneous wireless information and power (SWIPT), energy harvesting etc. could help achieve upcoming targets in the context of 5G D2D networks. D2D is also helpful in 5G network as it helps offload traffic from BS and provide direct peer-to-peer links [51]. Direct communication will also pave way for easy health monitoring, public safety networks, disaster area networks, multimedia services etc.

D2D has also been studied in the context of energy harvesting. A resource allocation algorithm for D2D system with energy harvesting is proposed in [52]. The algorithm investigates the interference and cellular links of a D2D system which results in optimal power allocation and maximized sum rate. The algorithm outperforms the exiting algorithms with respect to sum rate. D2D cooperated HetNet is analyzed in [53]. An amplify-and-forward scheme is used to engage the idle femtocell users and enhance coverage to macrocell users. Closed form expressions for outage probability and SNR are derived to show performance improvement through femtocell users cooperation.

D2D has also been investigated in the context of network coding in [54]. A comparison is presented between relay-aided D2D and relay-aided network-coded D2D network. D2D pairs are prioritized during transmission based on the channel characteristics. The success probability for both schemes is quantified based on SNR margin regions. A cooperative multi-hop D2D network is studied in [55]. Relay nodes are deployed randomly in the network and expressions for end-to-end transmission and received power in a path loss and Rayleigh fading environment are obtained. An improved end-to-end communication is achieved through SNR based relay selection. D2D based on SWIPT is investigated in [56]. A PPP model is utilized for node distribution and intra-region signaling is performed by the central node. Expressions for end-to-end transmission and ergodic rates are derived and it is shown that

end-to-end transmission is successful for large distance between D2D nodes.

D2D is also studied in combination with mmWave system. The details are as following.

2.4.1 D2D in mmWave

D2D and mmWave are two key technologies that complement each other. mmWave provides high throughput and reduced interference through highly directional communication, whereas, D2D facilitates short-range communication [57]. Recently, D2D communications for mmWave systems have grabbed the attention of both academia and industry to overcome the limited power and blockage effects of a mmWave system. D2D systems can help improve coverage and connectivity through a relay network. A two-hop relay system for mmWave communication is studied in [58]. A threshold policy is designed to get a tradeoff between throughput gain and throughput loss due to the search for a better delay and higher relaying overhead, respectively. Similarly, a two-hop D2D mmWave network to overcome blockages is also discussed in [59]. Stochastic geometry is used to derive the coverage probability and spectral efficiency. A comparative study is conducted between microwave and mmWave D2D system and it is concluded that microwave D2D achieves better coverage as NLoS channel can be established. Whereas, the coverage for mmWave D2D is better with high number of interferers as NLOS interferers gets eliminated through blockages. Also, mmWave D2D uses less uplink resources as compared to microwave D2D relays.

D2D is also analyzed in [60] to discover the unblocked line-of-sight (LoS) links in a mmWave system. The communication occurs by either finding the unblocked LoS path or switching to microwave band. In addition, beam alignment is also investigated for directional communication and it is concluded that the combination of mmWave and microwave significantly improves the communication as compared to single band communication. Another hybrid scheme to overcome mmWave blockage effect through switching between microwave band and mmWave band in a D2D network is studied in [61]. A stochastic geometry model is used to analyze the coverage probability and area spectral efficiency (ASE) with the conclusion that standalone bands, i.e., mmWave or microwave perform worst as compared to hybrid mode.

The performance of D2D mmWave system is analyzed through Poisson bipolar model in [62]. A meta distribution for SINR and data rate is derived to study the number of users that achieve the target reliability. It is concluded that the meta distribution through beta approx-

imation doesn't work well with highly directional antennas or small node density. Hence, a modified algorithm is proposed to study the mean delay and outage capacity. A clustered D2D mmWave system is investigated through Poisson cluster process in [63]. Multiple antennas are deployed at the TX and RX. An analytical expression is derived for ASE and coverage probability and it is concluded that coverage probability is influenced by intra-cluster interference and an optimal number of simultaneously active TXs maximize the ASE.

A multi-tier HetNet with mmWave, microwave and D2D users is investigated in [64], [65]. Downlink dynamic resource sharing is studied to maximize the EE of users served by mmWave or microwave small cells. The QoS of D2D users is also maintained. An EE optimization problem is formulated to maximize the network EE. The optimization problem is studied in terms of two subproblems related to resource allocation management and EE maximization. The results highlight the tradeoffs between outage probability, EE and sum rate for different D2D pairs densities and QoS levels.

D2D network is also utilized for directional communication using oblivious directional neighbor discovery (ODND), Hunting-based Directional Neighbor Discovery (HDND) and Polya's Necklaces algorithms. The details of each of them are as following:

2.4.2 ODND

Neighbor discovery through directional communication in a decentralized network is a challenging task [66]. A node discovery algorithm is devised with heterogeneous antenna configuration. The discovery process begins when both RX and TX point their beams in different search sectors. The BF direction is calculated through an antenna scan sequence and the search process ends only when the beams of each device get aligned. An upper-bound has also been derived to prove that the nodes always discovery each other within the minimal bounded time. It is shown that the proposed algorithm can achieve a tradeoff between average and worst-case performance.

2.4.3 HDND

Another directional neighbor discovery algorithm for mmWave system is discussed in [67]. The device discovery process occurs through clockwise or anti-clockwise rotation of TX and

RX with a given angular velocity. Device discovery is made successful by driving certain conditions regarding the distribution of the overlap angle and beacon-ACK handshake between the beams of a D2D pair. A sequence design is adopted for a decentralized network to coordinate transmission and reception between nodes. The node discovery is ensured within a bounded worst-case discovery delay through the proposed algorithm.

2.4.4 Polya's Necklaces

Neighbor discovery in a decentralized network with heterogeneous antenna configuration is studied in [68] through Polya's Necklaces algorithm. The worst-case discovery delay is minimized through Polya's enumeration theorem and Fredricksen, Kessler and Maiorana (FKM) algorithm. It is shown that the proposed algorithm reduces the discovery delay through short and efficient antenna scan sequences.

2.5 Beamforming

It is a data transmission technique that relies on different antenna beams for communication. BF is discussed in multiple perspectives. An angle-based BF algorithm is proposed for mMIMO mmWave system in [69]. The user selection is pre-defined to reduce intra-cell interference. The scheme help reduce feedback bits and feedback frequency. Also, the overhead is far less as compared with CSI-based BF scheme. A UAV based BF in mmWave is studied in [70]. UAV is the BS that covers ground mobile users. A codebook for beam training is proposed for both sufficient and insufficient beam training scenarios. A prediction model is used for efficient beam tracking along with user mobility. The results show an increased downlink capacity and reduced mean angular error.

A maximum likelihood angle-of-departure (AoD) based hybrid BF in mmWave system is investigated in [71]. A discrete Fourier transform (DFT) BF is proposed for angle estimation. The Butler matrix is utilized to implement DFT matrix in analog domain. A Cramer-Rao lower bound is derived for performance analysis. Machine learning based beam tracking in mmWave is investigated in [72]. A prediction model is proposed where past CSI is used for predicting future CSI through machine learning. The number of channel estimates are reduced by this method, hence, reduced pilot overhead.

An analog beam tracking technique is proposed in [73] for accurate and fast tracking of

mobile users. A recursive phenomenon is used for monitoring both the static and dynamic scenarios. The proposed algorithm achieves convergence towards the minimum Cramer-Rao lower bound. Also, the algorithm can even track mobile devices accurately at very low SNR values.

A cell discovery mechanism that reduces the overhead in a mmWave system is proposed in [74]. A framework based on out-of-bound information is analyzed and relationship is established between mmWave parameters and BS detection performance. The results highlight the averaged undiscovered probability and beam pattern in the desired region.

A transmitter beam selection algorithm is proposed in [75]. The scheme relies on in-band position-aiding for improved beam alignment. A joint positioning and communication scenario along with scattering and LoS is analyzed. The results show reduced latency as compared to standard protocol.

2.6 Initial Access in mmWave

Recently, the research focus has shifted from microwave band to mmWave spectrum to satisfy the demands of massively increasing mobile traffic. mmWave is an ideal candidate due to high bandwidth and high frequencies. However, mmWave suffer from high propagation loss. To overcome this environmental loss, directional BF plays a vital role but at the cost of complicated IA process. IA becomes difficult because the BS and the mobile user search for each other over an angular directional region until a suitable communication path can be established between them [76]. To address this problem, several IA techniques have been proposed in literature. The details are as following:

2.6.1 Directional Cell Discovery

In [76], the BS transmits directional synchronous signals periodically in time-varying random directions. The mobile user scans the region for the received signal and obtains the direction and timing of arrivals from the BS. Generalized Likelihood Ratio Test (GLRT) is utilized for signal detectors. The BS scans the desired angular region for user detection through digital and analog BF. It is concluded that although digital BF utilizes very low quantization to recompense for power requirements, yet it outperforms analog BF. The BS also utilizes both omnidirectional and directional transmission to better understand the user

discovery process. It is observed that the omnidirectional transmission from BS is superior than random directional scanning in both analog and digital domains.

2.6.2 Exhaustive and Iterative Search

In [19], the exhaustive search method for IA is utilized where sequential BF is applied through brute-force. The BF directions are already known at the BS through a predefined codebook. The BS sends a signal in a sequential manner to scan the entire angular region for the mobile user. The mobile user organizes its antenna array to receive directional communication from the BS. A narrow beam is transmitted from the BS during different time slots. Upon reception of a signal from BS, the RX calculates the SNR and if the SNR is above a predefined threshold value, a feedback is sent to the BS. The BS determines the best beam for communication in the direction where the received SNR was highest after scanning the whole angular region.

Another IA scheme, known as iterative search, is discussed in [19]. Unlike exhaustive search, the iterative search is carried out in two stages. The scanning direction is determined through the predefined codebook. During the first phase, the BS utilizes wide beams to search different sectors in a sequential manner. After scanning the whole angular region, the BS determines the best sector where the received SNR was the highest. The RX also determines the best direction to reach the TX. In the second stage, the BS scans the best selected sector by utilizing more antenna elements and narrow beams. The total number of search sectors in both stages remain the same.

The performance for both exhaustive and iterative search methods is evaluated through probability of miss detection (PMD) and discovery delay (DD). PMD is the probability that the RX cannot be detected by the TX, perceiving the SNR is below the predefined threshold. Whereas, DD is total time taken by the BS to detect a mobile user. It is shown that there is a trade-off between DD and PMD. The iterative schemes utilize less time slots to detect a user through wide beams as compared to exhaustive method. Hence, the DD is low. Whereas, the PMD is high for iterative method due to wide beams and low BF gain. The exhaustive method is preferred for applications where coverage is required for end users and in urban, densely populated regions.

2.6.3 Context Information-based Search

The analog BF technique of context-information (CI) based search is proposed in [20]. The search process takes place in three stages. In the first stage, the BS uses omnidirectional antennas to spread the global positioning system (GPS) coordinates of mmWave devices. The mobile users detect their corresponding GPS coordinates and orientation in the second stage. Finally, in the third stage, the users select the best BS that is geographically close to the user for communication. Meanwhile, each BS utilizes the exhaustive search method to determine the best TX-RX direction. It is shown that the PMD is higher than exhaustive method when cell edge users are considered. However, the PMD and DD can be reduced if the CI-based algorithm is modified by refining the direct link and utilizing adjacent directions for beam steering.

2.6.4 Hybrid Search

A hybrid cell search algorithm is proposed in [77] that is the combination of both exhaustive and iterative search methods. The search process takes place in multiple stages until an upper bound on the number of stages is reached. The user discovery is based on two SNR thresholds, i.e., a loose threshold and a tight threshold. The BS utilizes the loose threshold value to reduce the search area in each stage, whereas, the tight threshold is utilized for link establishment. The BS starts the search process in an iterative way through wide beams during the first stage. The loose threshold is calculated for each search sector and if the received SNR is higher than the loose threshold value in any search sector, then that sector is selected for further scanning. The BS keeps scanning and reducing the search area in each stage until the upper bound on stages is reached. Once the upper bound is reached, then the BS begins the scanning process through exhaustive method and the received SNR is determined according to the tight SNR threshold. The performance analysis showed that the PMD is lower for hybrid method as compared to iterative search method. Also, the DD is lower for hybrid scheme than exhaustive method. The hybrid scheme is a trade-off between exhaustive and iterative search algorithms.

2.6.5 Context-Aware Sequential Search

IA access based on machine learning is investigated in [78]. A context-aware sequential algorithm is proposed. The basis of artificial intelligence is utilized for beamforming and connectivity between BS and users. GPS coordination is implemented to detect location of both mobile and static users. Furthermore, C-plane and U-plane systems are used for transferring signal information and data transmission, respectively. It is shown that PMD and DD are reduced with the proposed scheme as compared to the existing exhaustive and iterative methods.

2.6.6 Auxiliary Beam Pair

IA through auxiliary beam pair (ABP) in a narrow band MIMO system with hybrid precoding is discussed in [79]. A pair of beams is created at the TX side through uniform linear array (ULA), to scan the angular region. On the RX side, omnidirectional antenna is used to form a beam. The TX sends beam pairs in different angular directions and the RX calculates a ratio metric with respect to each transmitted pair. All the ratio metrices are fed back to the TX. The TX selects the best ratio metric and directs its beam in the desired direction for data transmission. The performance analysis showed that ABP can improve the spectral efficiency while reducing the implementation complexity.

ABP in a full-dimension MIMO system is also discussed in [80]. ULA and uniform planar array (UPA) are employed at RX and TX, respectively. The RX calculates a set of ratio metric through amplitude comparison of TX and RX beam pairs. The ratio metric help characterize the AoD and angle-of-arrival (AoA). It is concluded that the proposed BF scheme achieves good AoA and AoD estimates under various channel conditions and SNR levels. AoD and AoA in a closed-loop large-scale mmWave MIMO system through ABP is analyzed in [81]. The high-resolution and low overhead AoA and AoD estimates are obtained through amplitude comparison of ABPs. The RX sends back the best ratio metric or estimated AoD to TX for data communication. To reduce the IA delay, the proposed algorithm is also implemented into control channel design.

ABP is also utilized for a cross-polarized MIMO system with wideband in [82]. AoA and AoD is estimated through a multi-layer reference signal and a differential feedback mechanism is proposed for an improved angle estimation and data rate under various antenna

configurations, channel conditions and SNR levels. ABP is utilized for tracking mobile user in a wideband mmWave system [83]. Directional beams are utilized for angle variation in different directions. A differential and direct feedback mechanism is used for angle tracking in frequency-division duplex system and it is concluded that through differential feedback there is a considerable reduction in the feedback overhead. Also, an array calibration algorithm is proposed to study the impact of array calibration errors and it is shown that the proposed algorithm work well even with some calibration errors.

Custom designed ABPs are also used to analyze the 2D super-resolution AoA and AoD in a wideband mmWave MIMO system [84]. The antenna array utilizes the dual-polarized antennas. A novel multi-layer system based on signal structure along with differential feedback mechanism is proposed. The angle pairs estimated are fed back to the BS and good performance is achieved under variable channel conditions, SNR and antenna elements.

A modified ABP (mABP) is investigated in [85] to study the impact of angle estimation error in the presence of noise. In the mABP approach, each beam scans a distinct direction. It is shown that mABP achieves lower root mean square (RMS) angle estimation error as compared to ABP scheme. Similarly, an ABP pair is probed in time division manner to study the effect of wrong beam selection in [86]. The results show that although the SNR is high, yet 50% of the time, a wrong beam is selected. Also, a small reduction in beam spacing helps reduce the RMS error in the desired direction by about 55%

Chapter 3

Beamforming

In this chapter, the basic design principle of BF with respect to monopulse radars and mmWave systems is discussed in detail. We also shed some light on the analog, digital and hybrid BF techniques in mmWave systems. The details are as follows.

3.0.1 Beamforming in Radars

The electromagnetic waves radiate in all directions when broadcasted through a single antenna. However, to focus a signal in a particular direction, mutiple antennas should broadcast the same signal at slightly different time slots. This results in overlapping waves that produce both strong and weak signals. The strong waves are due to constructive interference and weak signal results from destructive interference. If executed properly, this whole BF process can focus the signal in a particualr direction [87]. BF is a signal processing technique for directional transmission or reception. The radar transmitter and receiver also utilize BF for directional communication. The beam can be pointed in azimuth or elevation direction, i.e., either side to side or up and down, respectively. Early radar systems utilized the parabolic antennas to focus energy in the direction of antenna [88]. The modern radar systems use monopulse tracking system to achieve refined angular measurements. A monopulse system usually consists of two identical antennas to get an angle estimate. The output signals are summed (Σ) up and subtracted (Δ) to determine a ratio metric. The angle information (θ) is obtained through this ratio metric. Mathematically [89],

$$\gamma = \frac{\Delta(\theta)}{\Sigma(\theta)}, \tag{3.0.1}$$

There are two types of monopulse systems, i.e., amplitude comparison monopulse and phase

comparison monopulse. The details are as follows [90]

3.0.2 Amplitude Comparison Monopulse

In this method, two overlapping radiation patterns are formed at an angle (θ_o) from the boresight angle. Fig. 3.1. shows the radiation pattern and the target location (black

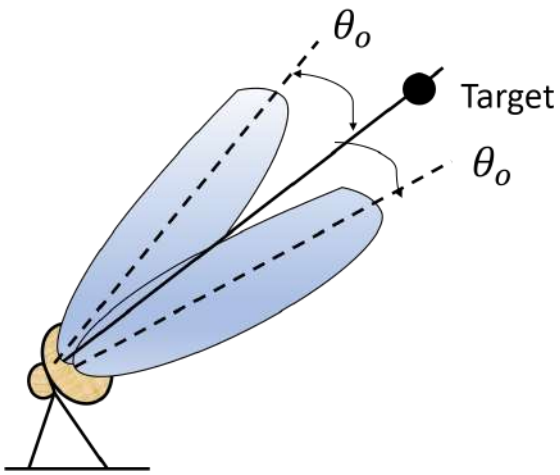

Figure 3.1: Amplitude comparison monopulse system

circle). Since, the target is located at the center or bore sight angle, both antennas receive an equal amount of energy. However, if the target is located at an angle away from boresight, then the antennas receive a different amount of energy. This difference in energy is used to determine an error signal.

The radar compares the amplitude and phase of beams continuously to determine the target location. The phase of all signals at both TX and RX is constant. To determine the accurate angle, sum and difference beams are used to generate a ratio metric as shown in Figs 3.2 and 3.3.

It is clear that a small angular separation between two beams results in better sum beams as compared to large angular separation. Moreover, the slope of difference beams is also steeper for small angular separation [91].

3.0.3 Phase Comparison Monopulse

It is based on different phases for the antenna beams as shown in Fig 3.4. The boresight angle for both beams is different and is parallel to each other. The target information is

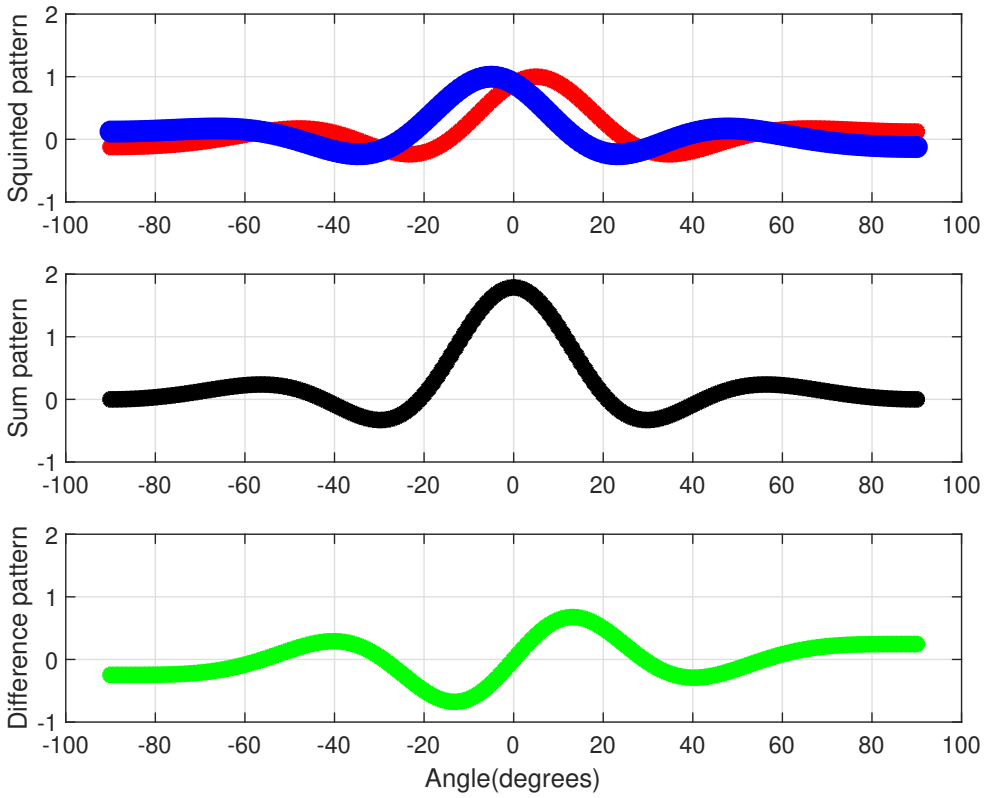

Figure 3.2: Amplitude comparison with angle deviation 1

calculated by phase difference comparison of the received signal. The AoA can be calculated through geometrical relation as shown in Fig 3.5 [92]. The AoA (Θ_o) is calculated as [92].

$$\Theta_o = arcsin\frac{\lambda\Delta\Upsilon}{2\pi\Delta x}, \tag{3.0.2}$$

where Δx is the distance between two antennas, $\Upsilon = \angle x_1 - \angle x_2$ is the phase difference of incoming signals at the two antennas and λ is the wavelength.

3.1 Beamforming in mmWave systems

Recently BF is studied in mmWave systems as well. BF plays a vital role in mmWave systems as the signals carried by mmWave are subject to blockage and reduced signal strength over long distances. Hence, BF help modify the signal shape and turns them in directional beams [93]. Also, the high frequencies and small wavelengths of mmWave makes it possible to pack large number of antennas elements into a small space to enable directional beams with high antenna gains [15].Usually the beamwidth of a single antenna element is very wide

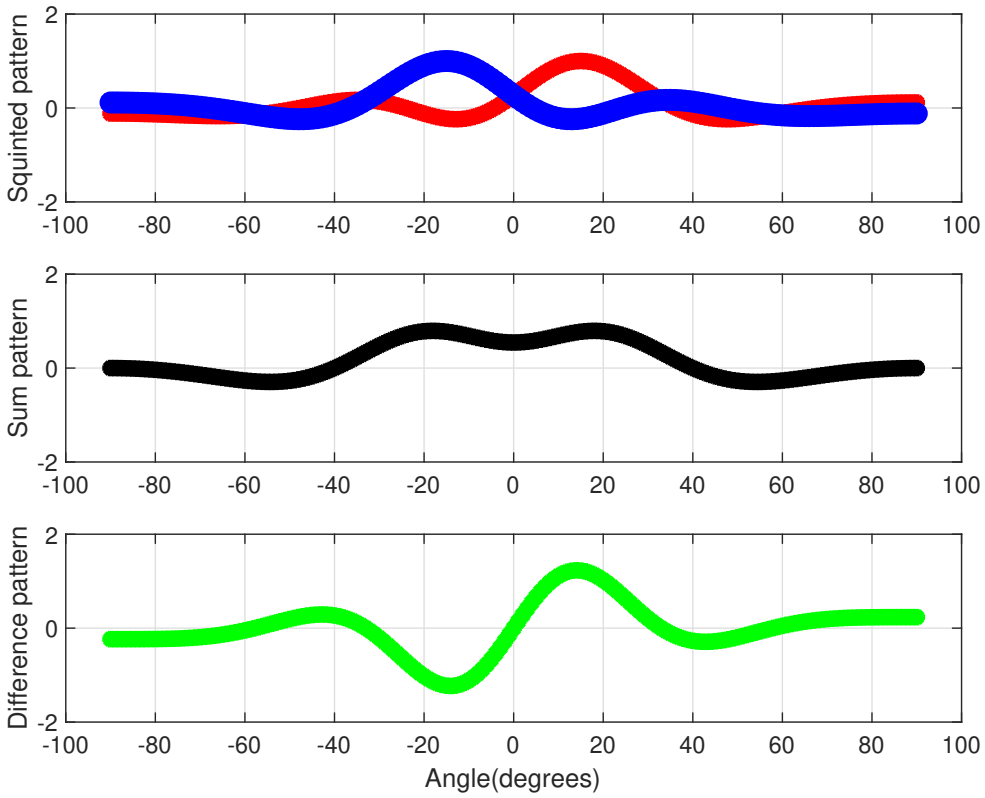

Figure 3.3: Amplitude comparison with angle deviation 2

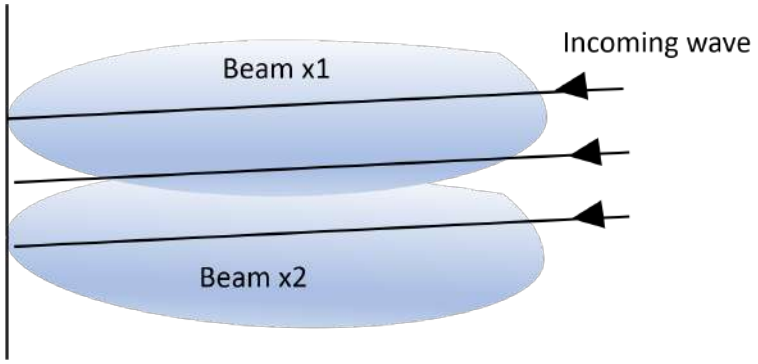

Figure 3.4: Phase comparison monopulse system

and the BF gain is very low. For long distance communication, highly directional antennas are required with a considerable gain. Such antennas can be constructed by increasing the radiating aperture (size much larger than wavelength (λ)). This approach is practically not feasible due to extremely large antenna size and appearance of many side lobes. Therefore, to make this happen in practice, the concept of antenna array emerged [94]. The most common antenna array techniques are ULA and UPA. The details are as follows

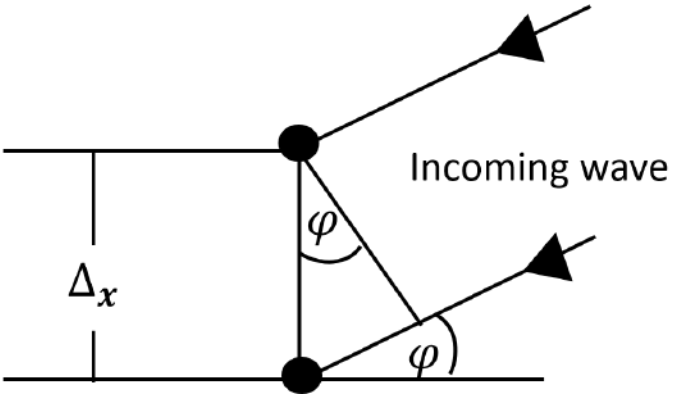

Figure 3.5: Phase comparison monopulse algorithm

3.1.1 Uniform Linear Array

ULA consists of a set of sensor elements that are spaced equally along a straight line. A dipole antenna is the most well-known sensor that transmits and receives electromagnetic waves. ULA is used to improve the SNR and directional gain [95]. The basic design principle of ULA is illustrated in Fig. 3.6. The antenna elements are aligned along a straight line

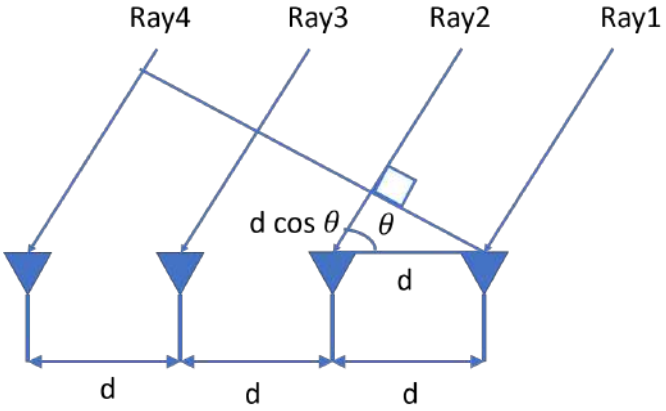

Figure 3.6: Uniform linear array with four antenna elements

with a separation of a distance d between them. The electromagnetic rays arrive as planar waves at the antenna array, i.e., each ray travels an excess distance as compared to the other ray. For example, the second ray arrives at an excess distance of $dcos(\theta)$ as compared to first ray. Similarly, the third ray arrives after travelling an excess distance of $2dcos(\theta)$ and so on. This excess distance is important in determining the constructive or destructive combinations of the signals [95]. Mathematically,

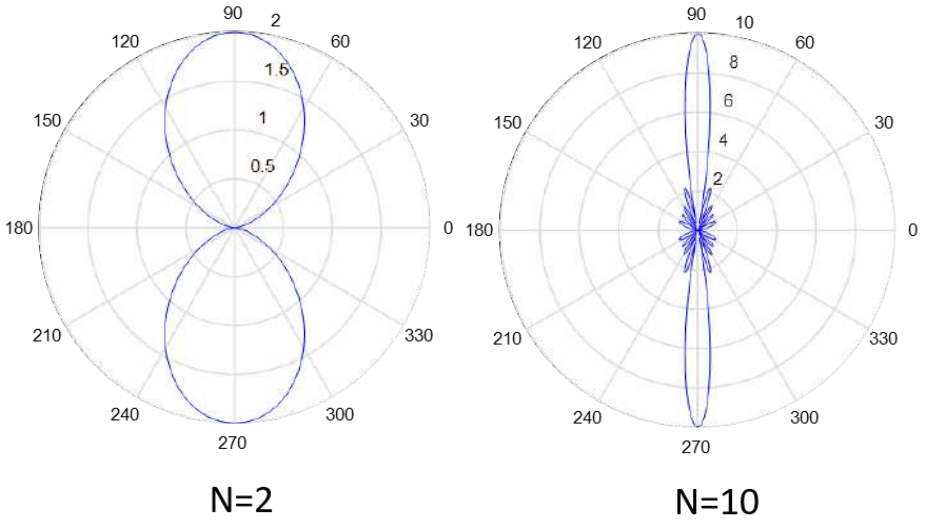

Figure 3.7: Beamforming with $N = 2$ and $N = 10$ antenna elements

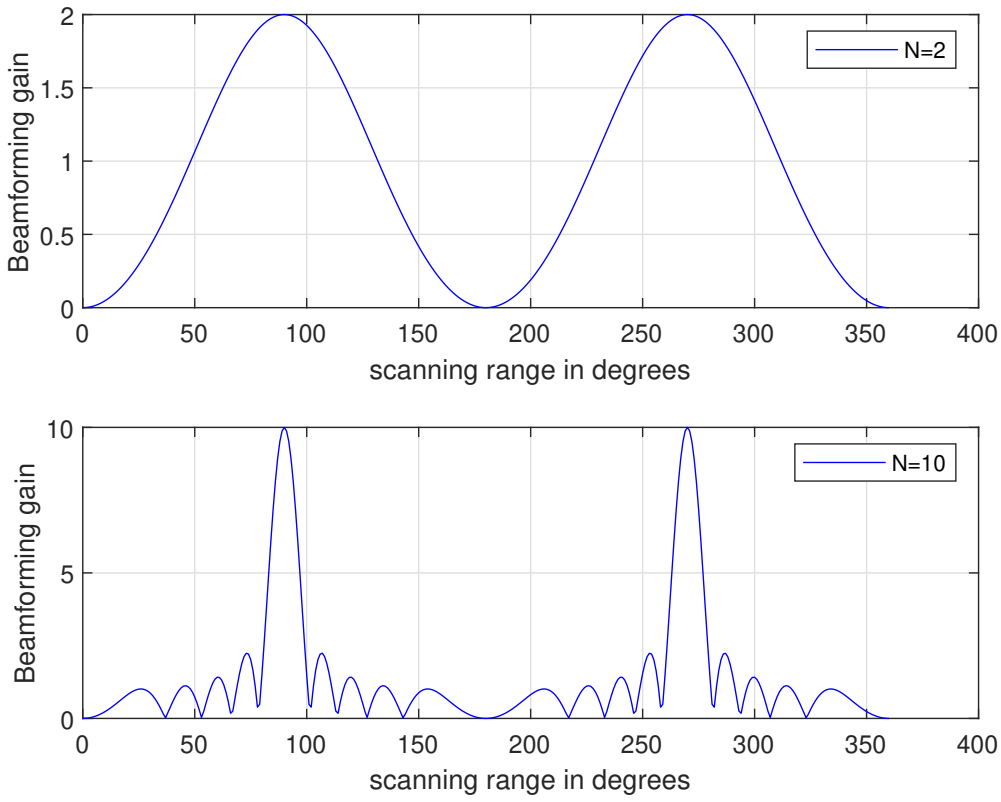

Figure 3.8: Beamforming gain of $N = 2$ and $N = 10$ antenna elements

$$\begin{aligned} r &= \sum_{n=1}^{N} e^{-j\omega t}, \\ &= e^{-j\phi} \sum_{n=1}^{N} e^{(-j2\pi d(n-1)\cos(\theta))/\lambda}, \end{aligned} \tag{3.1.1}$$

where N, λ, θ, and ϕ are the total antenna elements, wavelength, AoA and steering direction, respectively. The number of antenna elements play a vital role in determining the BF gain as shown in Figs. 3.7 and 3.8.

It is evident that as the number of antennas increase, so does the BF gain. Hence, large antenna elements help form narrow beams that travel a longer distance with high BF gain as compared to wide beams.

For directional scanning, the weights ($e^{-j\phi}$) can be adjusted in (3.1.1) and the beam can be pointed in desired direction as shown in Fig. 3.9.

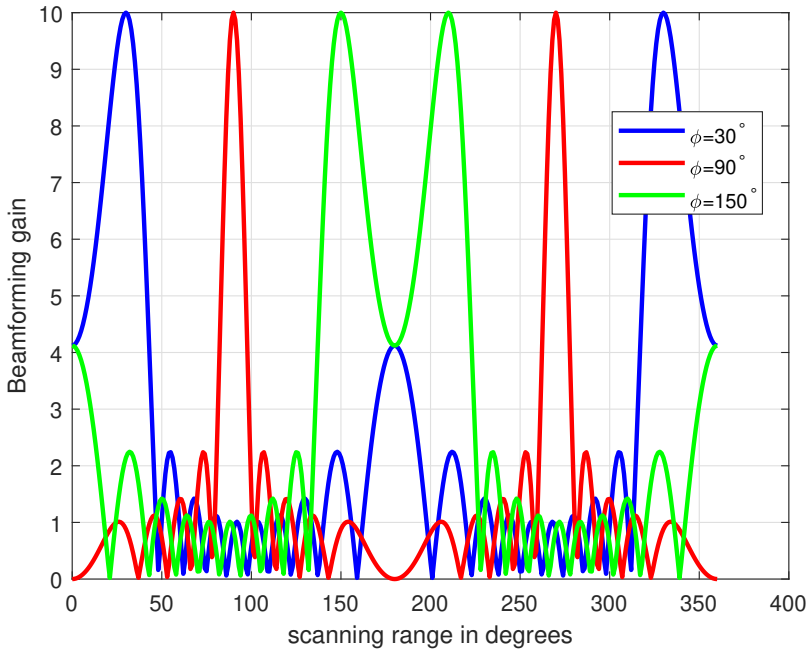

Figure 3.9: Random beam directions

3.1.2 Uniform planar array

UPA is shown is Fig 3.10. The antenna elements are arranged in xy plane uniformly along a rectangular grid. The spacing between elements in the x and y plane is represented as d_x and d_y, respectively. The radiation pattern is given as [96]

$$r = I_{mn} \sum_{m=0}^{M-1} e^{jk(nd_x sin(\theta)cos(\phi))} \sum_{n=0}^{N-1} e^{jk(nd_y sin(\theta)sin(\phi))} \tag{3.1.2}$$

where I_{mn} is the excitation amplitude.

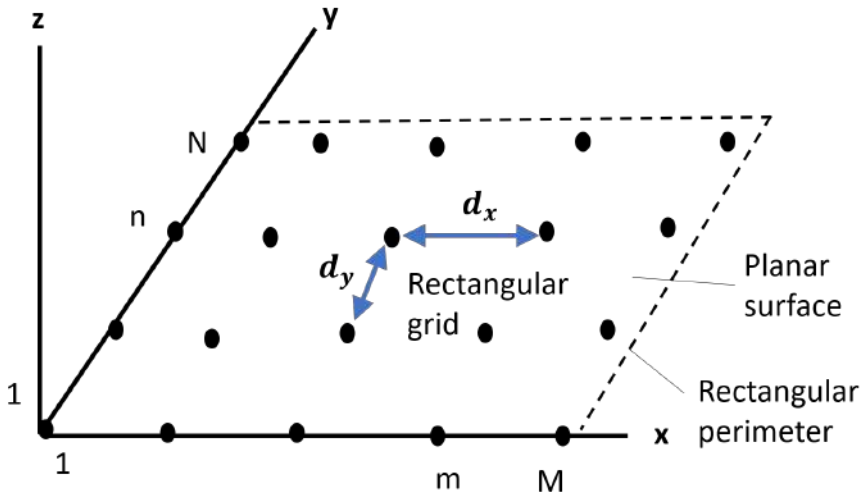

Figure 3.10: Uniform planar array

BF can also be implemented in three domains, i.e., analog, digital and hybrid. The details are as following

3.1.3 Analog Beamforming

In analog BF, same signal is fed to all antenna elements and the signal is steered in different directions through analog phase-shifters as shown in Fig 3.11. Single radio-frequency (RF) chain is utilized in analog BF, hence, the system is limited to a single user. The RF signal is manipulated through complex coefficients by controlling the phase shifters and variable gain amplifiers. Although, analog beamforming lacks spatial multiplexing yet it is simple technique that offers high BF gains [15], [97], [98].

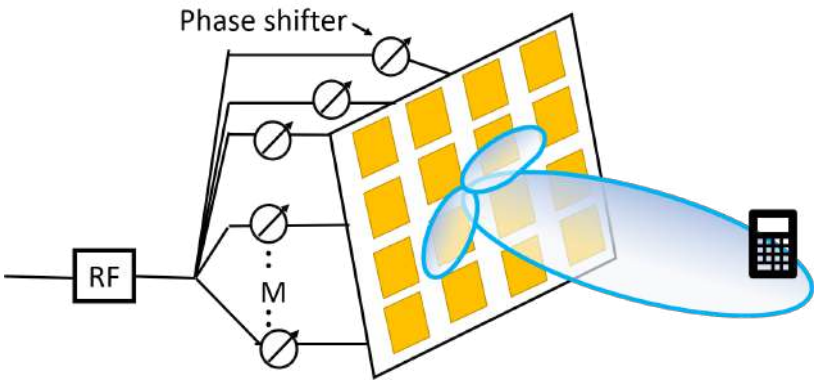

Figure 3.11: Analog beamforming.

3.1.4 Digital Beamforming

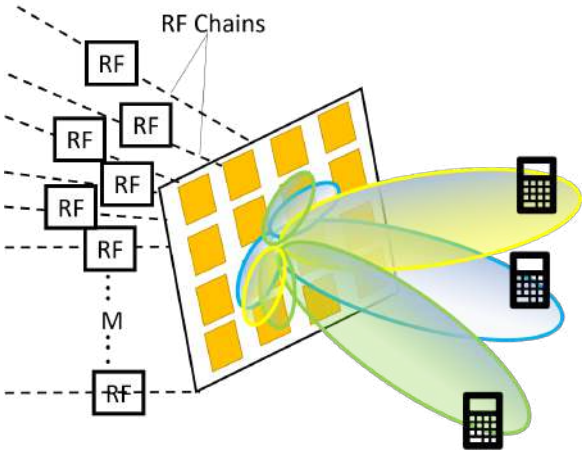

Figure 3.12: Digital beamforming.

In digital BF, different signals are fed to different antenna elements. Different phases and powers to different antennas can be applied in the digital domain as shown in Fig. 3.12. In digital BF, the beams are not steered instead they are created. Many RF chains are utilized for controlling the phase and amplitude of incoming signal at each antenna element. Digital BF is suitable for a multi-user system. Digital BF offers more flexibility and better performance at the expense of high complexity and increased cost because of independent fast Fourier transform (FFT)/ inverse fast Fourier transform (IFFT) blocks, analog-to-digital converters (ADCs) and digital-to-analog converters (DACs) per RF branch [15], [97], [98].

3.1.5 Hybrid Beamforming

It is the combination of both digital and analog BF. The upcoming 5G BS are expected to utilize hybrid BF, i.e., utilizing analog BF for coarse beams and digital BF within analiog technique as either SU-MIMO (transmit several data beams to a user for increased data rates) or MU-MIMO (simultaneous beam transmissions to many users at high load) [99], [100].

Chapter 4

Auxiliary Beam Pair Enabled Initial Access in mmWave Systems: Analysis and Design Insights

In this chapter, the novel AH and AF algorithms are discussed in detail with respect to BF and sequential scanning. ABP is implemented at the TX side only and the RX has an omnidirectional antenna. The well-known methods of IA, i.e., exhaustive and iterative search schemes also lack BF, hence, BF is employed in these existing techniques as well for a comprehensive analysis. This work has also been published in IEEE International Conference on Communication (2019) [101]. The details are as following.

4.1 Beamforming at TX

4.1.1 Auxiliary-Half

BF is employed at the TX side through a ULA. In AH, two beams, i.e., α and β are formed simultaneously at the TX as shown in Fig 4.1.

The beams at TX are formed by splitting the ULA equally into two halves. Mathematically,

$$N_t = N_{t1} + N_{t2}, \tag{4.1.1}$$

where N_{t1} and N_{t2} are the antenna elements forming α and β beams, respectively. The vector contribution from elements N_{t1} and N_{t2} is summed up and eq. (3.1.1) can be re-

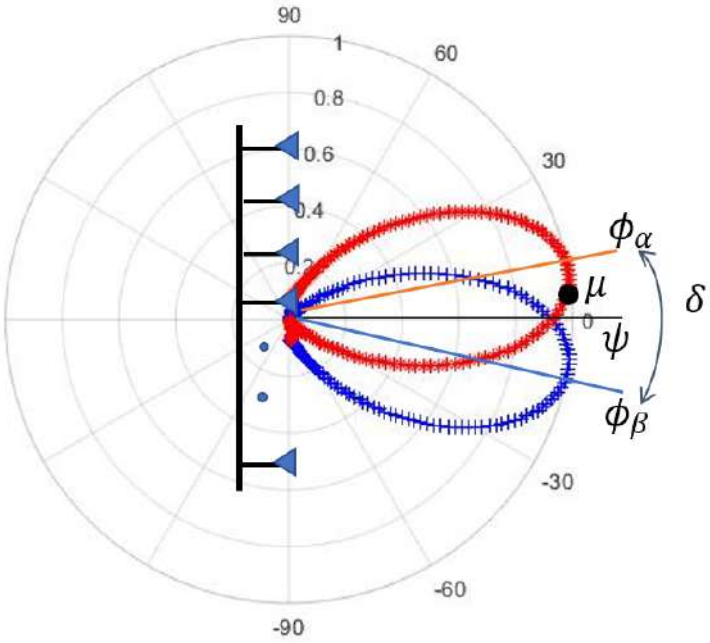

Figure 4.1: Beamforming for AH scheme

written as

$$X_{t1}(\theta_t) = \frac{1}{\sqrt{N_{t1}}} \sum_{n=0}^{N_{t1}-1} e^{(-j2\pi d(n)\sin(\theta_t))/\lambda}, \tag{4.1.2}$$

$$X_{t2}(\theta_t) = \frac{1}{\sqrt{N_{t2}}} \sum_{m=0}^{N_{t2}-1} e^{(-j2\pi d(m)\sin(\theta_t))/\lambda}, \tag{4.1.3}$$

It is to be noted that $\theta_t \in [-\pi/2, \pi/2]$ is the AoD and the chosen range is set to avoid the grating lobes [102]. Also, the beam steering directions, i.e., $\phi_{t\alpha}$ and $\phi_{t\beta}$ for α and β beams is given as

$$W(\phi_{t\alpha}) = \frac{1}{\sqrt{N_{t1}}} \sum_{n=0}^{N_{t1}-1} e^{(j2\pi d(n)\sin(\phi_{t\alpha}))/\lambda}, \tag{4.1.4}$$

$$W(\phi_{t\beta}) = \frac{1}{\sqrt{N_{t2}}} \sum_{m=0}^{N_{t2}-1} e^{(j2\pi d(m)\sin(\phi_{t\beta}))/\lambda}, \tag{4.1.5}$$

where $W(\phi_{t\alpha})$ and $W(\phi_{t\beta})$ are the weights adjusting the signal phase. Hence, the radiation pattern for α and β beams is given as

$$
\begin{aligned}
Y_{t\alpha} &= X_{t1}(\theta_t) \times W(\phi_{t\alpha}), \\
&= \frac{1}{\sqrt{N_{t1}}} \sum_{n=0}^{N_{t1}-1} e^{(-j2\pi d(n)\sin(\theta_t))/\lambda} \times \frac{1}{\sqrt{N_{t1}}} \sum_{n=0}^{N_{t1}-1} e^{(j2\pi d(n)\sin(\phi_{t\alpha}))/\lambda}, \\
&= \frac{1}{N_{t1}} \sum_{n=0}^{N_{t1}-1} e^{(-j2\pi dn/\lambda)(\sin(\theta_t)-\sin(\phi_{t\alpha}))}, \\
&= \frac{1}{N_{t1}} \sum_{n=1}^{N_{t1}} e^{(-j2\pi d(n-1)/\lambda)(\sin(\theta_t)-\sin(\phi_{t\alpha}))},
\end{aligned}
\tag{4.1.6}
$$

Using the identity

$$
\sum_{n=1}^{N} e^{-j(n-1)x} = \frac{sin(Nx/2)}{sin(x/2)} \tag{4.1.7}
$$

Equation (4.1.6) can be written as

$$
Y_{t\alpha} = \frac{\sin(N_{t1}\pi d(\sin(\theta_t) - \sin(\phi_{t\alpha}))/\lambda)}{N_{t1} \times \sin(\pi d(\sin(\theta_t) - \sin(\phi_{t\alpha}))/\lambda)}, \tag{4.1.8}
$$

Similarly, the radiation pattern for β beam is calculated as

$$
Y_{t\beta} = \frac{\sin(N_{t2}\pi d(\sin(\theta_t) - \sin(\phi_{t\beta}))/\lambda)}{N_{t2} \times \sin(\pi d(\sin(\theta_t) - \sin(\phi_{t\beta}))/\lambda)}. \tag{4.1.9}
$$

For IA, the TX starts searching for the UE by directing a beam pair in a particular direction. Let N_{tAH} be the total number of search sectors that the TX scans. Mathematically,

$$
N_{tAH} = \frac{180^\circ}{BW^\circ_{tAH}}, \tag{4.1.10}
$$

where the scanning region is limited to 180° to avoid grating lobes and BW°_{tAH} is the TX search beamwidth. Grating lobes are secondary lobes or side lobes with amplitude same as the main lobe. It is to be noted that the limited scanning region can be extended by utilizing additional ULAs to give full 360° coverage but that is out of scope of this work. The TX BW°_{tAH} is calculated by finding the half-power beam width (HPBW). Mathematically,

$$
HPBW^\circ_{tAH} = \frac{50.8^\circ}{(N_x dcos(\varphi)/\lambda)}, \tag{4.1.11}
$$

where $HPBW^\circ_{tAH}$ is obtained by equating (4.1.8) or (4.1.9) to $1/\sqrt{2}$ and solving for θ [102]. $N_x \in \{N_{t1}, N_{t2}\}$, φ is the scan angle, i.e., $\varphi = \phi_{t\alpha}$ or $\varphi = \phi_{t\beta}$. The HPBW changes at different scan angles and the smallest value is achieved at $\varphi = 0^\circ$. Therefore, for simplicity, the HPBW is fixed according to 0° for our entire analysis. Furthermore, the search beamwidth [1] is determined from the HPBW as

$$
BW^\circ_{tAH} = HPBW^\circ_{tAH} + \delta, \tag{4.1.12}
$$

[1] A sector or search beamwidth is defined by the HPBW of α (β) beam plus the separation between α (β) and β (α) beams.

where δ is the separation between α and β beams.

4.1.2 Auxiliary-Full

The basic design principle of AF is illustrated in Fig. 4.2.

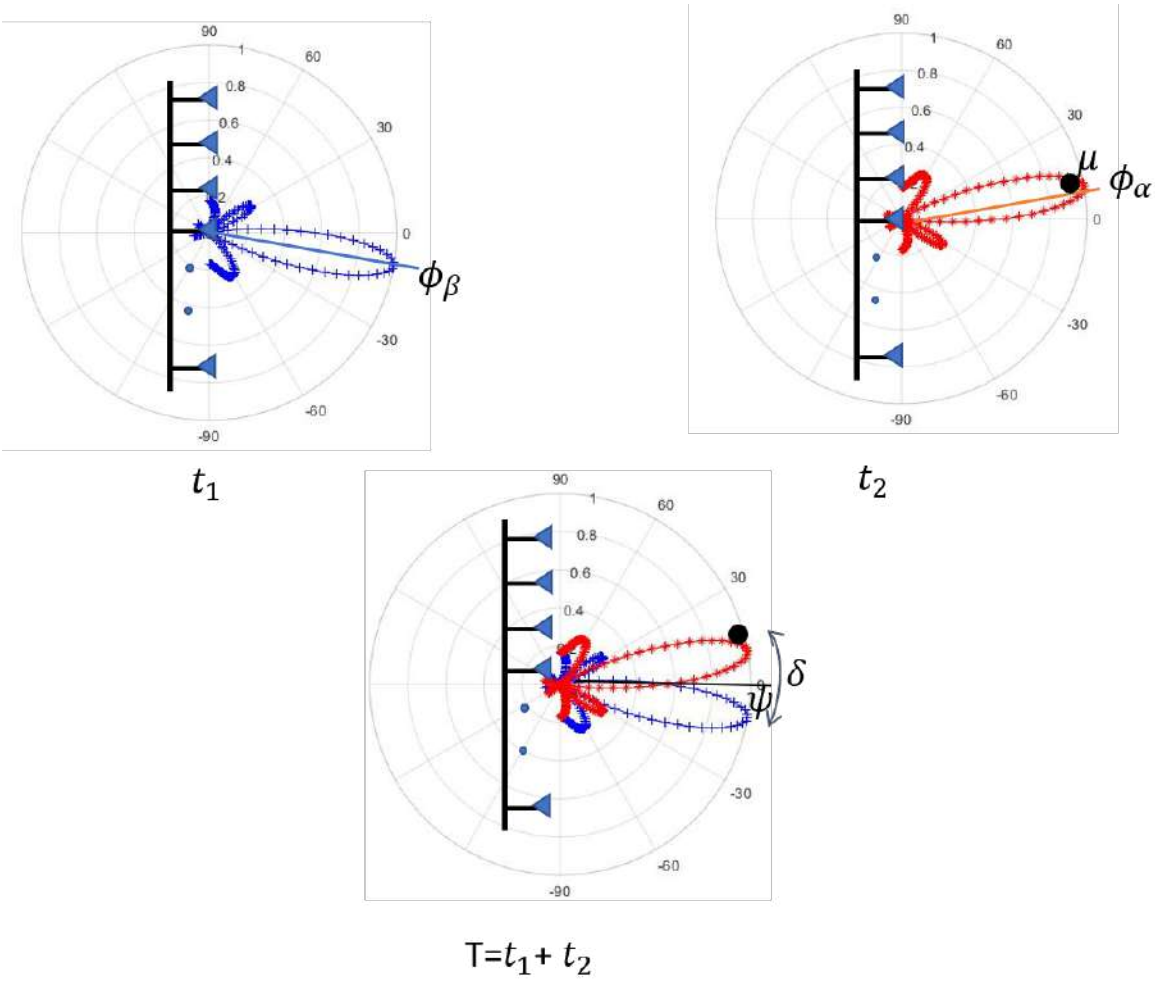

Figure 4.2: Beamforming for AF scheme

In AF, all antenna elements combine together to form a TX beam during one time slot. AF is similar to AH with the only difference that two beams are formed in two different time slots but in the same search sector. TX beam searches the same sector twice in a time division manner.

For example, in time slot 1, TX forms a beam with N_t antenna elements. The beam is directed at an angle ϕ_α within a search sector. If TX and RX discover each other, than the search process ends. However, if TX and RX have not detected each other, then in time

slot 2, the TX will search the same sector again but at a slight different angle ϕ_β. Both ϕ_α and ϕ_β are δ distance apart from each other. In this way, time diversity is achieved and the device detection probability increases.

The TX, radiation pattern during one time slot is given as

$$Y_{t\alpha}(t_1) = \frac{\sin(N_t \pi d(\sin(\theta_t) - \sin(\phi_{t\alpha}))/\lambda)}{N_t \times \sin(\pi d(\sin(\theta_t) - \sin(\phi_{t\alpha}))/\lambda)}, \tag{4.1.13}$$

$$Y_{t\beta}(t_2) = \frac{\sin(N_t \pi d(\sin(\theta_t) - \sin(\phi_{t\beta}))/\lambda)}{N_t \times \sin(\pi d(\sin(\theta_t) - \sin(\phi_{t\beta}))/\lambda)}, \tag{4.1.14}$$

where t_1 and t_2 are two different time slots in which beams α and β are formed. The $HPBW^{\circ}_{tAF}$ and BW°_{tAF} is given as

$$HPBW^{\circ}_{tAF} = \frac{50.8^{\circ}}{(N_t d \cos(\varphi)/\lambda)}, \tag{4.1.15}$$

$$BW^{\circ}_{tAF} = HPBW^{\circ}_{tAF} + \delta. \tag{4.1.16}$$

4.1.3 Exhaustive Search

Exhaustive search method utilizes all the antenna elements to form a single beam. The TX forms one directional beam to search a particular sector during one time slot as shown in Fig.4.3.

Unlike AF, the search process is not repeated in the same sector during different time slots. The radiation pattern at TX is calculated as

$$Y_t = \frac{sin(N \pi d(sin(\theta_t) - sin(\phi_t))/\lambda)}{N \times sin(\pi d(sin(\theta_t) - sin(\phi_t))/\lambda)}, \tag{4.1.17}$$

The number of search sectors, i.e., N_{EX} at the TX are determined as

$$N_{tEX} = \frac{180^{\circ}}{BW^{\circ}_{tEX}} = \frac{180^{\circ}}{HPBW^{\circ}_{tEX}}, \tag{4.1.18}$$

The $HPBW^{\circ}_{tEX}$ is equal to BW°_{tEX} in this case and is calculated according to (4.1.15). The BS searches for a UE in a particular sector.

4.1.4 Iterative Search

Iterative search algorithm narrows down the search beamwidth to detect the user as shown in Fig. 4.4. The radiation pattern is calculated in a similar way as (4.1.17). Let N_{IT} be

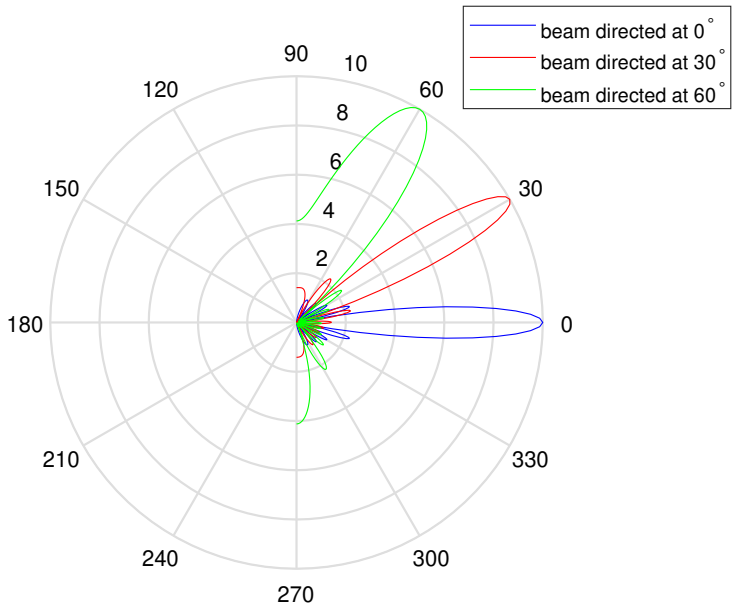

Figure 4.3: Beamforming for exhaustive search scheme

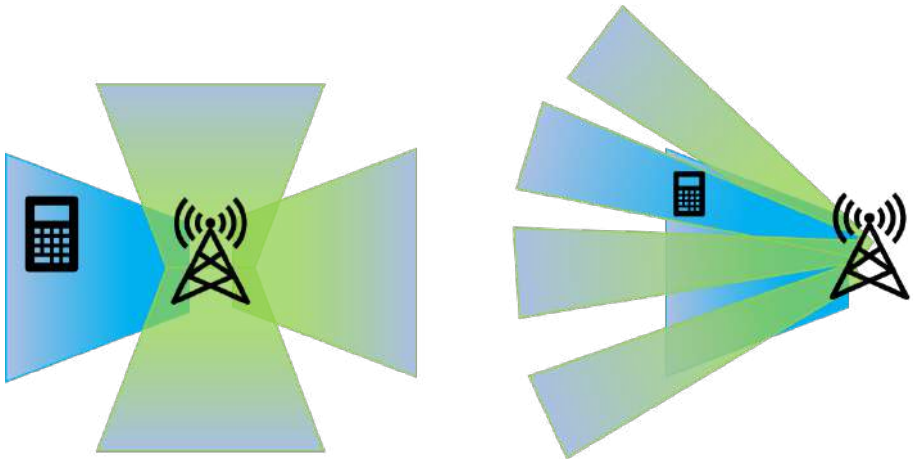

Figure 4.4: Beamforming for iterative search scheme

an integer that represents the number of search sectors, such as

$$N_{IT} = h, \tag{4.1.19}$$

where $h > 1$ is a positive integer. For example, bisection method is utilized, than $h = 2$. The entire search region is divided into two halves, each having a width of 90°.

Iterative search is based on the principle of *Stages*. The algorithm successively narrows down the beamwidth in a particular stage, S. Let *Stages* be the upper bound on S, i.e., $S \leq Stages$. *Stages* is a design parameter, whose value is determined according to

the narrowest allowable beamwdith that the transmit or receive antenna array can support. Since, the total antenna elements (N) are known, so the bound on S for TX can be calculated as

$$\begin{aligned} HPBW^{\circ}_{tIT} &= \frac{180^{\circ}}{h^S}, \\ S &\leq \frac{log_2(180^{\circ}/HPBW^{\circ}_{tIT})}{log_2(h)}, \end{aligned} \tag{4.1.20}$$

where $HPBW^{\circ}_{tIT}$ is calculated according to (4.1.15). The search beamwdith, i.e., BW°_{tIT} for a particular stage is determined as

$$BW^{\circ}_{tIT} = \frac{180^{\circ}}{h^S}, \tag{4.1.21}$$

4.2 User Detection through Sequential Search

In this method, BF is implemented in a sequential manner, i.e., the beam is rotated in either clockwise or anti-clockwise direction to search each sector. Sequential search is implemented in both AH and AF schemes and compared with the existing exhaustive and iterative sequential search methods. The details are as following

4.2.1 Auxiliary-Half

Two simultaneous beams are pointed in a particular direction and the search process begins through scaning of each adjacent sector. Let $K = \{1, 2, ..., N_{AH}\}$ be the set that represents the search sector index. The search area spanned by the two beams at TX for a particular $k \in K$ is found as

$$\begin{aligned} \theta^{\circ}_{start} &= (k-1)BW^{\circ}_{tAH} - 90^{\circ}, \\ \theta^{\circ}_{end} &= (k)BW^{\circ}_{tAH} - 90^{\circ}, \end{aligned} \tag{4.2.1}$$

where θ°_{start} and θ°_{end} marks the start and end of search sector, respectively. The direction of both the beams is given as

$$\begin{aligned} \phi_{\alpha} &= \psi + \frac{\delta}{2}, \\ \phi_{\beta} &= \psi - \frac{\delta}{2}, \end{aligned} \tag{4.2.2}$$

where $\psi = (\theta^{\circ}_{start} + \theta^{\circ}_{end})/2$ is the direction of main probing region. The gain at user location μ is determined by substituting $\theta = \mu$ in (4.1.8) and (4.1.9) such that

$$Y_{t\alpha} = \frac{sin(N_{t1}\pi d(sin(\mu) - sin(\phi_{t\alpha}))/\lambda)}{N_{t1} \times sin(\pi d(sin(\mu) - sin(\phi_{t\alpha}))/\lambda)}, \tag{4.2.3}$$

$$Y_{t\beta} = \frac{sin(N_{t2}\pi d(sin(\mu) - sin(\phi_{t\beta}))/\lambda)}{N_{t2} \times sin(\pi d(sin(\mu) - sin(\phi_{t\beta}))/\lambda)}, \tag{4.2.4}$$

Also,

The BF gain at TX is determined through eqs (4.2.3) and (4.2.4) as

$$G_{t\alpha} = |Y_{t\alpha}|^2, \tag{4.2.5}$$

$$G_{t\beta} = |Y_{t\beta}|^2, \tag{4.2.6}$$

where $G_{t\alpha}$ and $G_{t\beta}$ are the BF gains of α and β beams, respectively. Hence, the total transmit BF gain is given as

$$G_{BF_{TX}} = G_{t\alpha} + G_{t\beta}, \tag{4.2.7}$$

If G is the total antenna gain, then

$$G(dB) = G_{TX} + G_{RX} + G_{BF_{TX}} + G_{BF_{RX}}, \tag{4.2.8}$$

where G_{TX}, G_{RX} and $G_{BF_{RX}}$ are the transmit and receive antenna gains and BF gain at the RX, respectively.

Now, the signal passes through either a LoS or NLoS channel. The path loss can be calculated as

$$L(dB) = \begin{cases} \rho + 10\alpha_L log(r) + \chi_L, & \text{if } LoS. \\ \rho + 10\alpha_N log(r) + \chi_N, & \text{otherwise.} \end{cases} \tag{4.2.9}$$

where ρ is the fixed path loss factor, r denotes the distance between the TX and RX, α_L and α_N are the LoS and NLoS path loss exponents, respectively. χ_L and χ_N denote the zero mean lognormal random variables for LoS and NLoS links, respectively, which represents shadowing [103].

When the RX receives a signal from the TX, then the received power is calculated as

$$P_r = \frac{P_t G \zeta}{L}, \tag{4.2.10}$$

where P_t is the transmit power and ζ is the squared envelope of multipath fading channel. The envelope follows a Rician or Rayleigh distribution depending on whether the link between the BS and UE is LoS or NLoS, respectively. The SNR is thus calculated as

$$\tau = \frac{P_r}{\sigma^2}, \tag{4.2.11}$$

where σ^2 is the noise variance. A decision regarding the BS-UE link establishment is made according to the SNR threshold, α_{th}, such that if

$$\begin{cases} \tau \geq \alpha_{th}, & \text{link is established.} \\ \tau < \alpha_{th}, & \text{otherwise.} \end{cases} \tag{4.2.12}$$

The TX starts the search process for a RX by sending a synchronization signal, T_{syn}, with beamwidth BW°_{tAH}, for T_{sig} seconds (s) in a particular sector. If the RX has been detected, i.e., $\tau \geq \alpha_{th}$, then the TX stops its search process immediately. However, if the RX is not detected in a sector, then the TX waits for $T_{per}(s)$ and repeat the whole process for the next sector. This search process continues until all sectors have been scanned by the TX in a sequential manner. Hence, the total time taken by the TX to search for a RX in its coverage range is known as DD. Mathematically,

$$DD_{AH} = (k)T_{sig} + (k-1)T_{per}, (for\ k \in K). \tag{4.2.13}$$

4.2.2 Auxiliary-Full

In this scheme, the BF gain is calculated for each time slot. Following the same steps as AH, the BF gain during time slot 1 is determined through eq (4.1.13) as

$$G_{\alpha - BF_{TX}}(t_1) = |Y_{t\alpha}(t_1)|^2, \tag{4.2.14}$$

From this gain, the SNR at time slot 1 is determined following (4.2.8)-(4.2.11). It is to be noted that unlike AH, the gain experienced at RX is not the sum of BF gains. If the RX is detected according to (4.2.12), then the TX stops its search process. Otherwise, the TX searches the same sector again during time slot 2. If the RX is not detected in time slot 2, then the TX waits $T_{per}(s)$ and repeat the entire process for other search sectors. The DD_{AF} is calculated for each time slot according to (4.2.13).

4.2.3 Exhaustive Search

In this scheme, the TX performs sequential scanning by pointing a single beam in a particular sector using eqs (4.1.17), (4.2.1) and (4.2.2). The BF gain at TX is calculated using (4.1.17) as

$$G_{BF_{TX}} = |Y_t|^2, \tag{4.2.15}$$

The device detection is successful when $\tau \geq \alpha_{th}$ according to (4.2.10). The total time taken by TX to discover RX, i.e., DD_{EX} is calculated according to (4.2.13).

4.2.4 Iterative Search

The sequential search is carried out in different stages. The number of antenna elements required to achieve the BW°_{IT} in a particular stage is calculated according to (4.1.21). A similar process to that of previous search methods follows here. Let $K = \{1, 2, ..., N_{IT}\}$, then the search area spanned by the beam for a particular $k \in K$ at a certain stage S is found as

$$\begin{aligned} \theta^{\circ}_{start}(S) &= (k-1)BW^{\circ}_{AH} - 90^{\circ} + \theta^{\circ}_{start}(S-1), \\ \theta^{\circ}_{end}(S) &= (k)BW^{\circ}_{AH} - 90^{\circ} + \theta^{\circ}_{start}(S-1), \end{aligned} \tag{4.2.16}$$

where $\theta^{\circ}_{start}(S)$ and $\theta^{\circ}_{end}(S)$ is the start and end of a search beam in a particular stage S, while $\theta^{\circ}_{start}(S-1)$ marks the angular offset from previous stage. The radiation pattern and the BF gain is calculated similar to (4.1.17) and (4.2.15). If a signal is received at the RX, the RX determines τ by using (4.2.8) - (4.2.11). Subsequently, the TX-RX link is established according to following scheme

$$\begin{cases} \tau \geq \alpha_{th}, & \text{link is established.} \\ \tau \geq \alpha_{l}, & \text{narrow down search sector.} \\ \tau < \alpha_{l}, & \text{RX not present in the sector.} \end{cases} \tag{4.2.17}$$

where α_l is the loose threshold that determines the region to be narrowed down to locate the RX.

The DD_{IT} is the sum of delay incurred at a stage, DD_S. It is the time taken by the TX to firstly track the RX and secondly, the time incurred while searching each sector to detect the RX.

$$\begin{aligned} DD_S &= (N_{IT})T_{sig} + (N_{IT}-1)T_{per}, (for\ \tau \geq \alpha_l) \\ DD_S &= (k)T_{sig} + (k-1)T_{per}, (otherwise) \end{aligned} \tag{4.2.18}$$

Hence, the total delay, DD_{IT} is given as

$$DD_{IT} = \sum_{S=1}^{Stages} DD_S, \tag{4.2.19}$$

4.3 Simulation Results for Sequential Search

We analyze the performance of our proposed ABP schemes with respect to sequential scanning algorithm. We implement BF in the existing techniques in literature, i.e., exhaustive and iterative search schemes and compare all the schemes for a comprehensive analysis. For simplicity, we have assumed fixed distance r between the TX and RX. The channel is generated as NLoS and LoS by following a Bernoulli distribution and the result is approximated using 10^5 Monte Carlo simulations via MATLAB. The simulation parameters are summarized in Table 4.1.

Table 4.1: System Parameters

Parameter	**Value**	**Parameter**	**Value**
f_c	73 GHz	h	2
P_t	30 dBm	T_{sig}	10 μs
G_{TX}	0 dBi	T_{per}	200 μs
G_{RX}	0 dBi	ρ	70 dB
α_L	2	$Std(\chi_L)$	5.2 dB
α_N	2.5	$Std(\chi_N)$	7.2 dB

The sequential search employs BF at the TX side only. The transmitter employs ULA with $N_t = 16$ antenna elements. The RX has an omnidirectional antenna. The BF gain at RX is set as $G_{BF_{RX}} = 0dBi$. The search beamwidth for each scheme is determined individually. We also assume a single user, located randomly at a distance $r = 10m$ from the TX. The simulation results are as follows

4.3.1 SNR vs. PMD and DD for all schemes

Fig. 4.5 shows the PMD and DD performance for all four schemes against α_{th}. The loose threshold α_l has a value $20dB$ lower than α_{th}. It is observed that the iterative search performs the worst in terms of PMD. This is because the iterative method uses wide beams in initial stages, resulting in reduced BF gain and hence increased PMD. On the other hand, AF performs the best because it uses the concept of time diversity. A beam is formed with $N_t = 16$ antenna elements twice in one sector. Hence, the probability of detecting a user increases. Also, AH shows a high PMD as compared to exhaustive and AF. Since, AH forms

two beams simultaneously with $N_t = 8$ antenna elements, therefore, the BF gain decreases and so does the detection probability. For the DD it is observed that iterative is the best scheme as it scans the region very quickly. AF takes a lot of time to locate a user as it has time diversity in it, hence the DD is highest. AH and exhaustive schemes provide the mediocre results.

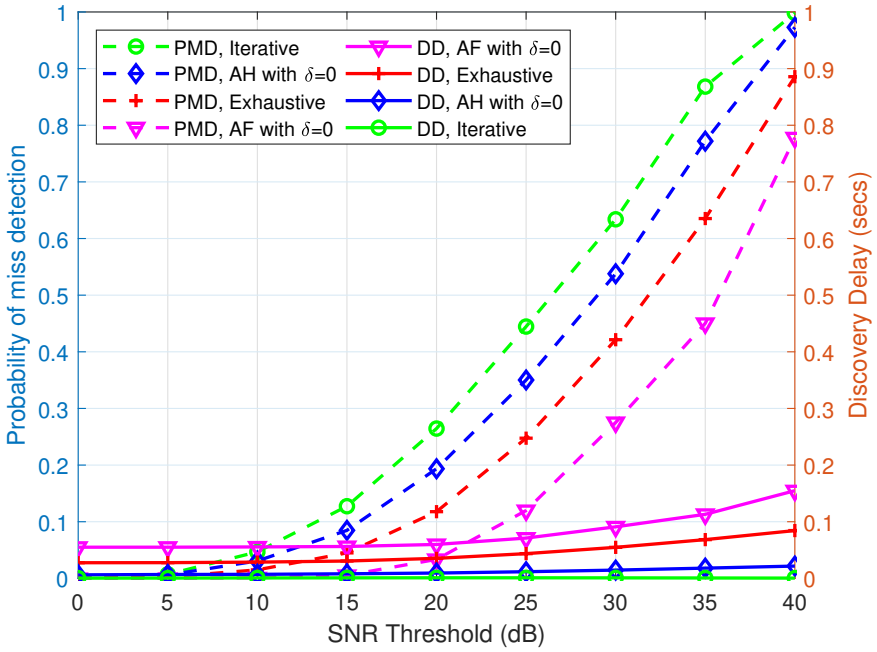

Figure 4.5: SNR vs. PMD and DD for all schemes, $\delta = 0$ for ABP

4.3.2 PMD vs. SNR for exhaustive, iterative and AH schemes

Next, we study the effect of δ on AH and AF. Fig. 4.6 shows that if we vary δ, then PMD starts increasing for AH. As δ increases, the width of search sector also increases, and AH starts approaching the iterative scheme. Furthermore, for $\delta = 20°$, AH performs worse than iterative scheme at lower α_{th}. It is because for lower α_{th} values, iterative method can detect a UE successfully, even with less number of antenna elements, i.e., wider beams. However, as α_{th} increase beyond $30dB$, both iterative and AH schemes perform in a similar manner.

4.3.3 DD vs. SNR for exhaustive, iterative and AH schemes

In Fig. 4.7, for lower values of SNR, the DD is almost same for iterative scheme and AH with $\delta = 20°$. For higher SNR values, DD is low for iterative method as it searches the scan

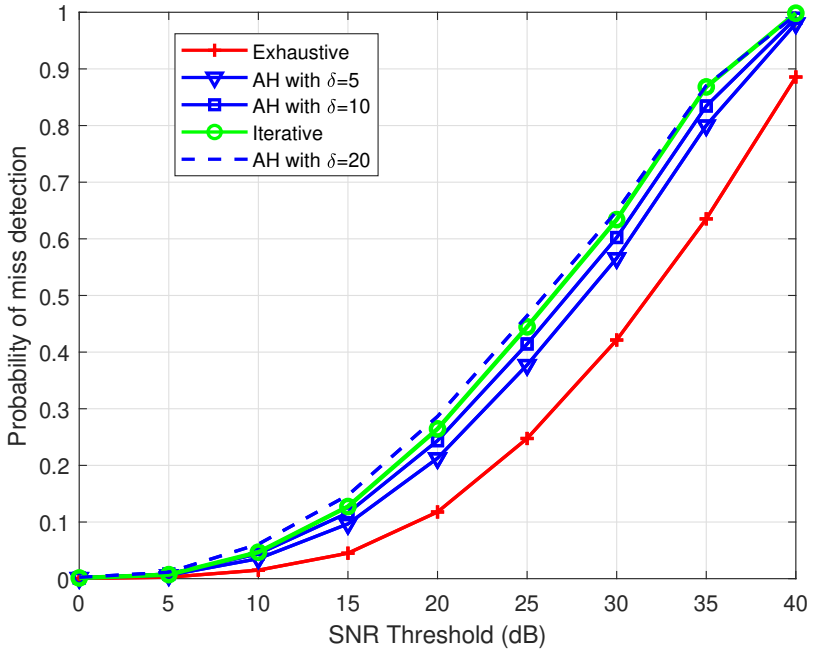

Figure 4.6: PMD vs. SNR for exhaustive, iterative and AH schemes

area very quickly as compared to AH.

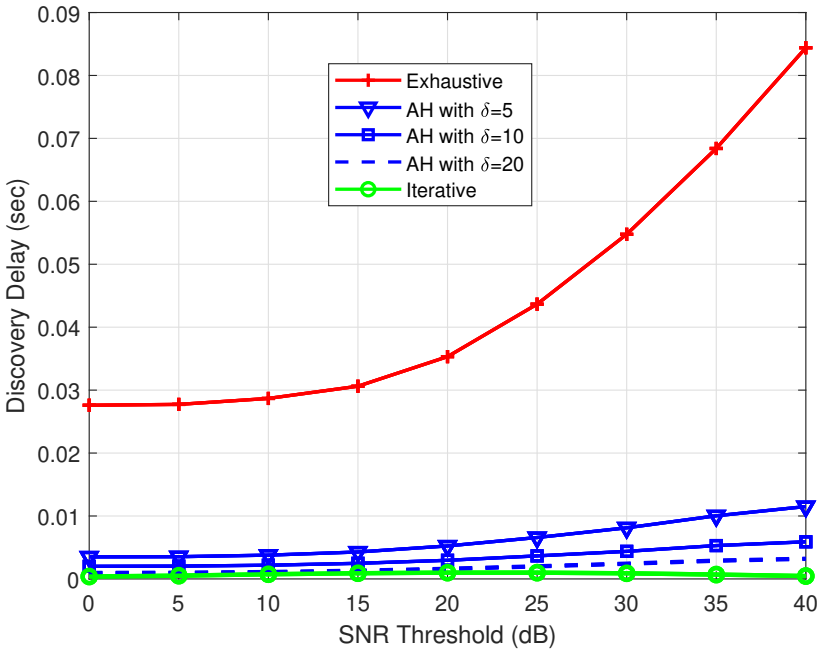

Figure 4.7: DD vs. SNR for exhaustive, iterative and AH schemes

4.3.4 PMD vs. SNR for exhaustive, iterative and AF schemes

Fig. 4.8 shows that by varying δ, AF is not always the best scheme with respect to PMD. If we start increasing δ, AF outperforms both exhaustive and iterative schemes for $\delta < 10°$. However, for higher values of δ, exhaustive search outperforms AF. It is because, as δ starts increasing, the sector width increases. Hence, the SNR also degrades because the two beams now cover different regions within a sector. The probability of detecting a user twice at the same location reduces, which leads to increased PMD. It is observed that when the separation between two beams is 10°, then AF gives same performance as exhaustive search. It is to be noted that although δ increases to 20°, yet iterative scheme performs the worst. It is because AF is using time diversity.

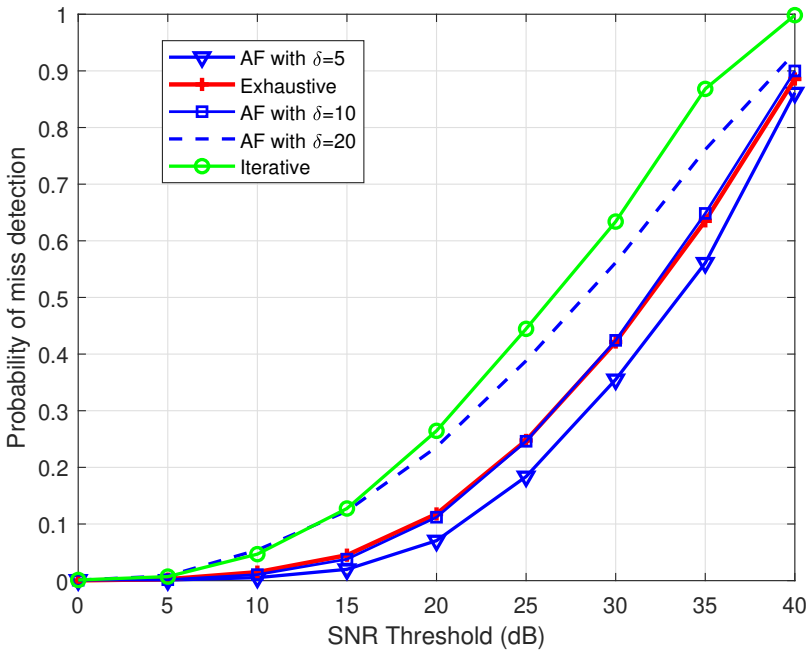

Figure 4.8: PMD vs. SNR for exhaustive, iterative and AF schemes

4.3.5 DD vs. SNR for exhaustive, iterative and AF schemes

In Fig. 4.9, it is observed that for different values of δ, AF has a low DD as compared to exhaustive search. As δ is increasing, the separation between the two beams increases. However, the separation is not significant for $\delta < 10°$. The beams are covering some portion twice within the same sector at different time slots. Hence, the DD is low because the probability of detecting a user in a sector increases. In this case, AF outperforms exhaustive

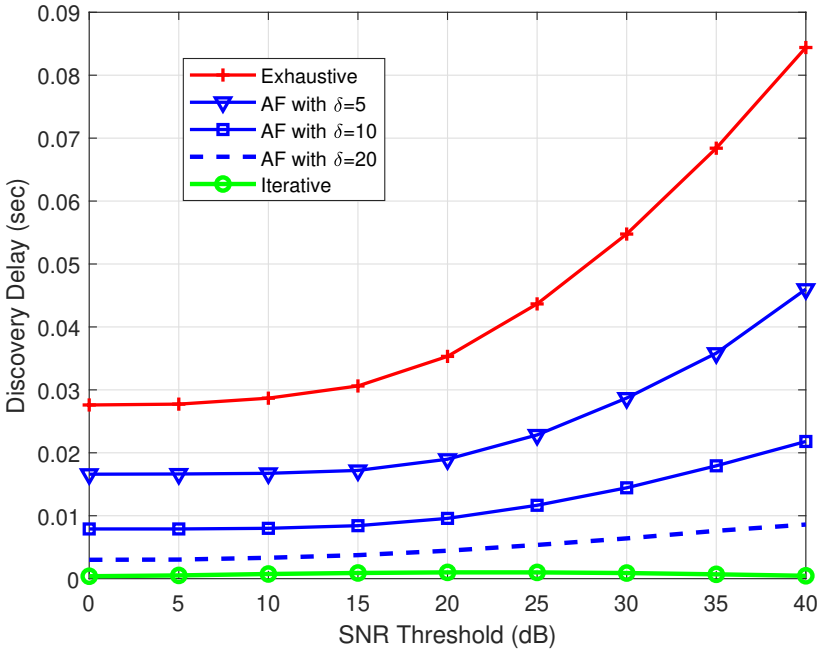

Figure 4.9: DD vs. SNR for exhaustive, iterative and AF schemes

search for a variable δ.

4.3.6 LoS probability vs. PMD and DD for all schemes

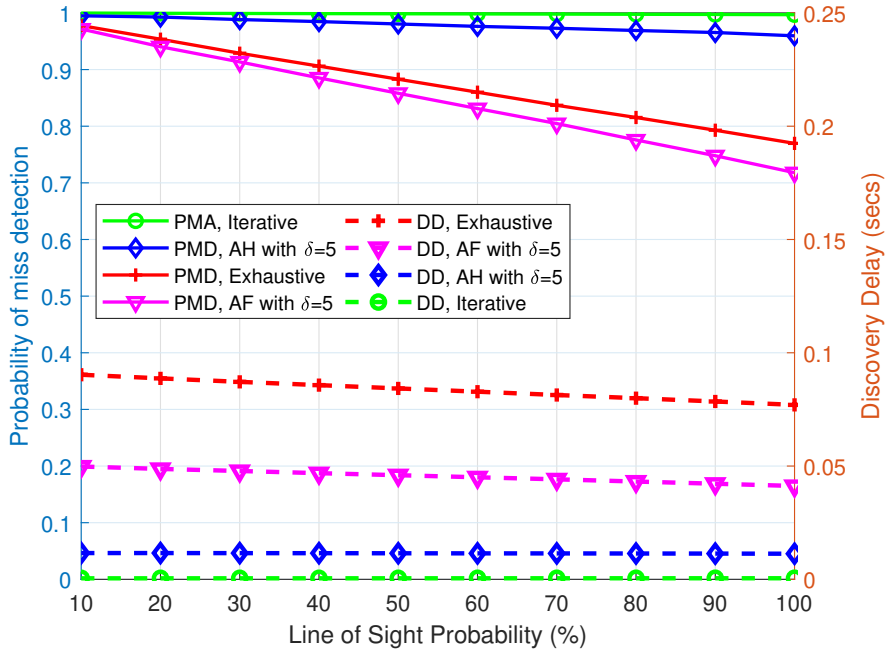

Figure 4.10: LoS probability vs. PMD and DD for all schemes

Fig. 4.10 shows the performance of schemes with respect to PMD and DD when the probability of a LoS/NLoS channel is varied. We set $\alpha_{th} = 40dB$ and $\delta = 5°$. The PMD decreases as the probability of having a LoS channel increases. It is observed that the PMD is highest for iterative scheme and lowest for AF. However, in terms of DD, the delay is least for iterative and highest for exhaustive method. AF performs better than exhaustive in terms of both PMD and DD. It is because the beams cover same search area twice but with a higher probability of detection, which results in a lower DD.

4.3.7 UE orientation vs. PMD and DD for all schemes

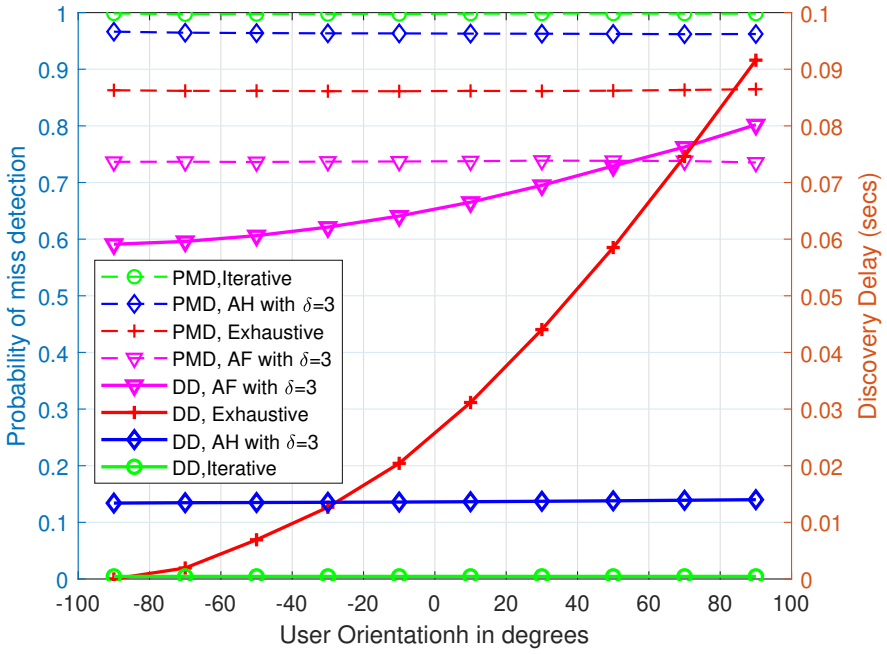

Figure 4.11: UE orientation vs. PMD and DD for all schemes

Fig. 4.11 shows the performance of PMD and DD with respect to user orientation. We have assumed constant BF gain value in each sector. We set $\alpha_{th} = 40dB$ and $\delta = 3°$. It is observed that the UE orientation does not have an impact on PMD. The PMD remains constant irrespective of UE location. In terms of DD, AF and exhaustive schemes are most sensitive to initial UE orientation while AH and iterative methods are relatively robust. It is because the probability of detecting a user is extremely low for both AH and iterative, hence the BS has to search the entire region to locate a UE, which results in constant DD.

4.4 Conclusions

In this chapter, we have analyzed and compared the performance of different IA schemes, i.e., exhaustive, iterativeand ABP schemes. Simulation results show that formation of beam pairs with respect to δ has a huge impact on the PMD and DD performance. For a moderate seperation between the beam pair, AF outperforms all other schemes in terms of PMD. Also, AF achieves lower DD than exhaustive scheme, whereas, AH achieves a lower DD and PMD than both exhaustive and iterative schemes, respectively. Furthermore, PMD and DD show similar trend with respect to varying SNR. If the SNR threshold in low, the probability of user detection is high, hence, low discovery delay. Similarly, for higher SNR threshold, it takes more time to search for a user, hence increased DD and PMD.

Chapter 5

Auxiliary Beam Pair Enabled Initial Access for mmWave D2D Networks

In this chapter, BF is implemented at both the TX and RX side in the proposed AH and AF schemes along with non-sequential scanning at both TX and RX. BF is also implemented in the existing ODND and Polya's Necklaces schemes for a comprehensive analysis. This work has also been published in Physical Communication Journal (2020) [104]. The details are as following.

5.1 Beamforming at RX

5.1.1 Auxiliary-Half

BF is implemented at both TX and RX by employing ULA as shown in Fig 5.1. Both TX and RX generate two simultaneous beams at a given time instant. The radiation pattern for RX is given as

$$Y_{r\alpha} = \frac{\sin(N_{r1}\pi d(\sin(\theta_r) - \sin(\phi_{r\alpha}))/\lambda)}{N_{r1} \times \sin(\pi d(\sin(\theta_r) - \sin(\phi_{r\alpha}))/\lambda)}, \tag{5.1.1}$$

$$Y_{r\beta} = \frac{\sin(N_{r2}\pi d(\sin(\theta_r) - \sin(\phi_{r\beta}))/\lambda)}{N_{r2} \times \sin(\pi d(\sin(\theta_r) - \sin(\phi_{r\beta}))/\lambda)}. \tag{5.1.2}$$

where $\theta_r \in [\pi/2, 3\pi/2]$ is the AoA.

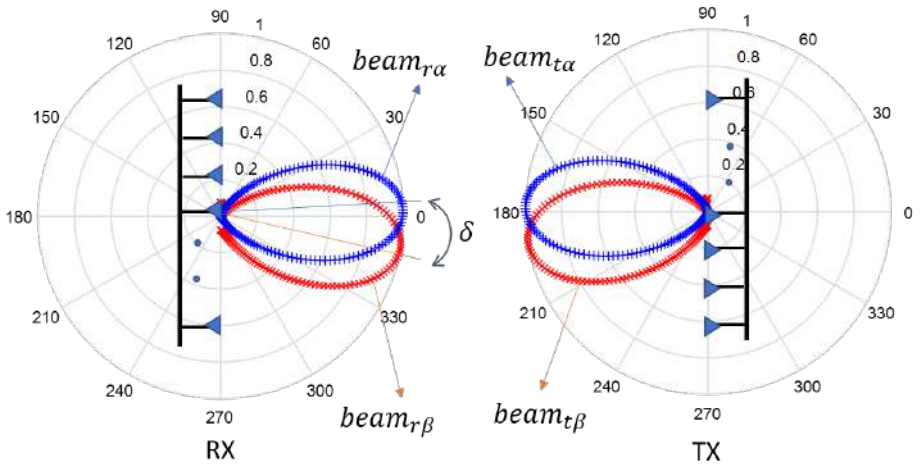

Figure 5.1: Beamforming for AH scheme

The number of search sectors in the desired scanning area of RX is given as

$$N_{rAH} = \frac{180^\circ}{BW^\circ_{rAH}}, \tag{5.1.3}$$

where the scanning range of RX is limited to 180° to avoid grating lobes. Also, the RX HPBW and beamwidth is calculated as

$$HPBW^\circ_{rAH} = \frac{50.8^\circ}{(N_x d cos(\varphi)/\lambda)}, \tag{5.1.4}$$

$$BW^\circ_{rAH} = HPBW^\circ_{rAH} + \delta. \tag{5.1.5}$$

where $N_x \in \{N_{r1}, N_{r2}\}$, φ is the scan angle, i.e., $\varphi = \phi_{r\alpha}$ or $\varphi = \phi_{r\beta}$. The TX beamwidth is calculated in a similar way as (5.1.1)-(5.1.5).

5.1.2 Auxiliary-Full

The basic design principle of AF is illustrated in Fig. 5.2. The RX radiation pattern and beamwidth is given as

$$Y_{r\alpha}(t_1) = \frac{\sin(N_{rAF}\pi d(\sin(\theta) - \sin(\phi_{r\alpha}))/\lambda)}{N_{rAF} \times \sin(\pi d(\sin(\theta) - \sin(\phi_{r\alpha}))/\lambda)}, \tag{5.1.6}$$

$$Y_{r\beta}(t_2) = \frac{\sin(N_{rAF}\pi d(\sin(\theta) - \sin(\phi_{r\beta}))/\lambda)}{N_{rAF} \times \sin(\pi d(\sin(\theta) - \sin(\phi_{r\beta}))/\lambda)}, \tag{5.1.7}$$

$$HPBW^\circ_{rAF} = \frac{50.8^\circ}{(N_{rAF} d \cos(\varphi)/\lambda)}, \tag{5.1.8}$$

$$BW^\circ_{rAF} = HPBW^\circ_{rAF} + \delta. \tag{5.1.9}$$

The TX beamwidth is calculated in a similar way as (5.1.6)-(5.1.9).

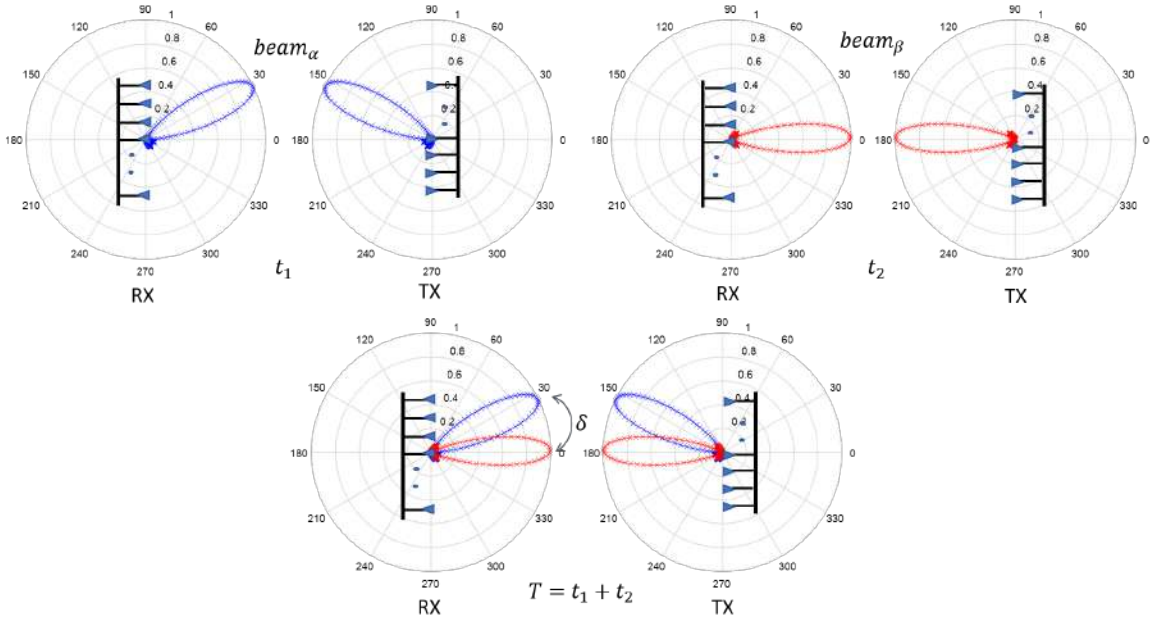

Figure 5.2: Beamforming for AF scheme

5.1.3 ODND and Polya's Necklaces

ODND and Polya's Necklaces utilize all the antenna elements to form a single directional beam at a time. BF is implemented by utilizing the ULA at both TX and RX. The radiation pattern at RX for ODND scheme is calculated as

$$Y_r = \frac{\sin(N_{rOdnd}\pi d(\sin(\theta) - \sin(\phi_r))/\lambda)}{N_{rOdnd} \times \sin(\pi d(\sin(\theta) - \sin(\phi_r))/\lambda)}. \tag{5.1.10}$$

The search area is divided into N_{rOdnd} sectors such as

$$N_{rOdnd} = \frac{180^\circ}{BW^\circ_{rOdnd}} = \frac{180^\circ}{HPBW^\circ_{rOdnd}}. \tag{5.1.11}$$

The $HPBW^\circ_{rOdnd}$ and BW°_{rOdnd} are equal in this case. Similar calculations follow for TX part of ODND and Polya's necklaces.

5.2 User Detection through Non-Sequential Search

In non-sequential search method, both TX and RX point their beams in a random search sector at a given time instant. TX and RX keep scanning random sectors until the maximum allowed time to search the desired region is not reached or $\tau \geq \alpha_{th}$ is not achieved. The search method is based on the generation of antenna scan sequences. The antenna scan

sequence generation for ODND and Polya's Necklace is well discussed in [66], [68], [105]. We modify the scan sequence for the generation of ABP in our proposed algorithms. The details of non-sequential scanning is as following

5.2.1 ODND

In this method, there are total M devices in the network. The devices can detect each other only when the TX and RX beams get aligned. For example, the number of antennas per device are A_m, where, m refers to device index, $m \in \{0, 1, ..., M-1\}$. Based on A_m, each device scans the search region according to the beamwidth B_m, where $(0 < B_m < 2\pi)$. Each device has $N_{odnd} = 2\pi/B_m$ search sectors. For example, in Fig. 5.3, Node a and Node b have 3 and 4 search sectors, respectively. Both devices point their beams in different sectors according to a scan sequence. The scan sequence is used for directional BF in a specific sector at a given time instant. The scenario given in Fig. 5.3 is described in Fig. 5.4 with respect to the discovery process and scanning sequence. It is clear from Fig. 5.4 that the devices discover each other when device a points its beam in sector 2 and device b directs it in sector 1.

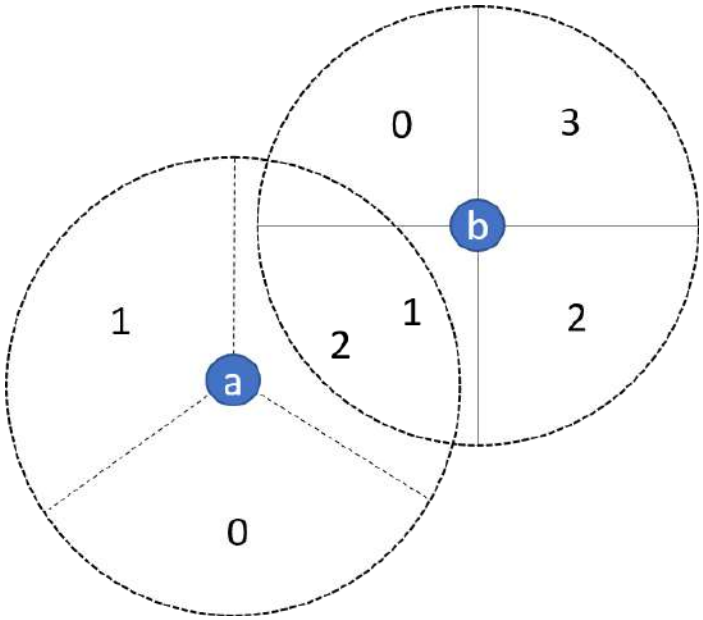

Figure 5.3: Antenna configuration of *Node a* and *Node b* with 3 and 4 antenna sectors, respectively.

A unique ID, known as device ID is associated with each device in the network. The device ID can be represented by a binary number. The minimum number of bits for a device ID is determined by the total number of devices in the network. For example, if there exist M

Slot Index	0	1	2	3	4	5	6	7
Node a	0	1	2	0	1	2	0	1
Node b	3	2	1	0	3	2	1	0

Figure 5.4: Example of antenna scan sequences where *Node a* and *Node b* discover each other in time slot 2.

devices in the network, then the least number of bits must be $\lceil \log_2(M) \rceil$. The device ID is utilized by each device to construct its extended address. The extended address is created such that it is mutually cyclically rotationally distinct for each device, i.e., each extended address is unique and cannot be obtained by cyclic rotation of any other extended addresses. This condition ensures neighbor discovery for arbitrary device orientations that may not be synchronous. The extended address length L_{odnd} is a key parameter in determining the neighbor discovery latency. The construction of extended ID sequence proposed in [66] is summarized as follows.

- Let $\mathbf{m}$ denote the ID of device m, which is l_a bits long binary sequence and $m(i)$ denoting the i^{th} bit of $\mathbf{m}$. Typically, l_a is chosen such that $l_a = \lceil \log_2(M) \rceil$.
- Let $\mathbf{m}_1$ and $\mathbf{m}_2$ represent the sequence from $m(1)$ to $m(i_a - 1)$ and from $m(i_a)$ to $m(l_a - 2)$, where $i_a = \lfloor l_a/2 \rfloor$.
- The extended ID sequence E and its length L_{odnd} is calculated as

$$E = [\mathbf{0}(l_b), \mathbf{m}_1, 1, 0, \mathbf{m}_2, \mathbf{1}(l_c)], \tag{5.2.1}$$

$$L_{odnd} = l_a + l_b + l_c + 2, \tag{5.2.2}$$

  where $\mathbf{0}(l_b)$ and $\mathbf{1}(l_c)$ are string of all zeros and ones of length l_b and l_c, respectively. l_b and l_c are chosen such that the total length of L_{odnd} is odd and minimum.

The antenna scan sequence is given as

$$U_t = \begin{cases} t \bmod p_m, & {e_t}^m = 0 \ \text{ and } \ t \bmod p_m < N_{odnd}. \\ t \bmod q_m, & {e_t}^m = 1 \ \text{ and } \ t \bmod q_m < N_{odnd}. \\ rand(N_{odnd} - 1), & \text{otherwise}, \end{cases} \tag{5.2.3}$$

where $t \in \{0, 1, ..., T\}$ is the number of time slots, p_m is the smallest odd prime number not less than N_{odnd} and co-prime to L_{odnd}. q_m is the smallest power of 2 not less than N_{odnd}

and ${e_t}^m$ denotes a bit in E at a given time instant and $rand(N_{odnd} - 1)$ is uniform random integer in $[0, N_{odnd} - 1]$. The worst-case discovery delay between two devices, i.e., RX and TX, is dependent on L_{odnd} and is upper-bounded by

$$W = L_{odnd} \max\{p_r q_t, p_t q_r\}. \tag{5.2.4}$$

The generation of antenna scan sequence and user discovery can be well understood by Fig. 5.5. Here, both TX and RX have 7 search sectors each and the extended IDs, p_m, q_m, L_{odnd} and W is calculated according to (5.2.1)-(5.2.4). It is shown that the nodes can discover each other only when their beams point in search sector 3. Hence, the devices get aligned in time slots 3 and 10 for successful discovery.

$L_{odnd} = 3, Extended\ ID = 101, N_{odnd} = 7, p_r = 7, q_r = 8$

t:	0	1	2	3	4	5	6	7	8	9	10	11
e_t^{RX}	1	0	1	1	0	1	1	0	1	1	0	1
U_t	0	1	2	3	4	5	6	0	0	1	3	3

$L_{odnd} = 3, Extended\ ID = 100, N_{odnd} = 7, p_t = 7, q_t = 8$

t:	0	1	2	3	4	5	6	7	8	9	10	11
e_t^{TX}	1	0	0	1	0	0	1	0	0	1	0	0
V_t	0	1	2	3	4	5	6	0	1	1	3	4

$Discovery\ between\ TX\ and\ RX, U_t = 3, V_t = 3$

t:	0	1	2	3	4	5	6	7	8	9	10	11
U_t	0	1	2	3	4	5	6	0	0	1	3	3
V_t	0	1	2	3	4	5	6	0	1	1	3	4

Figure 5.5: Example of antenna scan sequences where TX and RX discover each other in time slots 3 and 10.

5.2.2 Polya's Necklaces

Polya's Necklaces is also a device discovery technique based on antenna scan sequence. The antenna sequence is generated in a similar way as ODND. However, the algorithm is more energy efficient in terms of reduced worst-case discovery delay. The length of extended address L_{poly} is calculated in a different way. The algorithm proposed in [68] is summarized as follows.

- It is a technique which consists of N necklaces. The necklaces are made of b beads of c different colors, connected circularly and invariant to rotation. For example, in Fig. 5.6 two necklaces can be created if $b = 1$ (one bead in each necklace) and $c = 2$ (two colors, black and white).

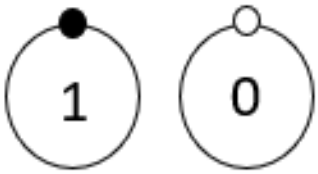

Figure 5.6: Two unique necklaces with different colored beads (bits)

- Alternatively, necklaces can also be represented as binary strings, i.e., black and white beads are represented by 0 and 1, respectively.

- Hence, the total number of necklaces that can be generated according to b and c, is calculated by Polya's Enumeration theorem as

$$N(b,c) = \frac{1}{b}\sum_{m=1}^{v}\varphi(g_m)e^{b/g_m}, \tag{5.2.5}$$

where g_m represents the v divisors of b and φ is the Euler's totient function which can be expressed as

$$\varphi(g) = g\prod_{n=1}^{v}(1-\frac{1}{\rho_m}), \tag{5.2.6}$$

where ρ_m represents the v distinct prime factors of g. For example, if $g = 8$, then there are three numbers that are co-prime to g, i.e., 1, 3 and 7. Hence $\varphi(8) = 3$.

- To determine the smallest odd L_{poly}, the Polya's Necklaces method is used where

$$\begin{aligned} L_{poly} &= \text{minimize } b \\ \text{s.t. } N(b,2) &\geq M, \text{and mod } (b,2) = 1. \end{aligned} \tag{5.2.7}$$

- Once the L_{poly} is selected, the extended addresses can be assigned to generate all the binary necklaces through FKM algorithm.[1]

[1]The details of FKM algorithm can be seen in [68].

5.2.3 Auxiliary-Half

In AH, two simultaneous beams are formed at a given time instant. Hence, two antenna scan sequences will be generated. The number of scan sectors is determined by N_{AH} and both beams are formed within one main scan sector as shown in Fig 5.7.

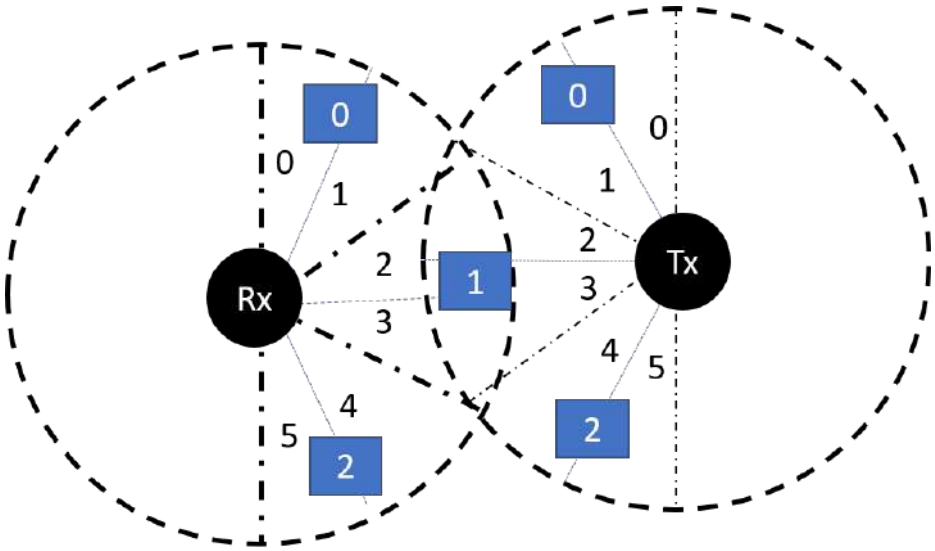

Figure 5.7: Antenna configuration of RX and TX with 3 main sectors ($N_{AH} = 3$) each having 6 subsectors. Devices discover each other when sectors 2, 3 of both TX and RX get aligned.

The antenna sequences generated for subsectors U_α and U_β are given as

$$U_\alpha = \begin{cases} 2(x_{p_m} \bmod p_m), & {e_t}^m = 0,\ 0 \le 2(x_{p_m} \bmod p_m) \le 2(N_{AH}-1). \\ 2(x_{q_m} \bmod q_m), & {e_t}^m = 1,\ 0 \le 2(x_{q_m} \bmod q_m) \le 2(N_{AH}-1). \\ 2y, & \text{otherwise}, \end{cases} \tag{5.2.8}$$

$$U_\beta = \begin{cases} 2(x_{p_m}+1 \bmod p_m)-1, & {e_t}^m = 0,\ 1 \le 2(x_{p_m}+1 \bmod p_m)-1 \le 2N_{AH}-1. \\ 2(x_{q_m}+1 \bmod q_m)-1, & {e_t}^m = 1,\ 1 \le 2(x_{q_m}+1 \bmod q_m)-1 \le 2N_{AH}-1. \\ 2y+1, & \text{otherwise}, \end{cases} \tag{5.2.9}$$

where $y = rand(N_{AH}-1)$, $x_{p_m} = t + p_m$ and $x_{q_m} = t + q_m$. Both TX and RX detect each other if the beams of both devices face each other as shown in Figs. 5.7 and 5.8. In Fig. 5.8, both TX and RX form two beams simultaneously. When the beams are formed in subsectors 2 and 3 of TX and RX, it is assumed that the devices have discovered each

other. It is to be noted that discovery time for AH is lower (1 time slot) than ODND (3 time slots) because the number of search sectors in AH is reduced when two simultaneous beams are formed.

$L_{odnd} = 3, Extended\ ID = 101, N_{AH} = 3, p_r = 5, q_r = 4$

t:	0	1	2	3	4	5	6	7	8	9	10	11
e_t^{RX}	1	0	1	1	0	1	1	0	1	1	0	1
U_α	0	2	4	2y	2y	2	4	4	0	2	0	2y
U_β	1	3	5	2y+1	2y+1	3	5	5	1	3	1	2y+1

$L_{odnd} = 3, Extended\ ID = 100, N_{AH} = 3, p_t = 5, q_t = 4$

t:	0	1	2	3	4	5	6	7	8	9	10	11
e_t^{TX}	1	0	0	1	0	0	1	0	0	1	0	0
V_α	0	2	4	2y	2y	0	4	4	2y	2	0	2
V_β	1	3	5	2y+1	2y+1	1	5	5	2y+1	3	1	3

$Discovery\ between\ TX\ and\ RX, U_\alpha = 2, U_\beta = 3, V_\alpha = 2, V_\beta = 3$

t:	0	1	2	3	4	5	6	7	8	9	10	11
U_α	0	2	4	2y	2y	2	4	4	0	2	0	2y
U_β	1	3	5	2y+1	2y+1	3	5	5	1	3	1	2y+1
V_α	0	2	4	2y	2y	0	4	4	2y	2	0	2
V_β	1	3	5	2y+1	2y+1	1	5	5	2y+1	3	1	3

Figure 5.8: Example of antenna scan sequences where TX and RX discover each other in slots 1 and 9.

Based on the antenna scan sequence, BF is implemented at both TX and RX. It is to be noted that when BF is implemented, (5.2.4) may no longer be valid. This is because the worst-case discovery delay is independent of the SNR, τ in (5.2.4). However, τ plays a vital role in device discovery and is the main focus of our study. The system model is summarized as follows.

The search area spanned by two TX beams at a given time instant is found as

$$\begin{aligned} \theta_{s_\alpha}^\circ &= 90^\circ - \left(\frac{U_\alpha}{2}\right) BW_{AH}^\circ, \\ \theta_{e_\alpha}^\circ &= 90^\circ - \left(\frac{U_\alpha + 1}{2}\right) BW_{AH}^\circ, \end{aligned} \tag{5.2.10}$$

$$\theta^{\circ}_{s_\beta} = 90^{\circ} - \left(\frac{U_\beta}{2}\right) BW^{\circ}_{AH},$$
$$\theta^{\circ}_{e_\beta} = 90^{\circ} - \left(\frac{U_\beta + 1}{2}\right) BW^{\circ}_{AH}, \tag{5.2.11}$$

where $\theta^{\circ}_{s_\alpha}$, $\theta^{\circ}_{e_\alpha}$ and $\theta^{\circ}_{s_\beta}$, $\theta^{\circ}_{e_\beta}$ mark the start and end of α and β beams, respectively. The direction of both the beams is given as

$$\phi_{t\alpha} = \theta^{\circ}_{e_\alpha} + \frac{\delta}{2},$$
$$\phi_{t\beta} = \theta^{\circ}_{s_\beta} - \frac{\delta}{2}. \tag{5.2.12}$$

The total BF gain and SNR is calculated by following eqs (4.2.8)- (4.2.12). The DD is calculated according to the number of time slots. Mathematically,

$$DD_{AH}(t) = (t+1)T_{sig} + (t)T_{per}, \tag{5.2.13}$$

It is to be noted that unlike the worst-case discovery delay given by ODND scheme in (5.2.4), the DD for AH cannot be upper-bounded. It is because the DD is highly dependent on the SNR as shown in Fig. 5.9.

Discovery between TX and RX, $U_\alpha = 2, U_\beta = 3, V_\alpha = 2, V_\beta = 3$

t:	0	1	2	3	4	5	6	7	8	9	10	11
U_α	0	2	4	2y	2y	2	4	4	0	2	0	2y
U_β	1	3	5	2y+1	2y+1	3	5	5	1	3	1	2y+1
V_α	0	2	4	2y	2y	0	4	4	2y	2	0	2
V_β	1	3	5	2y+1	2y+1	1	5	5	2y+1	3	1	3
τ	$< \gamma_{th}$	$< \gamma_{th}$	$< \gamma_{th}$	$< \gamma_{th}$	$< \gamma_{th}$	$< \gamma_{th}$	$< \gamma_{th}$	$< \gamma_{th}$	$< \gamma_{th}$	$\geq \gamma_{th}$	$< \gamma_{th}$	$< \gamma_{th}$

Figure 5.9: Example of TX and RX beam alignment in slot 1 but no device discovery as $\tau < \gamma_{th}$. Devices discover each other in slot 9 when $\tau \geq \gamma_{th}$

5.2.4 Auxiliary-Full

AF consists of two beams which are created within one main sector as shown in Fig. 5.2. The two beams are δ distance apart from each other. Hence, the scan sequence is calculated

as

$$U_\alpha(t_{even}) = \begin{cases} 2(x_{p_m} \bmod p_m), & {e_t}^m = 0,\ 0 \le 2(x_{p_m} \bmod p_m) \le 2(N_{AF}-1). \\ 2(x_{q_m} \bmod q_m), & {e_t}^m = 1,\ 0 \le 2(x_{q_m} \bmod q_m) \le 2(N_{AF}-1). \\ 2y, & \text{otherwise}, \end{cases} \tag{5.2.14}$$

$$U_\beta(t_{odd}) = \begin{cases} 2(z_{p_m} \bmod p_m)+1, & {e_{t-1}}^m = 0,\ 1 \le 2(z_{p_m} \bmod p_m)+1 \le 2N_{AF}-1. \\ 2(z_{q_m} \bmod q_m)+1, & {e_{t-1}}^m = 1,\ 1 \le 2(z_{q_m} \bmod q_m)+1 \le 2N_{AF}-1. \\ 2y+1, & \text{otherwise}, \end{cases} \tag{5.2.15}$$

where $U_\alpha(t_{even})$ and $U_\beta(t_{odd})$ are the $beam_\alpha$ and $beam_\beta$ formed at even and odd time slots, respectively, $y = rand(N_{AF}-1)$, $z_{p_m} = x_{p_m} - 1$ and $z_{q_m} = x_{q_m} - 1$. It is to be noted that the starting time index is assumed to be $t = 0$ or any even index. However, if the starting time index is odd then (5.2.14) and (5.2.15) are interchanged, i.e., (5.2.14) is used for odd indices and (5.2.15) is used for even index calculation.

Similar to AH, the search area spanned by both RX and TX is calculated according to (5.2.10)-(5.2.12). However, the BF gain at RX and TX is calculated independently in each time slot by following eq. (4.2.14). Also, the SNR for each time slot is determined through eqs. (4.2.8)-(4.2.11). Similar to AH, AF is also dependent on SNR for device discovery as shown in Fig. 5.10. Thus, the DD_{AF} is calculated according to (5.2.13) for each time slot.

$L_{odnd} = 3, N_{AF} = 7, p_r = 7, q_r = 8.$ *Discovery between TX and RX,* $U_\alpha = 0, V_\alpha = 2$

t:	0	1	2	3	4	5	6	7	8	9	10	11
U_α	0		4		8		12		0		4	
U_β		1		5		9		13		1		5
V_α	0		4		8		12		2		4	
V_β		1		5		9		13		3		5
τ	$< \gamma_{th}$	$< \gamma_{th}$	$< \gamma_{th}$	$< \gamma_{th}$	$< \gamma_{th}$	$< \gamma_{th}$	$< \gamma_{th}$	$< \gamma_{th}$	$\geq \gamma_{th}$	$< \gamma_{th}$	$< \gamma_{th}$	$< \gamma_{th}$

Figure 5.10: Example of antenna scan sequences where TX and RX discover each other in slot 8 when $\tau \geq \gamma_{th}$

5.3 Non-Sequential Search

In non-sequential search, we analyze the performance of AH, AF, ODND and Polya's Necklaces in terms of DD and PMD. Both transmitter and receiver employ a ULA with $N_r = N_t = 4$ antenna elements. The distance between TX and RX is set as $r = 15m$. The simulation paramters are same as given in Table 4.1. The simulation results are as follows

5.3.1 ODND vs. AH

Fig. 5.11 shows the PMD performance for ODND and AH against γ_{th}. The values of $L_{odnd} = L_{AH} = 3$ is calculated according to (5.2.2) for ODND and AH. For two devices, E is calculated according to (5.2.1) such that ${e_t}^r = 101$ and ${e_t}^t = 100$. During one Monte Carlo simulation, both TX and RX keep scanning the region until the devices have not discovered each other or the worst-case discovery delay is not reached according to (5.2.4). For AH, we calculate the worst-case delay in a similar way as given in (5.4.4) for better understanding of the DD upper-bound proposed in [66]. In ODND, the RX and TX utilize all the antenna elements to form one beam, hence, the PMD is low for ODND. The BF gain at both TX and RX is high and there is high probability of device detection since the SNR is high. On the other hand, the PMD=0 for lower values of γ_{th} when AH scheme is employed. Although the BF gain is low for AH but for lower values of γ_{th}, both TX and RX keep scanning the region for maximum time slots ($W = L_{AH}p_rq_t$) and detect each other within this time. However, as the γ_{th} increases beyond $22dB$, it becomes difficult for AH to detect the devices because of low BF gain. Hence, even after scanning the region for maximum time slots, TX and RX cannot find each other all the time. So, the PMD is higher as compared to ODND.

It is to be noted that the worst-case discovery delay does not ensure 100% device discovery for both ODND and AH. Hence, the upper-bound given in (5.2.4) is not always valid. The discovery process in highly dependent on the SNR. In [66] the SNR parameter is not considered while calculating the upper-bound, hence worst-case discovery delay does not always ensure device detection. Fig. 5.12 shows that the DD is the least for AH with $\delta = 25°$. It is because the beamwidth has increased due to increased separation between $beam_\alpha$ and $beam_\beta$. This in turn increases the coverage area. Hence, it takes less time to scan the region. However, it is to be noted that for lower values of γ_{th}, AH with variable

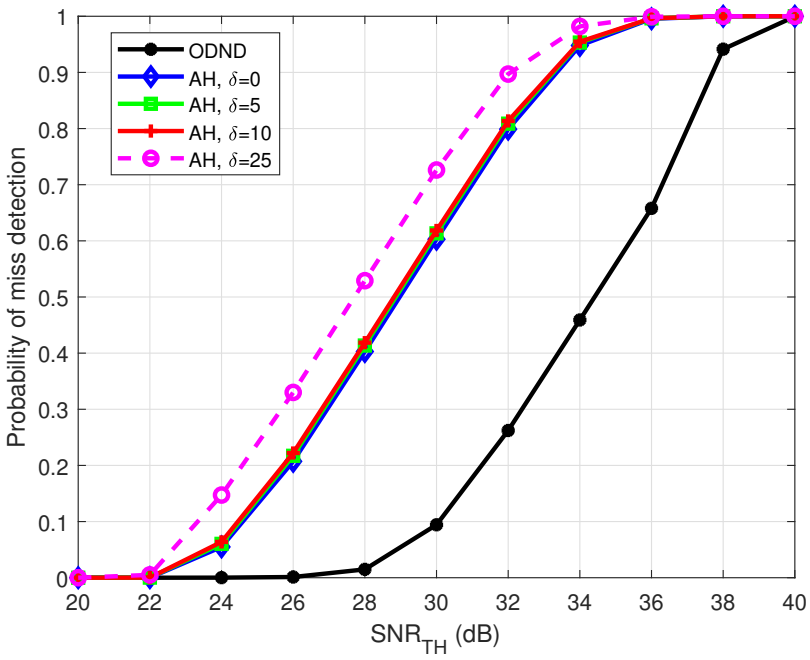

Figure 5.11: PMD for ODND and AH with variable δ

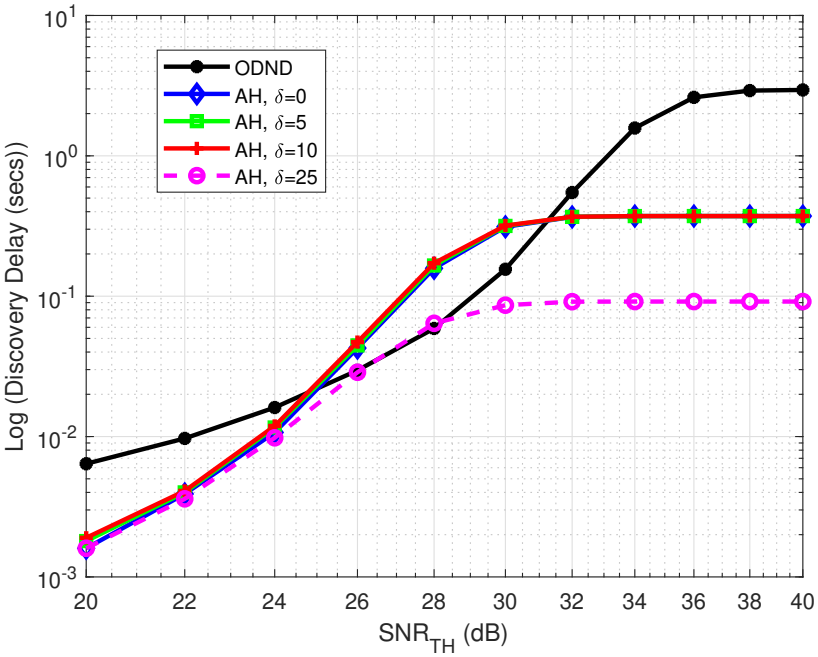

Figure 5.12: DD for ODND and AH with variable δ

δ still performs better than ODND. It is due to the fact that the γ_{th} value is low and even with low BF gain, AH can discover the devices. But for $\gamma_{th} = 26dB$ it is seen that ODND starts performing better than AH with $\delta = 0°, 5°, 10°$. It is because since the γ_{th} is high,

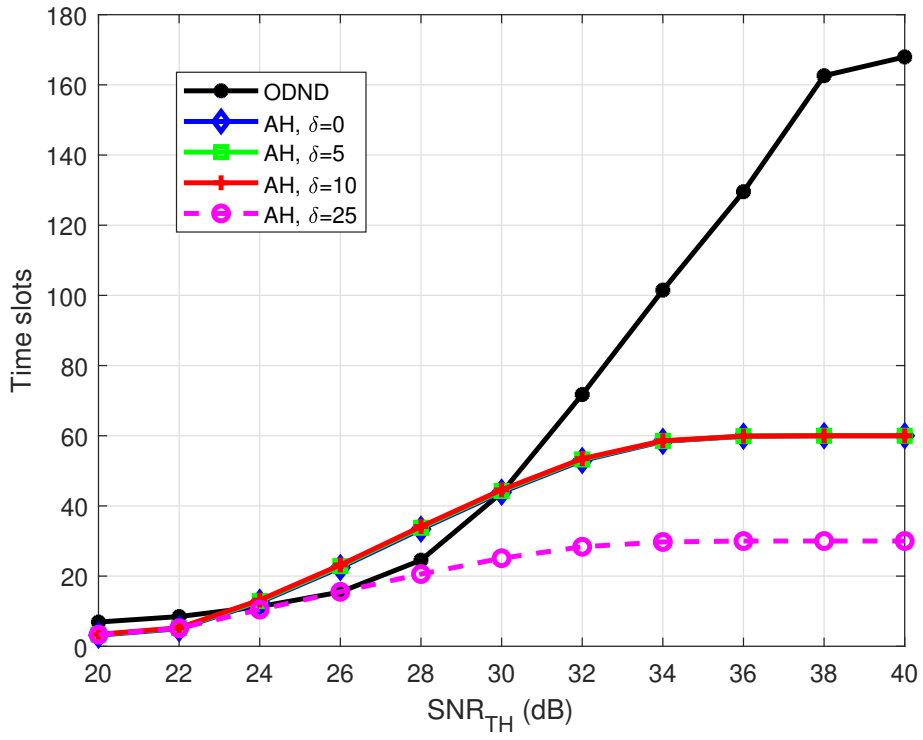

Figure 5.13: Time slots required for device discovery in ODND and AH with variable δ

it becomes difficult for AH to detect a device because of low BF gain. AH has to scan maximum time slots (as shown in Fig. 5.13) to detect a device, hence it takes more time during each Monte Carlo simulation. Whereas, since the BF gain is high for ODND, it can scan and detect the user within short span (does not need to scan region for maximum time slots) as shown in Fig. 5.13. It can detect a user quickly as compared to AH, so the DD is low for ODND. However, for $\gamma_{th} > 30dB$, even ODND cannot detect the devices because the BF gain is not enough, so ODND takes more time to scan a region as compared to AH (as shown in Fig. 5.13). Therefore, the DD is highest for ODND at $\gamma_{th} > 30dB$.

5.3.2 ODND vs. AF

Fig. 5.14 shows that for lower values of SNR, both ODND and AF performs the same. However, for $\gamma_{th} > 26dB$, AF performs better than ODND because AF is scanning one sector twice which increases the probability of detection. Also, for $\gamma_{th} = 40dB$, both ODND and AF show similar results since the γ_{th} value is very high and the signal strength for both ODND and AF is low, hence the PMD is high.

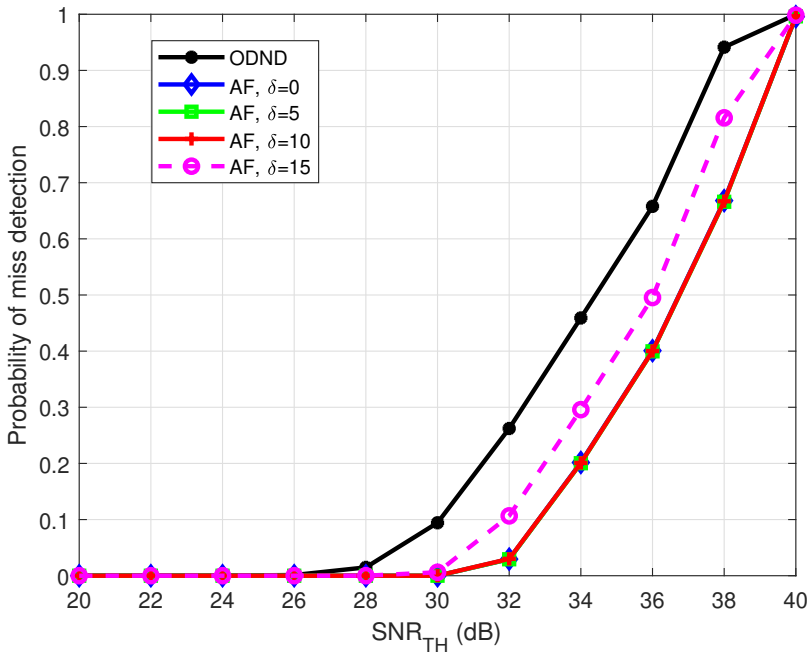

Figure 5.14: PMD for ODND and AF with variable δ

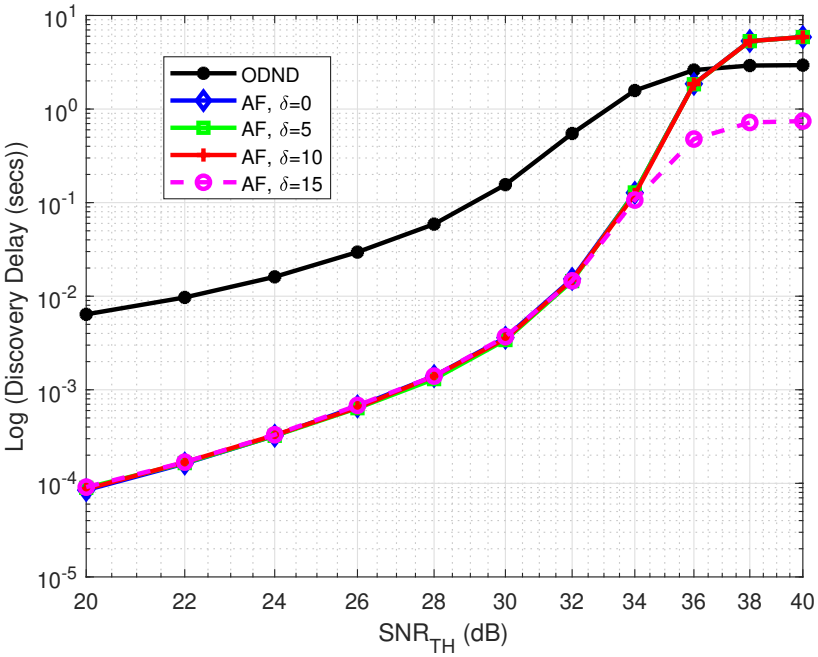

Figure 5.15: DD for ODND and AF with variable δ

In Fig. 5.15, for lower values of γ_{th} , AF performs better than ODND because AF scan a sector twice, hence the probability of detection in a short span increases. Therefore, DD is low. For higher values of γ_{th} , AF with $\delta = 0°, 5°, 10°$, performs worse than ODND because

the separation between two beams is not significant. AF keeps scanning one sector twice, hence the number of time slots increases as compared to ODND. On the other hand when $\delta = 15°$, then the beamwidth is high and AF can scan a region in less time as compared to ODND, so the DD is low.

5.3.3 Polya's Necklaces vs. AH

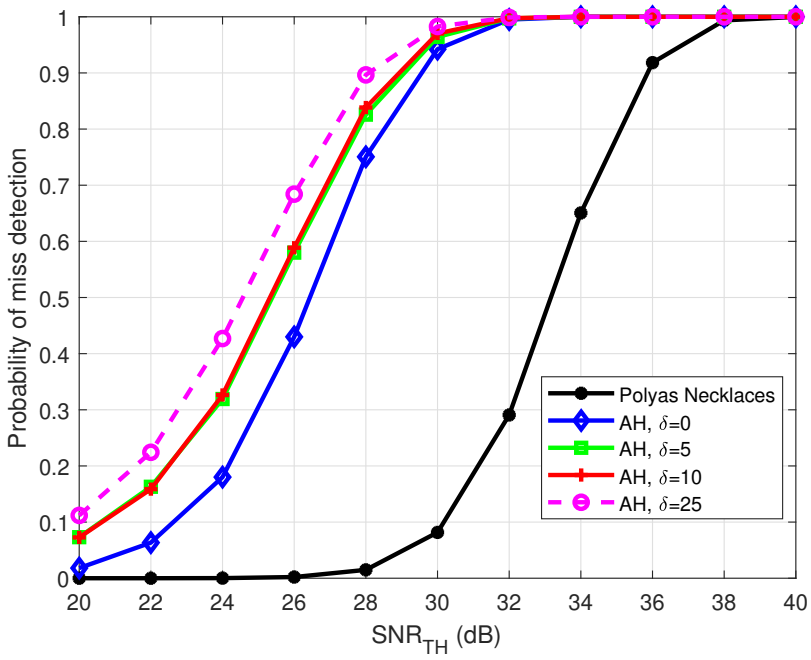

Figure 5.16: PMD for Polya's necklaces and AH with variable δ

In Polya's Necklaces scheme, the length of extended address in reduced i.e. $L_{poly} = 1$. We analyze both Polya's Necklaces and AH schemes with respect to this new length. Fig. 5.16 shows that the PMD is the lowest for Polya's scheme because BF gain is high. All antenna elements combine to form one beam at TX and RX, therefore the signal strength is higher for Polya's Necklaces. Whereas, the AH utilizes two simultaneous beams with reduced BF gain, hence the PMD is high. Fig. 5.17 shows that the DD is low for all values of δ in AH. It is because the beamwidth increases by increasing δ, hence it takes short time to scan a region. Whereas, the DD is high for Polya's Necklaces for all values of SNR. Here all antenna elements form a beam which is a narrow beam as compared to AH. Therefore, it takes more time to discover a device. It is to be noted that when the length of extended address is reduced, the performance of AH is better than both Polya's Necklaces and ODND in terms of DD.

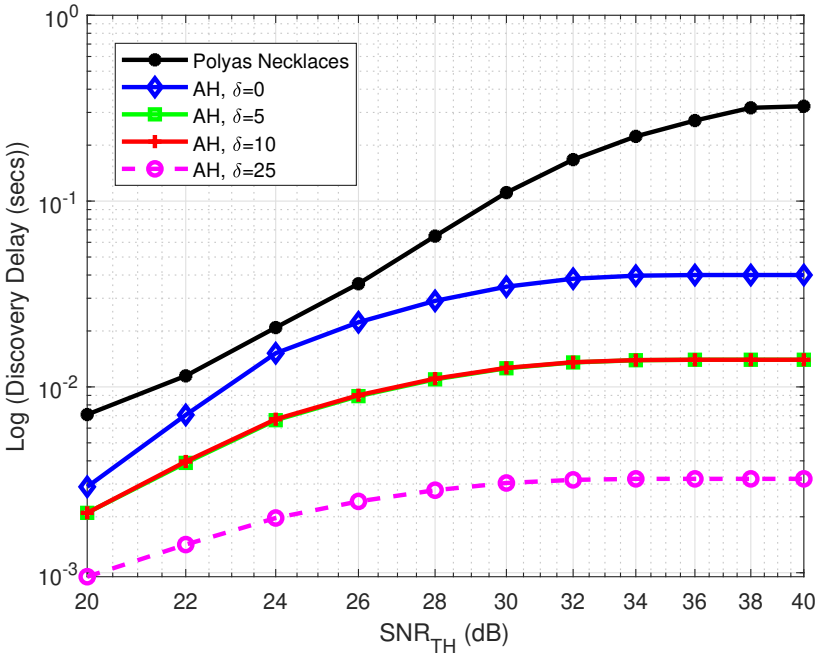

Figure 5.17: DD for Polya's necklaces and AH with variable δ

5.3.4 Polya's Necklaces vs. AF

Fig 5.18 shows that for AF with variable δ, the performance is better then Polya's Necklaces. AF scans a sector twice, which increases the probability of detection. Hence, the performance is better for any value of SNR.

The DD is lowest for AF with $\delta = 15°$ as shown in Fig. 5.19. It is because the beamwidth is increased, and it takes less time to scan the region. Whereas, the DD is highest for AF with $\delta = 0°, 5°$ when $\gamma_{th} > 35dB$ because the separation between beams is not significant. The beamwidth of AF is almost similar to beamwidth of Polya's Necklaces. Hence, when AF scans each sector twice, it takes more time to discover a device. Whereas, Polya's Necklaces can scan the region quickly, hence the DD is low.

5.3.5 Probability of miss detection and discovery delay vs. SNR

Figs. 5.20 and 5.21 show the behavior of PMD and DD for all schemes with $\delta = 15°$, $N_r = N_t = 8$ and $r = 50m$, respectively. In Fig. 5.20, it is observed that as the γ_{th} increases, the PMD starts increasing as well due to low BF gain. AH performs the worst in terms of PMD because the antenna array is split into two parts which reduces the BF gain as compared to ODND, Polya's Necklaces and AF. However, AF performs the best due

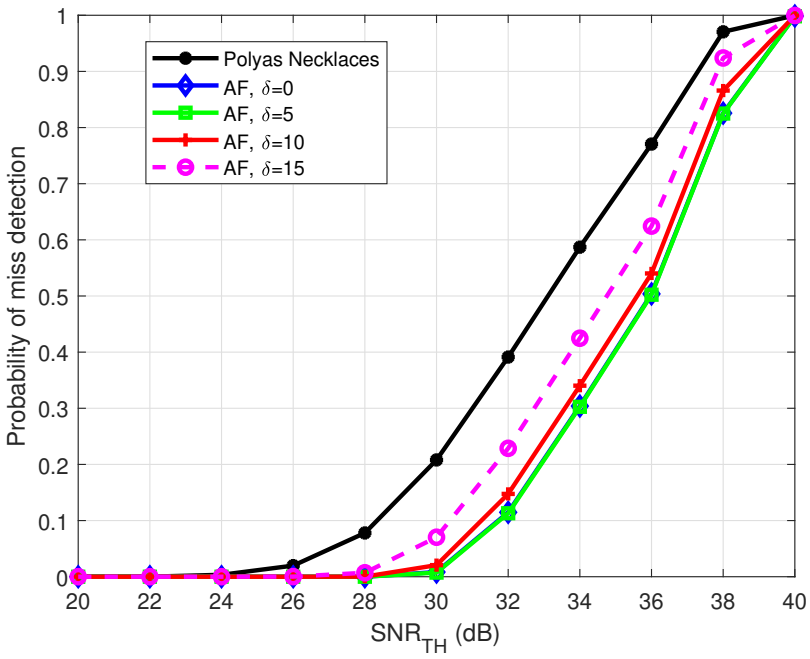

Figure 5.18: PMD for Polya's Necklaces and AF with variable δ

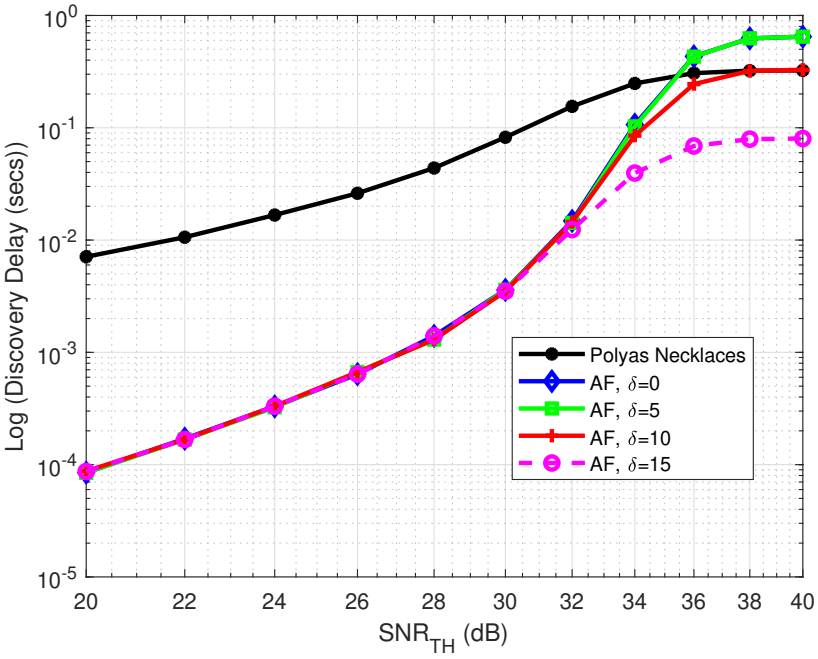

Figure 5.19: DD for Polya's Necklaces and AF with variable δ

to time diversity and by utilizing all the antenna elements of the ULA. AF_{odnd} performs better than AF_{poly} because the number of time slots is very high in AF_{odnd} as compared to AF_{poly}. It takes less time to scan the whole region through AF_{poly}, hence the PMD is high

than AF_{odnd}. Fig. 5.21 shows that AH_{poly} gives the best discovery delay due to reduced time slots as compared to AH_{odnd} and all other schemes. Whereas, ODND takes more time to discover a device due to high number of time slots. Since, AF_{odnd} scans a region twice so the probability of discovering a device in shorter time span increases. Hence, AF_{odnd} performs better than both ODND and Polya's Necklaces.

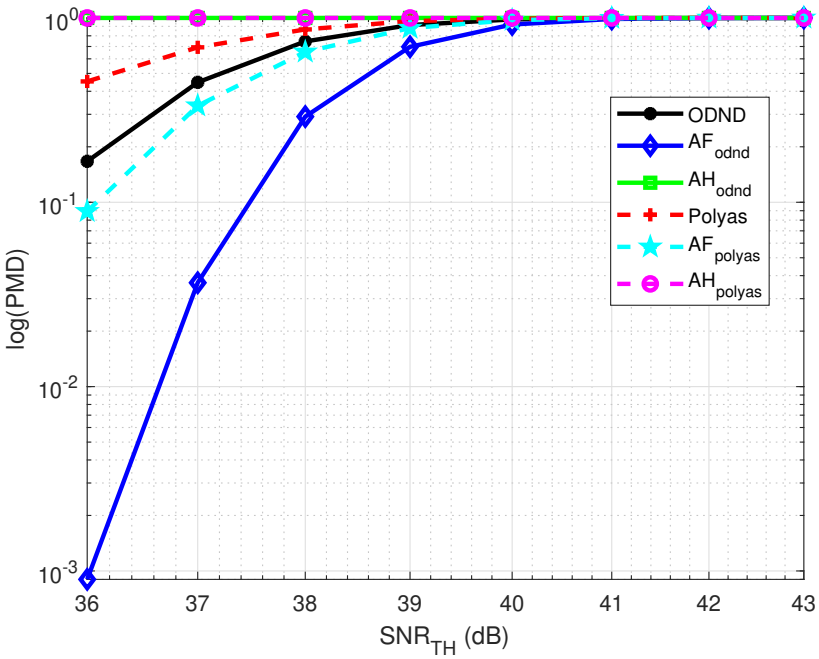

Figure 5.20: PMD for all schemes

5.3.6 Probability of miss detection vs. Number of antennas

Fig. 5.22 shows the PMD versus the number of antenna elements at both TX and RX. The values of δ, r and γ_{th} are taken as 15°, $40m$, and $38dB$, respectively. It is observed that the PMD is highly dependent on the number of antennas in the ULA. When the number of antennas is small, the device discovery is not possible because the BF gain is very low. Hence, the PMD is very high. However, as the number of antenna elements increases, the BF gain becomes high and the PMD starts decreasing. The AH scheme performs the worst due to wide beams and low BF gain, whereas, AF outperforms all other schemes due to narrow beams, time diversity and high BF gain with respect to various antenna elements.

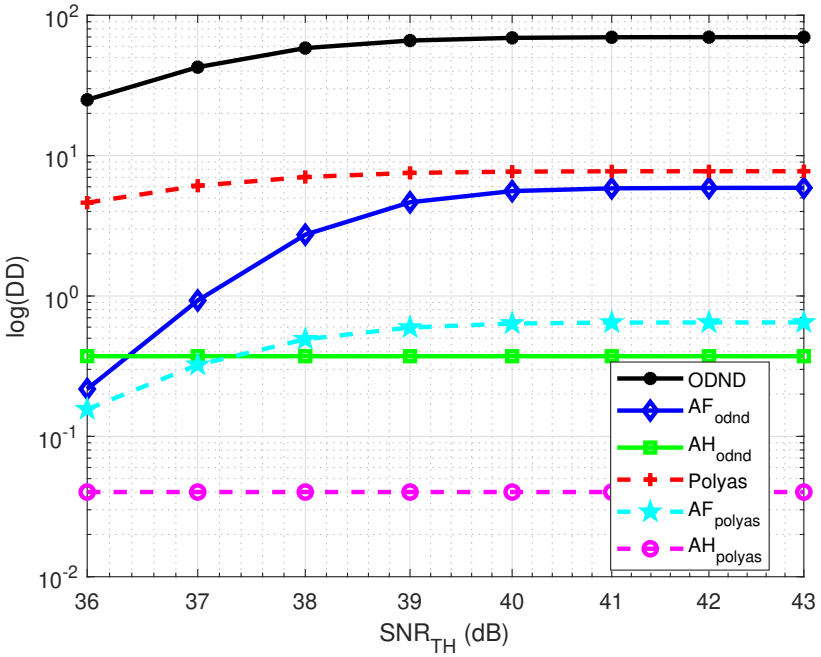

Figure 5.21: DD for all schemes

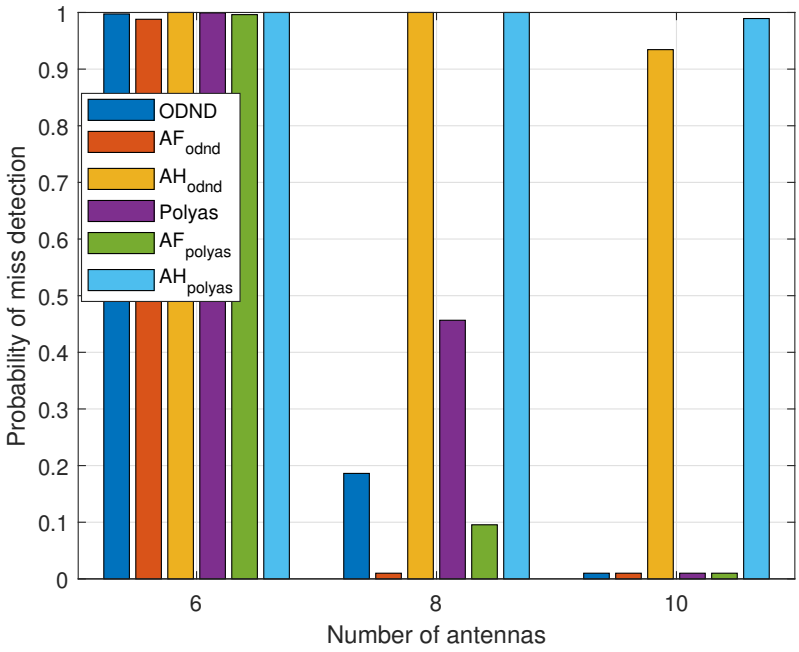

Figure 5.22: PMD for varying number of antennas

5.3.7 Time slots vs. Distance between RX and TX

Fig. 5.23 shows the number of time slots required to detect a device for variable TX-RX separation. The values of δ, N_r, N_t and γ_{th} are taken as 10°, 8, 8 and $30dB$, respectively.

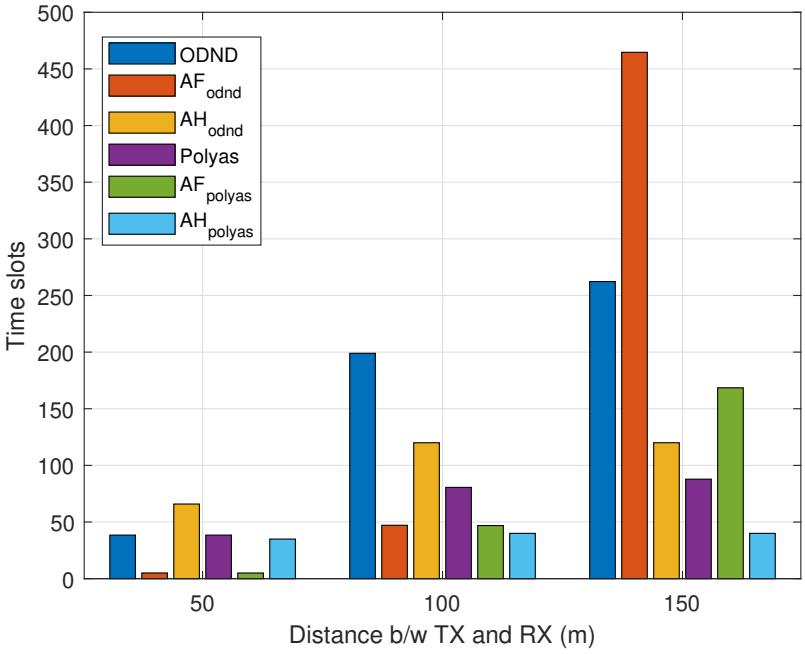

Figure 5.23: Time slots required for device detection for all schemes

It is observed that both AF_{odnd} and AF_{poly} require the least number of time slots for device detection. Since, AF utilizes the full antenna array and time diversity, hence it can detect a device quickly when the distance between TX and RX is small. However, as the distance starts increasing, AF_{odnd} takes more time to scan a region as AF_{odnd} scans twice the time slots as compared to ODND. On the other hand, all other schemes can scan the entire region according to the maximum number of time slots as given by (5.2.4). The maximum time slots for ODND, Polya's Necklaces and AH is less than AF because of time diversity in AF.

5.4 Conclusions

In this chapter, we have analyzed and compared the performance of different IA schemes, i.e., ODND, Polya's Necklaces and ABP schemes for D2D in mmWave systems. The numerical results show that the proposed ABP schemes are highly dependent on the beam separation, δ, that has a significant impact on the DD and PMD performance. AH achieves a lower DD than all other schemes for higher values of γ_{th} and r, whereas, AF outperforms all other schemes in terms of PMD for a moderate δ value. AF also provides a lower DD as compared to ODND, Polya's Necklaces and AH for a lower γ_{th} and r. Furthermore, we showed that the DD is highly dependent on the SNR which contradicts the worstcase DD upper-bound

proved by ODND algorithm.

Chapter 6

Optimal Beam Separation in Auxiliary Beam Pair-based Initial Access in mmWave D2D Networks

In this chapter, we propose the optimization of beam separation in ABP schemes to optimize the device discovery process in a mmWave D2D network. BF is employed at both TX and RX and both TX and RX discover each other through non-sequential scanning of the desired region. Antenna scan sequences are generated for AH and AF schemes and the performance is evaluated by varying the separation between a beam pair. This work has also been published in IEEE Vehicular Technology Conference (2020) [106]. The details are as follows.

6.1 Beamforming at TX and RX

6.1.1 Auxiliary-Half

BF is implemented at TX and RX through ULA. The radiation pattern for two simultaneous beams is given as

$$Y_{x\alpha} = \frac{sin(N_{x1}\pi d(sin(\theta) - sin(\phi_{x\alpha}))/\lambda)}{N_{x1} \times sin(\pi d(sin(\theta) - sin(\phi_{x\alpha}))/\lambda)}, \tag{6.1.1}$$

$$Y_{x\beta} = \frac{sin(N_{x2}\pi d(sin(\theta) - sin(\phi_{x\beta}))/\lambda)}{N_{x2} \times sin(\pi d(sin(\theta) - sin(\phi_{x\beta}))/\lambda)}, \tag{6.1.2}$$

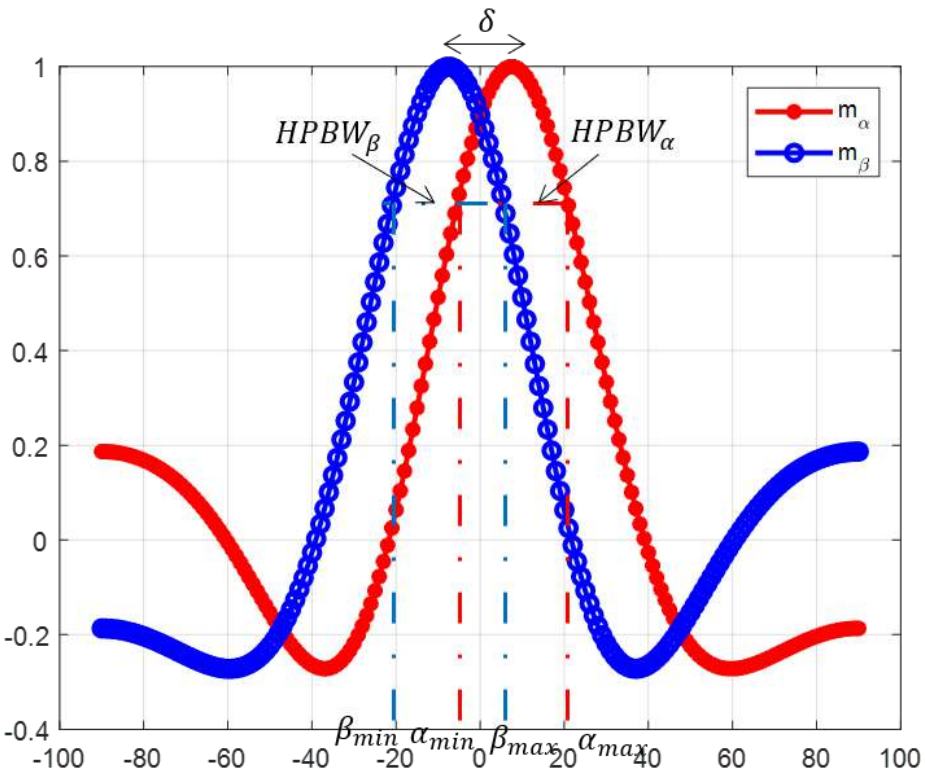

Figure 6.1: Beamwidth estimation for AH scheme

where $x \in \{TX, RX\}$, N_{x1} and N_{x2} are the antenna elements that generate α_x and β_x, respectively. For IA, the total scan region of both TX and RX is split into a number os search sector. Mathematically,

$$N_{AH} = \frac{180^\circ}{BW^\circ_{AH}}, \tag{6.1.3}$$

where BW°_{AH} is the beamwidth. BW°_{AH} is calculated by finding the HPBW of both α_x and β_x and then determining the minimum and maximum points of both beams as shown in Fig. 6.1. Mathematically

$$HPBW^\circ_\alpha = \frac{50.8^\circ}{(N_{x1} d cos(\delta/2)/\lambda)}, \tag{6.1.4}$$

$$m_\alpha = \frac{\delta}{2} \pm \frac{HPBW^\circ_\alpha}{2}, \tag{6.1.5}$$

where $HPBW^\circ_\alpha$ is obtained by equating (6.1.1) or (6.1.2) to $1/\sqrt{2}$ and solving for θ [102]. δ is the separation between α_x and β_x and $m_\alpha \in \{\alpha_{min}, \alpha_{max}\}$. The starting and ending points of α_x are represented by α_{min} and α_{max}, respectively. Similar calculations follow for $HPBW^\circ_\beta$ and BW°_{AH} is calculated as

$$BW^\circ_{AH} = [\beta_{min}, \alpha_{max}]. \tag{6.1.6}$$

where β_{min} is the starting point of BW°_{AH} and α_{max} is the ending value.

The antenna scan sequence and BF direction is calculated by following (5.2.8)- (5.2.12).The total BF gain of RX and TX is calculated as

$$G_{rBF} = |Y_{r\alpha}|^2 + |Y_{r\beta}|^2, \tag{6.1.7}$$

$$G_{tBF} = |Y_{t\alpha}|^2 + |Y_{t\beta}|^2, \tag{6.1.8}$$

$$G_{BF}(dB) = \max\,(G_{rBF} + G_{tBF}) - 3dB. \tag{6.1.9}$$

The total BF gain is assumed constant in a search sector at a particular time. Hence, the total antenna gain G is given as

$$G(dB) = G_{TX} + G_{RX} + G_{BF}, \tag{6.1.10}$$

The SNR is calculated similar to (4.2.9)-(4.2.11) and the discovery delay is estimated through (5.2.13).

6.1.2 Auxiliary-Full

A full antenna array is utilized to generate ABP is two different time slots at both TX and RX. The radiation pattern and beamwidth in different time slots is calculated through Eqs. (6.1.1)-(6.1.6) by utilizing N_x antenna elements in each time slot. The antenna scan sequence is generated according to (5.2.14)-(5.2.15). The total BF gain is calculated individually for each time slot, i.e.,

$$G_{\alpha-rBF}(t_1) = |Y_{r\alpha}(t_1)|^2, \tag{6.1.11}$$

$$G_{\alpha-tBF}(t_1) = |Y_{t\alpha}(t_1)|^2. \tag{6.1.12}$$

According to the calculated BF gain in t_1, γ is determined according to (4.2.12) and DD_{AF} is determined by (5.2.13)

6.2 Simulation Results

For optimal beam separation, we analyze the performance of AH and AF in terms of DD and PMD for variable δ. The value of δ highly impacts the BF gain. For example, when δ is small the overlapping between α_x and β_x is high, resulting in increased BF gain. Also,

TX and RX form beam pairs according to δ and scan the desired region for finite time slots. Hence, the maximum number of time slots are calculated as

$$T = L \max\{p_r q_t, p_t q_r\}. \tag{6.2.1}$$

It is to be noted that $L \in \{L_{odnd}, L_{poly}\}$. We have assumed $N_x = 6$ and the RX-TX separation is set as $r = 250m$. The simulation parameters are same as shown in Table 4.1.

6.2.1 PMD with variable δ_r and δ_t for AH

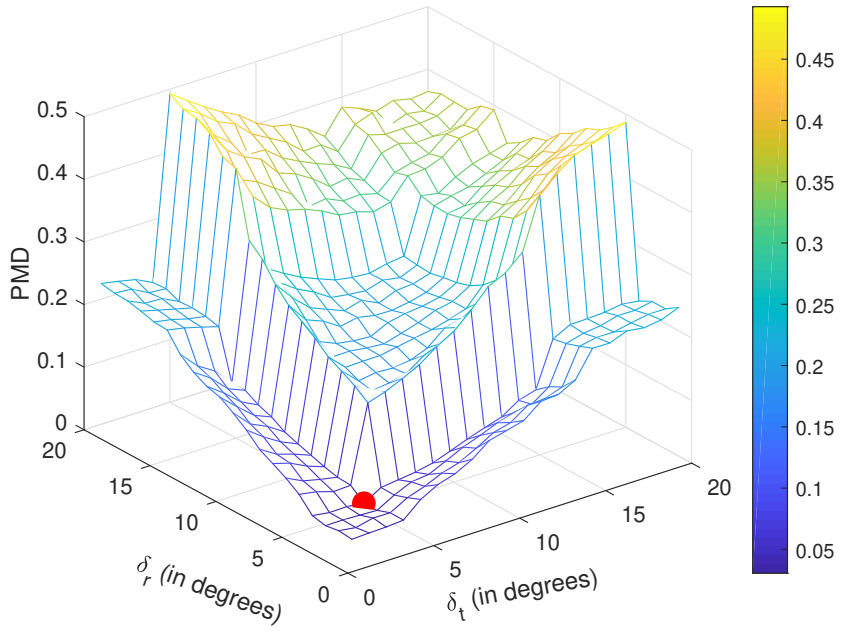

Figure 6.2: PMD vs. variable δ_t, δ_r and L_{odnd} for AH.

Fig. 6.2 shows the PMD for variable δ_t and δ_r with L_{odnd} and $\gamma_{th} = 13dB$. It is shown that the PMD is not least when $\delta_t = 1°$ and $\delta_r = 1°$. However, the minimum PMD is obtained when $\delta_t = 4°$ and $\delta_r = 4°$, because for this combination the beams are a bit wide but still have a high BF gain. The probability of wide beams facing each other is more than narrow beams. However, for higher values of δ, the beamwidth increases which reduces the BF gain, thereby, increasing PMD. In Fig. 6.3, the PMD is evaluated utilizing L_{poly} and the optimum value is obtained for $\delta_t = 4°$ and $\delta_r = 4°$. It is to be noted that the PMD is high when L_{poly} is utilized, i.e., at optimal δ, the PMD is 55% for L_{poly} compared to PMD of 3% for L_{odnd}. Since, the maximum time slots for scanning a region are less for L_{poly}, the beams scan the region for a short time period, and therefore increases the PMD.

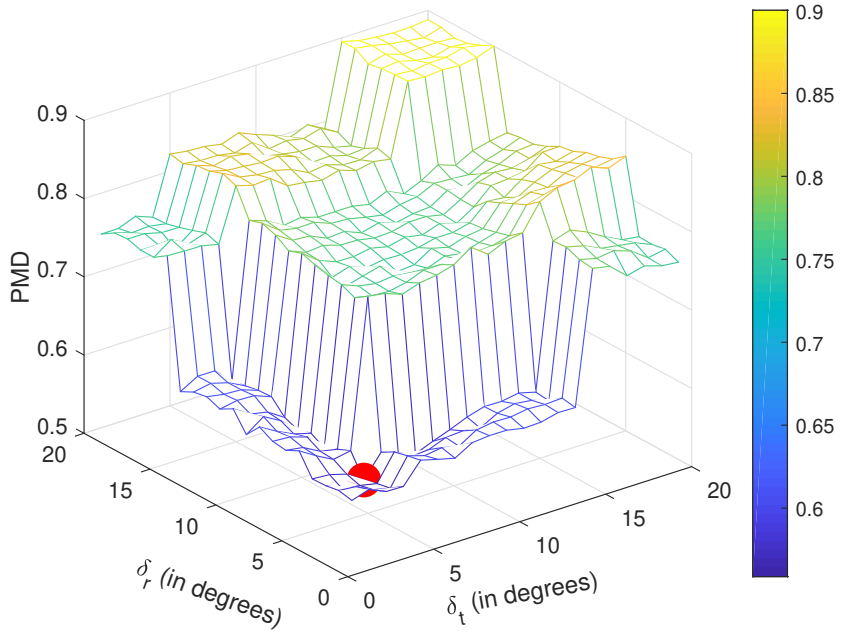

Figure 6.3: PMD vs. variable δ_t, δ_r and L_{poly} for AH.

6.2.2 DD with variable δ_r and δ_t for AH

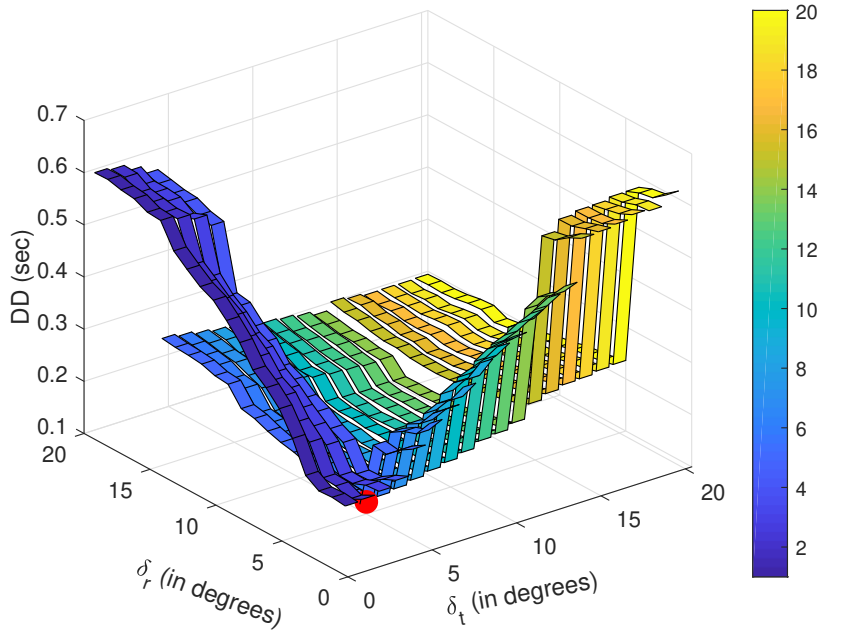

Figure 6.4: DD vs. variable δ_t, δ_r and L_{odnd} for AH.

Fig. 6.4 shows the DD for L_{odnd} and variable δ_r, δ_t. It is observed that the DD is minimized

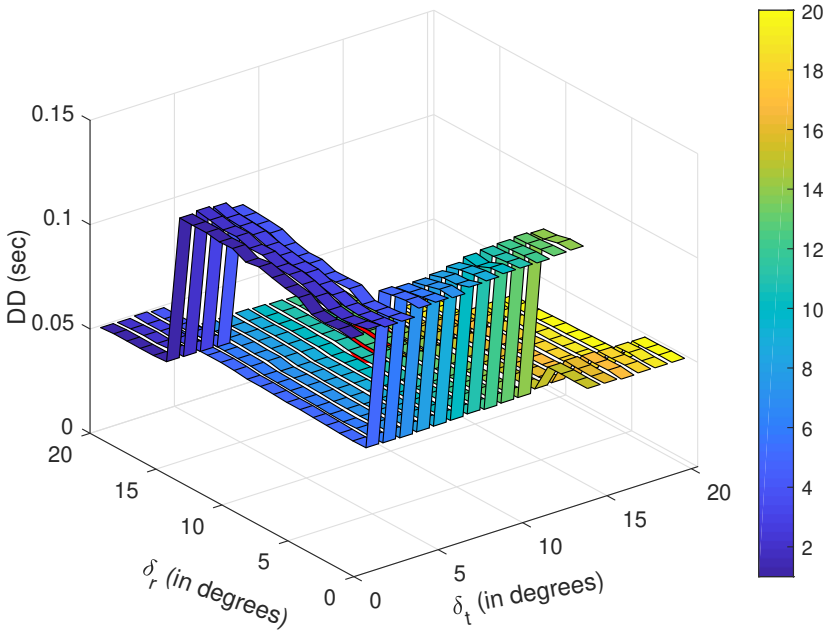

Figure 6.5: DD vs. variable δ_t, δ_r and L_{poly} for AH.

for $\delta_t = 5°$ and $\delta_r = 5°$. It is because for this combination, the beams are wide but have a considerable BF gain, hence it takes, on average, less time to detect each other. The maximum time slots required for this combination is calculated as $T = 60$ according to (6.1.7). It is observed that although $T = 60$ is also the maximum limit for other combinations where $\delta_t > 5°$ and $\delta_r > 5°$, yet the DD is not least. It is because, as δ increases, the beams are more wide but the BF gain is very low. Hence, it takes on average more time slots to scan before the devices discover each other. Fig. 6.5 shows the DD for L_{poly} and the optimum value is obtained for $\delta_t = 15°$ and $\delta_r = 18°$. Since, the maximum time slots for L_{poly} are less than L_{odnd}, it takes less time for beams to scan the entire region. Hence, the DD obtained at optimum values of L_{poly} and L_{odnd} is 0.01261 sec and 0.1232 sec, respectively.

6.2.3 PMD and DD with variable δ_r and δ_t for AF

Fig. 6.6 shows the PMD for AF with $\gamma_{th} = 23dB$. In AF, two beams are generated by utilizing the full antenna array in a time-division manner. It is observed that AF shows similar trend as AH, i.e., PMD is least for $\delta_t = 3°$ and $\delta_r = 3°$ due to high BF gain. As the beam separation starts increasing, the PMD also increases. In Fig. 6.7, the optimum value of DD is obtained for $\delta_t = 20°$ and $\delta_r = 20°$. DD is minimized for this combination

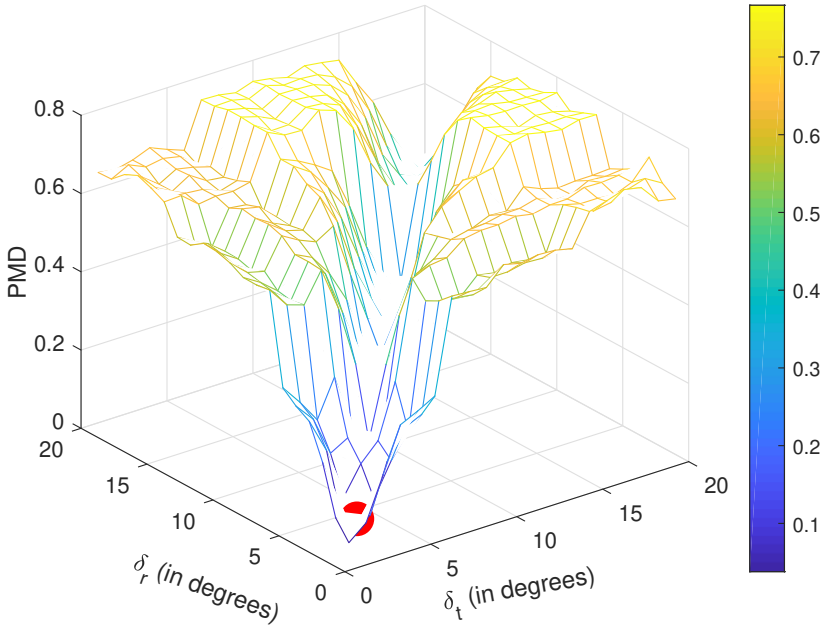

Figure 6.6: PMD vs. variable δ_t, δ_r and L_{odnd} for AF.

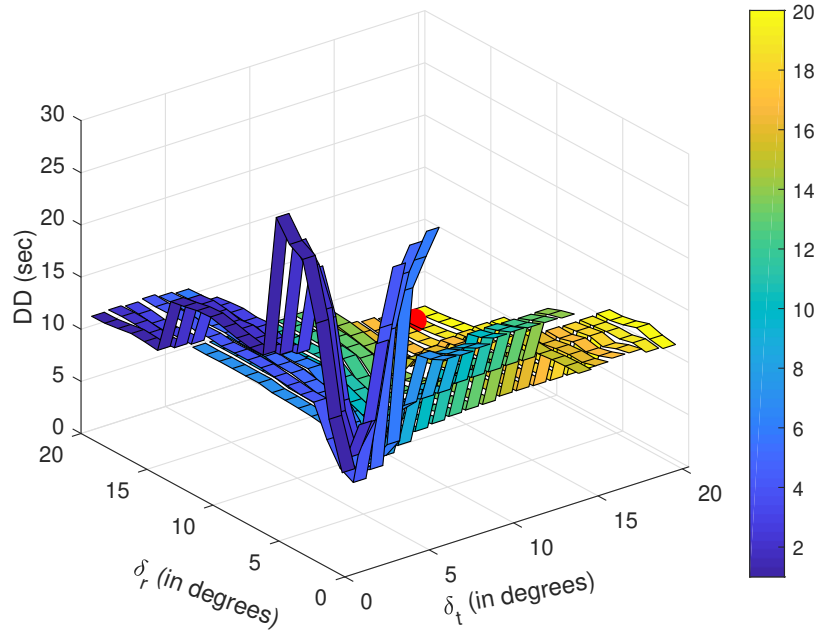

Figure 6.7: DD vs. variable δ_t, δ_r and L_{odnd} for AF.

because the beams are very wide and it takes very few time slots to scan the desired region. Since, AF utilizes all antenna elements so the BF gain is higher than AH and even with wide beams, the devices can discover each other in a shorter time span.

6.3 Conclusions

In this chapter, we have studied the performance of PMD and DD with respect to variable beam separation for AF and AH schemes. Simulation results show that the PMD and DD are minimized for a suitable combination of beam separation. A minimum beam separation does not ensure a minimum PMD or DD. The optimal combinations of δ_t, δ_r for both PMD and DD are highly dependent on the SNR threshold, $TX - RX$ separation, number of antenna elements and the maximum number of time slots allowed for beam sweeping in AH and AF schemes.

Chapter 7

Conclusions and Future Work

In this dissertation, we highlight the importance of initial access in a mmWave system. IA is a mechanism that helps the BS and users to connect with each other for successful link establishment. Therefore, IA should be a time saving mechanism that helps BS and users to discover each other as soon as possible. Our analysis revolves around this aspect of IA where we propose algorithms that help minimize the discovery delay and probability of miss detection. Some well know IA algorithms such as exhaustive search, iterative search, hybrid search, auxiliary beam pair-based search are proposed in literature, but they do not cover the aspects of DD and PMD in a detailed and efficient manner. Our proposed algorithms focus on the missing aspects in current literature by developing two novel auxiliary beam pair-based IA schemes in mmWave system. The two algorithms, i.e., auxiliary-half and auxiliary-full perform beamforming by a suitable combination of antenna arrays. AH splits the antenna array in two parts, whereas, AF utilizes the full array in a time division manner. The proposed schemes flow and performance analysis is summarized in different phases as following.

7.1 Phase 1

Two novel schemes, i.e., AH and AF are proposed, and a complete mathematical model is presented. Auxiliary beam pairs are formed at the BS side only by utilizing the ULA. The user utilizes the omnidirectional antenna. The BS performs sequential search algorithm and discover the user by sweeping the beam-pair in clockwise direction. We develop a mathematical model for the existing schemes in literature as well, i.e., exhaustive and iterative

search methods. The simulation results show a high dependence on the separation between the beam pairs for both AH and AF. AH is a balance between iterative and exhaustive search methods, i.e., it achieves a lower PMD than exhaustive scheme and a lower DD then iterative method. Moreover, AF performs the best as compared to all other schemes in terms of PMD. AF also has a low DD than exhaustive method.

7.2 Phase 2

BF is implemented at both TX and RX for a D2D network. The mathematical model proposed in paper 1 is extended for the RX side as well. We propose novel antenna scan sequences for both AH and AF schemes. Both TX and RX perform non-sequential search by the generation of antenna scan sequences. BF is also implemented in the existing techniques of ODND and Polya's necklaces for a comprehensive comparison. The simulations results show that both AH and AF exhibit high dependence on beam pair separation. We also prove that DD is highly dependent on the SNR, contrary to the worst-case DD upper bound proposed in ODND scheme. It is shown that AH achieves lower DD as compared to all other schemes for a reasonable beam-pair separation, high TX-RX distance and high SNR threshold. Also, for low RX-TX distance, low SNR threshold and considerable beam-pair separation, AF achieves the least DD than all other schemes. AF also outperforms all other schemes in terms of PMD.

7.3 Phase 3

For a D2D network, the optimal beam pair separation value that achieves the lowest DD and PMD is investigated in this paper. AH and AF implement BF at both TX and RX. The device discovery process takes place thought the generation of antenna scan sequences. Optimum values of DD and PMD are obtained through a suitable combination of beam pair separation. It is also proved that the narrowest existing beam separation value at both TX and RX do not improve the DD in either AF or AH schemes.

7.4 Future Work

The work in this dissertation can be extended in multiple directions. Some of the proposed future work ideas are as follows.

- To extend the work of phase 3 by solving an optimization problem for beam-pair separation. An optimization problem is to be solved that finds an optimal beam pair combination that maximizes the SNR. A unique combination of beam pair separation should exist at both TX and RX that minimizes the probability of miss detection. The optimization problem can be solved through langrage method under certain constraints on number of antenna elements, transmit power, TX-RX separation etc.

- The existing work is focused on fixed TX-RX separation and stationary devices. The BF algorithms can be implemented on mobile devices in the network with random distance between them. The effect of BF gains and beam pair separation will be interesting parameters to explore in a mobile D2D environment.

- The BF gain for a D2D network is considered constant in one search sector. This assumption can be modified and BF gain at each point in the desired search area should be estimated for realistic analysis.

- The consequence of beam misalignment can be another interesting future direction. Currently it is assumed that whenever the SNR is above a certain threshold value and TX and RX beams are facing each other, device discovery is successful. However, the effect of wrong beam pair selection should also be investigated.

- Currently, 2D BF is implemented at TX and RX. This work can be extended for 3D BF as well, where both azimuth and elevation angles are considered.

- The ABP algorithms should be implemented in a HetNet too. A D2D network with mmWave system and macro BS can be explored to improve the network capacity and coverage.

References

[1] M.Agiwal, A. Roy, and N. Saxena. Next generation 5g wireless networks: A comprehensive survey. *IEEE Communications Survey & Tutorials*, 18(3):1617–1655, February 2016.

[2] T. E. Bogale and L. B. Le. Massive mimo and mmwave for 5g wireless hetnet: Potential benefits and challenges. *IEEE Vehicular Technology Magazine*, 11(1):64–75, March 2016.

[3] Cisco visual networking index, 2016. URL `https://www.cisco.com/c/dam/m/en_in/innovation/enterprise/assets/mobile-white-paper-c11-520862.pdf`.

[4] T. S. Rappaport, W. Roh, and K. Cheun. Wireless engineers long considered high frequencies worthless for cellular systems. they couldn't be more wrong. *IEEE Spectrum*, 51(9):34–58, September 2014.

[5] J. G. Andrews et al. What will 5g be? *IEEE Journal on Selected Areas in Communications*, 32(6):1065–1082, June 2014.

[6] S. Chen and J. Zhao. The requirements, challenges, and technologies for 5g of terrestrial mobile telecommunication. *IEEE Communications Magazine*, 52(5):36–43, May 2014.

[7] S. Zeb, A. Mahmood, S. A. Hassan, S. H. Ahmed, and M. Gidlund. Impact of indoor multipath channels on timing advance for urllc in industrial iot. In *2020 IEEE International Conference on Communications Workshops (ICC Workshops)*, pages 1–6, 2020. doi: 10.1109/ICCWorkshops49005.2020.9145066.

[8] Qamar Abbas, Shah Zeb, and Syed Ali Hassan. Age of Information in Backscatter Communication. In *Wireless-Powered Backscatter Communications for Internet of Things*, pages 67–80. Springer, 2021.

[9] Understanding 5g: Perspectives on future technological advancements in mobile, 2014. URL https://www.gsma.com/futurenetworks/wp-content/uploads/2015/01/Understanding-5G-Perspectives-on-future-technological-advancement\s-in-mobile.pdf.

[10] S. Mumtaz, J. Rodrigues, and L. Dai. *mmWave Massive MIMO: A Paradigm for 5G*. Elsevier Inc., 2017.

[11] V. Jungnickel, K. Manolakis, W. Zirwas, B. Panzner, V. Braun, M. Lossow, M. Sternad, R. Apelfröjd, and T. Svensson. The role of small cells, coordinated multipoint, and massive mimo in 5g. *IEEE Communications Magazine*, 52(5):44–51, May 2014.

[12] K. N. R. S. V. Prasad, E. Hossain, and V. K. Bhargava. Energy efficiency in massive mimo-based 5g networks: Opportunities and challenges. *IEEE Wireless Communications*, 24(3):86–94, June 2017.

[13] R.W.Heath. Millimeter wave: The future of commerical wireless systems. In *IEEE Compound Semiconductor Integrated Circuit Symposium (CSICS)*, pages 1–4, October 2016.

[14] S. K. Yong and C. Chong. An overview of multigigabit wireless through millimeter wave technology: Potentials and technical challenges. *EURASIP Journal on Wireless Communications and Networking*, 2007. doi: https://doi.org/10.1155/2007/78907.

[15] W. Roh, J. Seol, J. Park, B. Lee, J. Lee, Y. Kim, J. Cho, and K. Cheun. Millimeter-wave beamforming as an enabling technology for 5g cellular communications: Theoretical feasibility and prototype results. *IEEE Communications Magazine*, 52(2): 106–113, February 2014.

[16] S. Zeb, A. Mahmood, H. Pervaiz, S. A. Hassan, M. I. Ashraf, Z. Li, and M. Gidlund. On TOA-based Ranging over mmWave 5G for Indoor Industrial IoT Networks. In *2020 IEEE Globecom Workshops (GC Wkshps*, pages 1–6, 2020. doi: 10.1109/GCWkshps50303.2020.9367555.

[17] M. N. Tehrani, M. Uysal, and H. Yanikomeroglu. Device-to-device communication in 5g cellular networks: Challenges, solutions and future directions. *IEEE Communications Magazine*, 52(5):86–92, May 2014.

[18] U. N. Kar and D. K. Sanyal. An overview of device-to-device communication in cellular networks. *ICT Express*, 4(4):203–208, December 2018.

[19] M. Giordani, M. Mezzavilla, C. N. Barati, S. Rangan, and M. Zorzi. Comparative analysis of initial access techniques in 5g mmwave cellular networks. In *Annual Conference on Information Science and Systems (CISS)*, pages 1–6, April 2016.

[20] M. Giordani, M. Mezzavilla, and M. Zorzi. Initial access in 5g mmwave cellular networks. *IEEE Communications Magazine*, 54(11):40–47, November 2016.

[21] R. I. Ansari, H. Pervaiz, C. Chrysostomou, S. A. Hassan, A. Mahmood, and M. Gidlund. Control-data separation architecture for dual-band mmwave networks: A new dimension to spectrum management. *IEEE Access*, 7:34925–34937, June 2019.

[22] S. A. Raza and S. A. Hassan. Combining noma and mmwave technology for cellular communication. In *IEEE Vehicular Technology Conference (VTC)*, pages 1–5, September 2016.

[23] Shah Zeb, Qamar Abbas, Syed Ali Hassan, Aamir Mahmood, and Mikael Gidlund. Enhancing Backscatter Communication in IoT Networks with Power-Domain NOMA. In *Wireless-Powered Backscatter Communications for Internet of Things*, pages 81–101. Springer, 2021.

[24] A. Ijaz, S. A. Hassan, S. A. R. Zaidi, and D. N. K. Jayakody. Coverage and rate analysis for downlink hetnets using modified reverse frequency allocation scheme. *IEEE Access*, 5:2489–2502, February 2017.

[25] H. Munir, S. A. Hassan, H. B. Parveiz, L. Musavian, and Q. Ni. Resource optimization in multi-tier hetnets exploiting multi-slope path loss model. *IEEE Access*, 5:8714–8726, May 2017.

[26] H. Munir, S. A. Hassan, H. Parveiz, Q. Ni, and L. Musavian. User association in 5g heterogeneous networks exploiting multi-slope path loss model. In *IEEE Second Workshop on Recent Trends in Telecommunications Research*, pages 1–5, February 2017.

[27] A. Ijaz, S. A. Hassan, and D. N. K. Jayakody. A multiple region reverse frequency allocation scheme for downlink capacity enhancement in 5g hetnets. In *Consumer Communications and Networking Conference (CCNC)*, pages 1–6, January 2017.

[28] S. Q. Gillani, S. A. Hassan, H. Pervaiz, and S. H. Ahmed. Performance analysis of flexible duplexing-enabled heterogeneous networks exploiting multi slope path loss models. In *IEEE International Conference on Computing, Networking nand Communications (ICNC)*, pages 1–6, February 2019.

[29] H. Munir, S. A. Hassan, H. Parveiz, and Q. Ni. A game theoretical network-assisted user-centric design for resource allocation in 5g heterogeneous networks. In *IEEE Vehicular Technology Conference (VTC)*, pages 1–5, May 2016.

[30] R. Zahid, A. Rahman, and S. A. Hassan. On the performance of multiple region reverse frequency allocation scheme in a single cell downlink heterogeneous networks. In *IEEE International Wireless Communications and Mobile Computing Conference (IWCMC)*, pages 1–6, August 2014.

[31] R. Zahid and S. A. Hassan. Stochastic geometry-based analysis of multiple region reverse frequency allocation scheme in downlink hetnets. In *IEEE International Wireless Communications and Mobile Computing Conference (IWCMC)*, pages 1–6, August 2015.

[32] S. Omar, S. A. Hassan, H. Pervaiz, Q. Ni, L. Musavian, S. Mumtaz, and O. A. Dobre. Multi-objective optimization in 5g hybrid networks. *IEEE Internet of Things Journal*, 5(3):1588–1597, June 2018.

[33] A. Umer, S. A. Hassan, H. B. Parveiz, L. Musavian, and Q. Ni. Coverage and rate analysis for massive mimo enabled heterogeneous networks with millimeter wave small cells. In *IEEE Vehicular Technology Conference (VTC)*, pages 1–5, June 2017.

[34] H. Munir, H. Pervaiz, S. A. Hassan, Q. Ni, L. Musavian, M. A. Imran, and R. Tafazolli. Computationally intelligent techniques for resource management in mmwave small cell networks. *IEEE Wireless Communications Magazine*, 25(4):32–39, August 2018.

[35] M. A. Jan, S. A. Hassan, and H. Jung. Qos-based performance analysis of mmwave uav-assisted 5g hybrid heterogeneous networks. In *IEEE Global Communications Conference (Globecom)*, pages 1–6, December 2019.

[36] H. Munir, S. A. Hassan, H. B. Parveiz, L. Musavian, and Q. Ni. Energy efficient resource allocation in 5g hybrid heterogeneous networks: A game theoretic approach. In *IEEE Vehicular Technology Conference (VTC)*, pages 1–5, September 2016.

[37] O. W. Bhatti, H. Suhail, U. Akbar, S. A. Hassan, H. Pervaiz, L. Musavian, and Q. Ni. Performance analysis of decoupled cell association in multi-tier hybrid networks using real blockage environments. In *IEEE International Wireless Communications and Mobile Computing Conference (IWCMC)*, pages 1–6, June 2017.

[38] Z. Mulk and S. A. Hassan. On achievable rates in massive mimo-based hexagonal cellular system with pilot contamination. In *IEEE Vehicular Technology Conference (VTC)*, pages 1–5, May 2015.

[39] M. T. Mushtaq, S. A. Hassan, and N. K. Jayakody. Ergodic rate analysis of massive mimo systems in k-fading environment. In *IEEE Vehicular Technology Conference (VTC)*, pages 1–5, September 2016.

[40] M. S. Zia and S. A. Hassan. On the impacts of composite fading on large-scale multi-user mimo systems. *IEEE Communication Letters*, 19(12):2286–2289, December 2015.

[41] M. S. Zia and S. A. Hassan. Outage analysis of multi-user massive mimo systems subject to composite fading. In *IEEE Vehicular Technology Conference (VTC)*, pages 1–5, May 2015.

[42] R. I. Ansari, M. A. Aslam, S. A. Hassan, and C. Chrysostomou. *Network Coding for Distributed Antenna Systems*. InTechOpen, 2018.

[43] S. A. R. Naqvi, S. A. Hassan, and Z. Mulk. *Encoding and Detection in mmWave Massive MIMO*. Springer, 2016.

[44] A. Umer, S. A. Hassan, H. Pervaiz, L. Musavian, Q. Ni, and M. A. Imran. Secrecy spectrum and energy efficiency analysis in massive mimo-enabled multi-tier hybrid hetnets. *IEEE Transactions on Green Communications and Networking*, 4(1):246–262, November 2019.

[45] A. Umer, S. A. Hassan, H. Pervaiz, Q. Ni, L. Musavian, and S. H. Ahmed. Secrecy outage analysis for massive mimo-enabled multi-tier 5g hybrid hetnets. In *IEEE International Conference on Communications (ICC)*, pages 1–6, June 2018.

[46] S. A. R. Naqvi, S. A. Hassan, and Z. Mulk. Pilot reuse and sum rate analysis of mmwave and uhf-based massive mimo systems. In *IEEE Vehicular Technology Conference (VTC)*, pages 1–5, May 2016.

[47] S. Nawaz, S. A. Hassan, S. A. R. Zaidi, and M. Ghogho. Throughput and energy efficiency of two-tier cellular networks: Massive mimo overlay for small cells. In *IEEE International Wireless Communications and Mobile Computing Conference (IWCMC)*, pages 1–6, September 2016.

[48] E. Björnson, M. Kountouris, and M. Debbah. Massive mimo and small cells: Improving energy efficiency by optimal soft-cell coordination. In *IEEE International Conference on Telecommunications (ICT)*, pages 1–5, May 2013.

[49] A. Adhikary, H. S. Dhillon, and G. Caire. Massive-mimo meets hetnet: Interference coordination through spatial blanking. *IEEE Journal on Selected Areas in Communications*, 33(6):1171–1186, March 2015.

[50] R. I. Ansari, C. Chrysostomou, S. A. Hassan, M. Guizani, S. Mumtaz, and J. Rodrigues. 5g d2d networks: Techniques, challenges, and future prospects. *IEEE Systems Journal*, 12(4):3970–3984, December 2018.

[51] R. I. Ansari, S. A. Hassan, and C. Chrysostomou. *Device-to-device communications for 5G*. IET, 2017.

[52] U. Saleem, S. Janghser, H. K.Qureshi, and S. A. Hassan. Joint subcarrier and power allocation in energy harvesting-aided d2d communication. *IEEE Transactions on Industrial Informatics*, 14(6):2608–2617, June 2018.

[53] A. Rahman and S. A. Hassani. Analysis of composite fading in a single cell downlink cooperative heterogeneous networks. In *IEEE Vehicular Technology Conference (VTC)*, pages 1–5, May 2015.

[54] C. Chrysostomou R. I. Ansari, S. A. Hassan. Ranc: Relay-aided network-coded d2d network. In *IEEE International Conference on Information, Communications and Signal Processing (ICICS)*, pages 1–5, December 2015.

[55] C. Chrysostomou R. I. Ansari, S. A. Hassan. Energy efficient relay selection in multihop d2d networks. In *IEEE International Wireless Communications and Mobile Computing Conference (IWCMC)*, pages 1–6, September 2016.

[56] C. Chrysostomou R. I. Ansari, S. A. Hassan. A swipt-based device-to-device cooperative network. In *IEEE International Conference on Telecommunications (ICT)*, pages 1–5, May 2017.

[57] G. H. Sim, A. Loch, A. Asadi, V. Mancuso, and J. Widmer. 5g millimeter-wave and d2d symbiosis: 60 ghz for proximity-based services. *IEEE Wireless Communications*, 24(4):140–145, August 2017.

[58] N. Wei, X. Lin, and Z. Zhang. Optimal relay probing in millimeter wave cellular systems with device-to-device relayingn. *IEEE Transactions on Vehicular Technology*, 65(12):10218–10222, December 2016.

[59] S. Wu, R. Atat, N. Mastronarde, and L. Liu. Improving the coverage and spectral efficiency of millimeter-wave cellular networks using device-to-device relays. *IEEE Transactions on Communications*, 66(5):2251–2265, May 2018.

[60] N. Bahadori, N. Namvar, B. Kelly, and A. Homaifar. Device-to-device communications in the millimeter wave band: A novel distributed mechanism. In *IEEE Wireless Telecommunications Symposium (WTS)*, pages 1–6, April 2018.

[61] F. Wang, H. Wang, H. Feng, and X. Xu. A hybrid communication model of mmwave and microwave in d2d network. In *IEEE 83rd Vehicular Technology Conference*, pages 1–5, May 2016.

[62] N. Deng and M. Haengg. A fine-grained analysis of millimeter-wave device-to-device networks. *IEEE Transactions on Communications*, 65(11):4940–4954, November 2017.

[63] W. Yi, Y. Liu, and A.Nallanathan. Modeling and analysis of d2d millimeter-wave networks with poisson cluster processes. *IEEE Transactions on Communications*, 65 (12):5574–5588, December 2017.

[64] S. A. R. Naqvi, H. Pervaiz, S. A. Hassan, L. Musavian, Q. Ni, M. A. Imran, X. Ge, and R. Tafazolli. Energy-aware radio resource management in d2d-enabled multi-tier hetnets. *IEEE Access*, 6:16610–16622, March 2018.

[65] S. A. R. Naqvi, S. A. Hassan, H. Parveiz, Q. Ni, and L. Musavian. Self-adaptive power control mechanism in d2d enabled hybrid cellular network with mmwave small cells: An optimization approach. *IEEE Transactions on Green Communications and Networking*, 4(1):246–262, November 2019.

[66] L. Chen, Y. Li, and A. V. Vasilakos. On oblivious neighbor discovery in distributed wireless networks with directional antennas: Theoretical foundation and algorithm design. *IEEE/ACM Transactions on Networking*, 25(4):1982–1993, August 2017.

[67] Y. Wang, S. Mao, and T. S. Rappaport. On directional neighbor discovery in mmwave networks. In *IEEE 37th International Conference on Distributed Computing Systems (ICDCS)*, pages 1–10, June 2017.

[68] A. Riaz, S. Saleem, and S. A. Hassan. Energy efficient neighbor discovery for mmwave d2d networks using polya's necklaces. In *IEEE Global Communications Conference (GLOBECOM)*, pages 1–6, December 2018.

[69] Y. Zhao, Y. Liu, G. Boudreau, A. Sediq, and X. Wang. Angle-based beamforming in mmwave massive mimo systems with low feedback overhead using multi-pattern codebooks. *IEEE China Communications*, 16(9):18–30, September 2019.

[70] W. Zhang, W. Zhang, and J. Wu. Uav beam alignment for highly mobile millimeter wave communications. *IEEE Transactions on Vehicular Technology*, pages 1–10, May 2020.

[71] F. Asim, J. A. Nossek, F. Antreich abd C. C. Cavalcante, and A. L. F. de Almeida. Maximum likelihood channel estimation for millimeter-wave mimo systems with hybrid beamforming. In *IEEE International ITG Workshop on Smart Antennas (WSA)*, pages 1–6, April 2019.

[72] Y. Guo, Z. Wang, M. Li, and Q. Liu. Machine learning based mmwave channel tracking in vehicular scenario. In *IEEE International Conference on Communications (ICC) Workshops*, pages 1–6, May 2019.

[73] J. Li, Y. Sun, L. Xiao, S. Zhou, and C. E. Koksal. Analog beam tracking in linear antenna arrays: Convergence, optimality, and performance. In *IEEE Asilomar Conference on Signals, Systems, and Computers*, pages 1–6, November 2017.

[74] Y. Xiu, J. Wu, C. Xiu, and Z. Zhang. Millimeter wave cell discovery based on out-of-band information and design of beamforming. *IEEE Access*, 7:23076–23088, February 2019.

[75] G. E. Garcia, G. S. Granados, E. Karipidis, and H. Wymeersch. Transmitter beam selection in millimeter-wave mimo with in-band position-aiding. *IEEE Transactions on Wireless Communications*, 17(9):6082–6092, September 2018.

[76] C. N. Barati, S. A. Hosseini, S. Rangan, P. Liu, T. Korakis, S. S. Panwar, and T. S. Rappaport. Directional cell discovery in millimeter wave cellular networks. *IEEE Transactions on Wireless Communications*, 14(12):6664–6678, December 2015.

[77] S. Habib, S. A. Hassan, A. A. Nasir, and H. Mehrpouyan. Millimeter wave cell search for initial access: Analysis, design and implementation. In *IEEE International Wireless Communications and Mobile Computing Conference (IWCMC)*, pages 1–6, June 2017.

[78] R. Mustafa and S. A. Hassan. Machine learning-based context aware sequential initial access in 5g mmwave systems. In *IEEE Global Communications Conference (Globecom)*, pages 1–6, December 2019.

[79] D. Zhu, J. Choi, and R. W. Heath. Auxiliary beam pair design in mmwave cellular systems with hybrid precoding and limited feedback. In *IEEE International Conference on Acoustics, Speech and Signal Processing (ICASSP)*, pages 1–5, March 2016.

[80] D. Zhu, J. Choi, and R. W. Heath. Auxiliary beam pair enabled aod and aoa estimation in mmwave fd-mimo systems. In *IEEE Global Communications Conference (GLOBECOM)*, pages 1–6, December 2016.

[81] D. Zhu, J. Choi, and R. W. Heath. Auxiliary beam pair enabled aod and aoa estimation in closed-loop large-scale mmwave mimo system. *IEEE Transactions on Wireless Communications*, 16(7):4770–4785, July 2017.

[82] D. Zhu, J. Choi, and R. W. Heath. Two- dimensional aod and aoa acquisition for wideband mmwave systems with cross-polarized mimo. *IEEE Transactions on Wireless Communications*, 16(12):7890–7905, December 2017.

[83] D. Zhu, J. Choi, Q. Cheng, W. Xia, and R. W. Heath. High-resolution angle tracking for mobile wideband millimeter-wave systems with antenna array calibration. *IEEE Transactions on Wireless Communications*, 17(11):7173–7189, November 2018.

[84] D. Zhu, J. Choi, and R. W. Heath. Two-dimensional aod and aoa acquisition for wideband millimeter-wave systems with dual-polarized mimo. *IEEE Transactions on Wireless Communications*, 16(12):7890–7905, December 2017.

[85] E. Ghunney, S. A. Hassan, and M. A. Weitnauer. Modified auxiliary beam pair for user discovery in mmwave systems. In *IEEE Vehicular Technology Conference (VTC)*, pages 1–5, June 2018.

[86] E. Ghunney, S. A. Hassan, and M. A. Weitnauer. Impact of wrong beam selection on beam pair scanning method for user discovery in mmwave systems. In *IEEE Vehicular Technology Conference (VTC)*, pages 1–5, May 2020.

[87] Beamforming explained: How it makes wireless communication fasters, 2019. URL `https://www.networkworld.com/article/3445039/beamforming-explained-how-it-makes-wireless-communication-faster.html`.

[88] Beamforming and radar digital processing, 2011. URL `https://www.eetimes.com/radar-basics-part-3-beamforming-and-radar-digital-processing/`.

[89] C. Fei, F. Hongqi, S. Zhiyong, and F. Qiang. Difference beam aided target detection in monopulse radar. *Chinese Journal of Aeronautics*, 28(5):1485–1493, August 2015.

[90] A. I. Leonov and K. I. Fomichev. *Monopulse Radar*. Foreign Technology Division, 1972.

[91] B. R. Mahafza. *Introduction to Radar Analysis*. CRC Press, 1998.

[92] W. Kederer and J. Detlefsen. Direction of arrival (doa) determination based on monopulse concepts. In *IEEE Asia-Pacific Microwave Conference. Proceedings*, pages 1–4, December 2000.

[93] What is beamforming and massive mimo in 5g?, 2020. URL `https://www.telit.com/blog/beamforming-massive-mimo-5g-technology/`.

[94] Linear array theory, 2019. URL `https://www.ece.mcmaster.ca/faculty/nikolova/antenna_dload/current_lectures/L13_Arrays1.pdf`.

[95] Fundamentals of a uniform linear array, 2018. URL `http://www.raymaps.com/index.php/fundamentals-of-a-uniform-linear-array-ula/`.

[96] Planar arrays, circular arrays, 2018. URL `http://www2.elo.utfsm.cl/~elo352/biblio/antenas/Lectura%62018.pdf`.

[97] What is the difference between beamforming and precoding, 2017. URL https://ma-mimo.ellintech.se/2017/10/03/what-is-the-difference-between-beamforming-and-precoding.

[98] A. Roze, M. Helard, M. Crussiere, and C. Langlais. Millimeter-wave digital beamsteering in highly line-of-sight environments for massive mimo systems. In *Conference: Forum WWRF35*, pages 1–6, October 2015.

[99] 5g nr: Massive mimo and beamforming – what does it mean and how can i measure it in the field?, 2018. URL https://www.rcrwireless.com/20180912/5g/5g-nr-massive-mimo-and-beamforming-what-does-it-mean-and-how-can\-i-measure-it-in-the-field.

[100] Advanced antenna systems for 5g networks, 2020. URL https://www.ericsson.com/en/reports-and-papers/white-papers/advanced-antenna-systems-for-5g-networks.

[101] S. Nawaz and S. A. Hassan. Auxiliary beam pair enabled initial access in wwwave systems: Analysis and design insights. In *IEEE International Conference on Communications (ICC) Workshops*, pages 1–6, May 2019.

[102] T. C. Cheston and J. Frank. *Array antennas*. The Johns Hopkins University, Applied Physics Laboratory, 1968.

[103] M. S. Omar, M. A. Anjum, S. A. Hassan, H. Pervaiz, and Q. Niv. Performance analysis of hybrid 5g cellular networks exploiting mmwave capabilities in suburban areas. In *IEEE International Conference on Communications (ICC)*, pages 1–6, May 2016.

[104] S. Nawaz, S. A. Hassan, and H. Jung. Auxiliary beam pair enabled initial access for mmwave d2d networks. *Physical Communication Journal*, pages 1–12, April 2020.

[105] L. Chen, Y. Li, and A. V. Vasilakos. Oblivious neighbor discovery for wireless devices with directional antenna. In *IEEE International Conference on Computer Communications (INFOCOM)*, pages 1–9, April 2016.

[106] S. Nawaz and S. A. Hassan. Optimal beam separation in auxiliary beam pair-based initial access in mmwave d2d networks. In *IEEE Vehicular Technology Conference (VTC)*, pages 1–5, May 2020.